Study on quantification of commercial fisheries echo sounder information for visualization of fish school distribution in Hyuga-nada, Miyazaki, Japan

日向灘における魚群分布の可視化に向けた漁業用魚群探知機の定量化に関する研究

Graduate School of Environmental Science

Hokkaido University

Yanhui Zhu

Contents

1. General introduction

1.1 Japan's fisheries

Oceans surround Japan, and many ocean currents, such as the Oyashio and Kuroshio currents, flow at crossings. Therefore, the surrounding seas are rich in fishery resources, and abundant fishing grounds have been formed. However, in recent years, the Japanese fisheries have experienced a continuous decline in fisheries production due to a decrease in the number of fishery workers, the aging of the fishery workers, and a decrease in fisheries resources due to changes in the marine environment. In 2018, 151,701 people were working in the fishery, with the most significant number of fishermen in the 65 and older age group (FY-2018, 2019). In coastal fisheries, many fishermen were working even at 75 or older. In addition, the recent rise in seawater temperature has changed the growth, behavior, and distribution of fish, shellfish, and algae, affecting the fishery in various ways (Shinada, 2021). Furthermore, most of Japan's fisheries resources are overfished, and only 20 % of fisheries resources can afford the catch quota. In Japan's 37 stock groups of fisheries resources, whose abundance is estimated by resource assessment, 46 % of the stocks were found to be at a low level (too much catch for the number of resources) (FY-2018, 2019).

On the other hand, technological advancements have led to high-performance machinery used in the fishery and the use of new technologies such as the Internet of Things (IoT) and Information and Communication Technology (ICT) (Kaneko, 2019; Takao et al., 2019). In addition, fishery workers have become more aware of resource conservation and management, and at production sites, fishery workers are engaged in various proactive activities to solve local fishery issues (Yakura et al., 2019; Hokimoto, 2019; Hokimoto, 2020). Furthermore, the Fisheries Law was partially amended in December 2018 to reform fisheries policy, aiming to balance the appropriate management of fishery resources and the growth industry of the fishery (FY-2018, 2019). It aims to maintain a stable supply of fishery resources and to operate efficiently with less effort. Under these circumstances, it is considered that Japan's fisheries need to change to a system that can sustain and develop.

1.2 Acoustic methods used in resource assessment

According to the United Nations Convention on the Law of the Sea, the primary management objectives of marine fisheries resources are not to deplete them by fishing. Additionally, take management measures to maintain or restore them to levels above which the maximum sustainable yield (MSY) can be achieved (Ichinokawa et al., 2022). However, half of Japan's fishery stocks were below the MSY level, and about two-thirds were under excessive fishing pressure (Katsugawa, 2020). One of the reasons why most of Japan's fishery resources are at low levels is that it is difficult to estimate fishery resources scientifically, and it is challenging to continue fishing without reducing the number of resources (Tanaka, 2021). Therefore, appropriate management of fishery resources based on scientific results is essential to achieve sustainable fisheries. Furthermore, to properly manage fishery resources, it is of utmost importance that they are in good condition. Therefore, it is necessary to evaluate fishery resources, maintain them when they are in good condition, and control them to recover when deterioration is observed promptly and accurately.

Accurate assessment of fishery resources requires two types of information: information from the fishery and information independent of the fishery. Information from the fishery is mainly information on the catch, fishing effort, and age composition of the catch, which is the most basic information for understanding the scale of the fishery. Information independent of the fishery is obtained from scientifically designed surveys to examine the abundance and its trend directly. For example, visual surveys are often conducted for cetaceans, catch surveys for bottom fish, and surveys using echo sounders for pelagic fish. By analyzing the data obtained from these surveys, an abundance index is calculated for use in resource estimation.

In echo sounder-based surveys, most survey methods use quantitative echo sounders onboard research vessels of government agencies and universities (Amakasu, 2019). In principle, quantitative echo sounder is not much different from general echo sounder; however, they convert the echoes of the target objects into distribution densities so that all responses can be quantified. For this reason, methods for discriminating fish species and three-dimensional behavior detection have been studied extensively. As a result, the level of resource survey methods using acoustic methods has been increasing yearly. However, the quantitative echo sounder is expensive and is often equipped with large research vessels, which limits the frequency and range of surveys or has the disadvantage of not being suited for surveys in coastal waters (Miyamoto et al., 2016). Therefore, there is a strong need to develop a simple data acquisition method that can collect the acoustic information necessary for resource assessment over a wide area and at high frequency.

From above, in this study, we considered a resource survey using a general echo sounder installed on most small fishing boats. Conventional general echo sounders could only determine the location of fish schools and could not be used for resource estimation. However, unlike conventional general echo sounders, today's general echo sounders can not only display the echoes reflected from an object. However, it can also calculate the backscattering strength of the object from the recorded electrical signals. Therefore, it is not too much to say that now is the time to realize resource assessment utilizing a general echo sounder. If a general echo sounder could be used like a quantitative echo sounder, surveying fish stocks using fishing vessels would be possible, significantly advancing resource management and utilization. Furthermore, since a general echo sounder is installed on daily fishing vessels, a large amount of data can be obtained each time a fishing trip is made. Combining the vast amount of acoustic information obtained from fishing vessels with environmental information such as ocean currents and sea surface temperatures is expected to provide a means of understanding the entire marine environment and ecosystems in coastal waters.

1.3 Acoustic survey using a general echo sounder

Since the data measured by conventional general echo sounders are not quantifiable, quantifying general echo sounders is necessary for resource assessment. Therefore, calibration of the transducer system is essential to provide quantifiability to the general echo sounder (Furusawa, 2019). In addition, calibration between vessels is also essential, primarily when several vessels conduct simultaneous surveys in the same ocean area, because all general echo sounders need to be adjusted to the same level. Furthermore, general echo sounders need to be calibrated more regularly than other measuring instruments because they are used for long periods in the constantly harsh environment of the ocean. Therefore, it is necessary to establish a simple calibration method that can calibrate multiple general echo sounders regularly because the measurement results of general echo sounders are directly linked to resource management.

Generally, the calibration of echo sounders is performed using a calibration ball, a standard reflector with known scattering strength (Furusawa, 2019). However, this method is a time- and manpower-intensive calibration method because the calibration ball must be placed on the sound axis of the transducer and worked onboard. Because of these reasons, performing periodic calibration on many fishing vessels takes much work. Therefore, this study considered a direct calibration method using the seabed instead of a calibration ball. This calibration method uses the scattering strength of the seabed, which does not change significantly in time or physically.

However, since calibration of the general echo sounder using the seabed backscattering strength has never been done before, it is necessary to examine the validity of this method. In addition, unlike calibration balls, there are various types of seabeds; therefore, it is also essential to examine seabed that can be used in place of calibration balls.

1.4 Objectives and outline in this study

This study was conducted in Miyazaki Prefecture, which has a well-developed fishery and is actively adopting reforms in the fishery. The first objective was to establish a new calibration method using seabed scattering strength. The second objective was to evaluate the fish resource in the coastal waters of Miyazaki Prefecture using a general echo sounder calibrated by seabed scattering strength.

The following is a summary of each chapter. Chapter 1 is an introduction, introducing the study's background, purpose, and outline. Chapter 2 describes the acoustic indices obtained from general echo sounders and the formulas used to calculate acoustic indices. Chapter 3 introduces the general calibration method and new calibration methods in this study. Chapter 4 discusses the validity of the calibration method using seabed scattering strength in the field. In Chapter 5, we calibrate one general echo sounder using the seabed scattering strength and try to evaluate the fish abundance and distribution in the coastal waters of Miyazaki Prefecture. Finally, chapter 6 presents a general discussion and prospects.

2. Mechanisms and formulas of general echo sounders

2.1 Introduction

Traditional echo sounders are not quantitative, and their primary purpose is to detect fish position. The system of general echo sounder amplifies the generated pulses, then discharges them into the ocean as ultrasonic pulses from the transducer, and either a single echo or a group of echoes of the target projects is reception. After receiving the echo, the transducer converts the reception echoes into electrical signals, and an echogram will finally be displayed. However, in recent years, processing such as TVG (time varied gain) has been incorporated into the reception echoes of general echo sounders, enabling quantification and advancement of general echo sounders (Figure 2-1). TVG processing serves as a distance correction and plays an essential role in the sonar equation on which various estimates are based (Furusawa, 1985; De Robertis and Higginbottom, 2007). The echoes carried include distance attenuation, such as diffuse attenuation and absorption attenuation caused by the propagation of sound waves. Therefore, TVG processing, which varies the gain of the amplifier over time so that the level of the returned signal is constant, can be used to accurately obtain the echo level of the target project (Yamatani, 1990; Furusawa, 1991). Whether this TVG processing can be processed automatically is the most significant difference between general and quantitative echo sounders.

The output data of the general echo sounder used in this study, manufactured by FURUNO, is the LOG conversion data (digit values from 0 to 255) proportional to the reception voltage level. The output data consists of three sentences: basic information, such as frequency and pulse width; environmental information, such as time and depth; and raw data, without TVG processing (Figure 2-2). To calculate the echo level from the target reflector, it is necessary to perform appropriate conversions for each transducer and add corrections such as absorption attenuation to the raw data. For example, the following formula can convert the raw output data (digit values from 0 to 255) to the reception signal level (EL, dBμV).

$$EL = digit * a + a' \tag{1}$$

where a is the specific coefficient of each transducer at the time of LOG conversion, and a' is a specific coefficient that includes each transducer's frequency and temperature variation characteristics. Since the available transducer differs depending on the frequency used, it is necessary to calculate the reception signal level by adding the transmitter sensitivity (SL, dBμPa), receiver sensitivity (ME, dB), and gain (RG, dB) of each transducer. Therefore, if the transducer used is known, the values of SL, ME, and RG will be known, and the reception signal level of the target reflector can be calculated. In addition, if the distance attenuation is known by TVG processing, the acoustic backscattering strength of the target reflector can be accurately calculated. Note that TVG processing differs for single echo and group echoes, so it is necessary to use the respective formulas (Furusawa, 2019).

2.2 Calculation of TS using TVG processing

The target strength (TS) is the backscattering strength of a single reflector, which is used to estimate the length of the reflector and distribution density (Furusawa and Takao, 1990). Since electrical pulses are discharged into the water as ultrasonic pulses by a transducer, the voltage E (V) and the sound pressure P (Pa) are considered equivalent in strength. These discharged sound waves are affected by diffuse attenuation and absorption attenuation, then reach the reflector. Diffuse attenuation is the attenuation due to spherical diffusion, with a characteristic of R^{-2} for the propagation distance R (m) to the reflector. Absorption attenuation is the attenuation due to the absorption of energy by the components of seawater, and it is exponential with the characteristic of exp (-2 α R) for the absorption attenuation coefficient α (dB/m). In addition to the effects of the two types of attenuation, the sound wave is also affected by the directivity function b in the direction θ (rad) of the reflector, and the sound wave becomes weaker as it moves away from the central axis. Became the sensitivity varies with direction, the sound pressure is direction θ times the directivity function b (θ). Therefore, if the sound pressure of the transmitted wave is P_o (sound pressure at 1 m from the transducer) and the sound pressure reaches the reflector is P_i, the following equation expresses the relationship between the P_o and P_i.

$$P_i^2 = P_o^2 R^{-2} \exp(-2 \alpha R) b^2 \quad (2)$$

The sound pressure P_{ts} from a single reflector is the strength of the return scattered wave at the point returned in the source direction by a unit distance from the target reflector (Figure 2-3, a). The sound wave at the reflector returns to the transducer is also affected by the same two types of attenuation in the return path, as shown in the following equation.

$$P_{ts}^2 = P_i^2 R^{-2} \exp(-2 \alpha R) b^2 ts$$

$$= P_o^2 R^{-4} \exp(-4 \alpha R) b^4 ts \quad (3)$$

where ts (m^2) denotes the sound scattering index of a single reflector. The transducer converts these sound pressures into electrical signals and sends them to the preamplifier. The receiver sensitivity M, which is the rate of conversion from sound pressure to voltage, and GR, which is the gain of the front-end amplifier, are then calculated using the following equation (Furusawa and Sawada, 1991), and output as the voltage Ets.

$$E_{ts}^2 = (P_{ts} M G_R)^2$$

$$= (P_o M G_R)^2 R^{-4} \exp(-4 \alpha R) b^4 ts \quad (4)$$

$P_o M G_R$ is called the factor of transmit and receive and is denoted by KTR (dB V). The value of KTR depends on the transducer and is obtained by calibration.

Finally, the distance attenuation term in equation (4) undergoes TVG processing, resulting in the following equation

$$G_{ts} R^2 \exp(2 \alpha R) \quad (5)$$

where G_{ts} is the TVG coefficient. In terms of decibel values, this equation yields

$$40 \log R + 2 \alpha R \tag{6}$$

Moreover, a distance characteristic of 40 log R is obtained (Yamatani, 1990; Imazeki et al., 1992). To decibel equation (4) and apply a TVG correction of 40 log R yields the following equation.

$$TS = EL - (SL + ME + RG) + 40 \log R + 2 \alpha R \tag{7}$$

Where TS is 10 log ts, EL is 20 log E_{ts}, SL is 20 log P_o, ME is 20 log M, and RG is 20 log G_R. This equation is the basic general echo sounder equation for the echo of an individual reflector (Traynor and Ehrenberg, 1990).

2.3 Calculation of SV using TVG processing

In calculating the volume backscatter strength (SV) of the group echoes, the same formula in P_i of TS can be used to calculate the P_i of SV. In addition, the strength of the scattered wave P_{sv} returned to the transducer is the strength of the group echoes combined with all echoes in the scattered volume V (m^3) for the propagation distance R (Saneyoshi and Nakamura, 1952; Foote, 1983), and expressed by the following formula (Figure 2-3, b).

$$P_{sv}^2 = P_o^2 R^{-4} \exp(-4 \alpha R) n\ ts$$

$$= P_o^2 R^{-4} \exp(-4 \alpha R) V\ sv \quad (8)$$

The time limit for distinguishing two things as two is the pulse width (τ, s), and its relation to the distance R is $\Delta R = c\ \tau / 2$. where c (m/s) is the speed of sound. Target echoes within this distance overlap and are combined to be recognized as one echo. Therefore, volume V can be calculated from the volume elements of the scattering cross section $d\Omega R^2$ and thickness $c\ \tau / 2$ within a small solid angle $d\Omega$ in each direction at a given instant using the pulse width τ.

$$dV = b^4\ d\Omega\ R^2\ c\ \tau / 2 \quad (9)$$

Integrating equation (9) yields the following equation:

$$V = \Psi R^2\ c\ \tau / 2 \quad (10)$$

$$\Psi = \int_{2\pi} b^4\ d\Omega \quad (11)$$

Ψ is the equivalent beamwidth for volume scattering. It indicates the solid angle representing the ideal beam spread where the intensity of the scattered wave is the same as that of the actual directivity case (MacLennan, 1989). If the actual equivalent beamwidth is unknown, the following approximate formula can be used to calculate it.

$$\Psi = 5.78 / (2\pi * ra / \lambda)^2 \quad (12)$$

Where ra (m) is the radius of the transducer, substituting equation (10) into equation (8), the group echo sound pressure P_{sv} becomes the following equation.

$$P_{sv}^2 = P_o^2 R^{-2} \exp(-4 \alpha R) (\Psi c \tau / 2) sv \quad (13)$$

n is the number of objects, sv (m^2 / m^3, the denominator is the unit volume $1m^3$) is the volume backscattering coefficient, the distribution density per unit volume.

Then, when converting the sound pressure obtained by equation (13) to a voltage, the receiver sensitivity M and the gain GR of the preamplifier are multiplied to obtain the E_{sv},

$$E_{sv}^2 = (P_o M G_R)^2 R^{-2} \exp(-4 \alpha R) (\Psi c \tau/2) sv \quad (14)$$

The distance attenuation term is subjected to TVG processing, yielding the following distance characteristics (Furusawa et al., 1995; Aoyama, 1999).

$$20 \log R + 2 \alpha R \quad (15)$$

Using this 20 log R TVG correction, the SV can be calculated by the following equation.

$$SV = EL - (SL + ME + RG) + 40 \log R + 2 \alpha R - 10 \log (\Psi c \tau/2) \quad (16)$$

SV is 10 log sv, EL is 20 log E_{sv}, SL is 20 log P_o, ME is 20 log M, and RG is 20 log G_R. This equation (16) is the basic general echo sounders formula for group echoes.

The SV obtained, as described above, is the raw SV and cannot be used directly for resource estimation. When calculating SV using the equivalent beam width Ψ, it is assumed that the fish are distributed evenly within the beam; therefore, the beam must be able to enter the fish school. However, not all fish schools are more significant in the natural environment than the beam spread. Therefore, it is challenging to calculate SV correctly when the fish school is smaller than the beam spread because it cannot be distributed evenly within the beam. From these, the raw SV data are subjected to a process called echo integration to obtain the mean distribution density over a wide area (Tang et al., 2003). When the raw SV pings are accumulated while running and averaged over a specific integration range, many distributions are superimposed, and a large school of fish is observed (Figure 2-4). Aggregating and averaging the raw SV of multiple pings in the horizontal and vertical directions can be applied to the formula for the volume backscattering strength SV of the school echoes, resulting in an accurate mean SV. When integrating over n' echoes in the direction of travel and R + R_w in the depth direction, the following equation can obtain the mean SV (SV_{mean}).

$$SV_{mean} = \int_{R}^{R+Rw} \left(\frac{1}{n'} \sum E_{sv}^2\right) dR \qquad (17)$$

This equation is the basic equation for the echo integral. Since fish schools in natural environments come in various sizes, echo integration is an essential process for resource estimation.

The echo integrated SV_{mean} is proportional to the distribution density per unit volume. Therefore, the final value used in the resource calculation is the distribution density per unit area SA (Figure 2-5). Finally, the SV_{mean} is integrated into the direction of depth and expressed by the following equation.

$$sa = \int_{R1}^{R2} SV_{mean}\, dR = \sum R_w\, SV_{mean} \quad (18)$$

Where sa (m^2 / m^2, the denominator is the unit area of $1m^2$) is the area backscattering coefficient, and SA is 10 log sa. By dividing this by the target strength TS, the number of the target species can be calculated, and the distribution density per area within a certain sea area can be obtained (Miyanohana, 1994).

2.4 Calculation of SS using TVG processing

When calculating the seabed reflection levels using acoustic data of the general echo sounder, the surface backscattering strength (SS) is the standard (Aoyama, 1999). When the pulse strikes the seabed surface, the scattering surface broadens from a circle to a ring (Figure 2-6). Also, when the scattering surface is a circle, the echo intensity reaches a maximum value as the area expands (Figure 2-6, a). Then, when the area of the scattering surface change to the circle, the backscattering strength decreases as the directional coefficient decreases (Figure 2-6, b). Therefore, the P_{ss} from a scattering area A (m^2) on the seabed surface can be calculated using the following equation.

$$P_{ss}^2 = P_o^2 R^{-4} \exp(-4 \alpha R) A / R \, ss \tag{19}$$

R is the water depth, A / R is the correction per unit area, and ss (m^2/m^2) is the surface backscattering coefficient per unit area.

The scattering area A is generally considered to be the beam width of the echoes reflected from the seabed and calculated from the beam width φ. However, due to the limitation of the pulse width τ of the general echo sounders, it is not always possible to receive all the reflected echoes from the seabed simultaneously. Since the sound waves transmitted by the echo sounder have a specific thickness, in the case of narrow pulse widths, the sound waves arrive quickly just below the transducer and take longer to reach the edges of the beam (Hamilton, 2001). Therefore, targets at the same depth cannot be detected simultaneously and may be perceived as different echoes. Similarly, in the case of the seabed, if the pulse width is narrow, the echo is cut off before the seabed of the beam width can be detected. As a result, only the seabed of the pulse width can be detected (Figure 2-7). Two parameters, therefore, calculate the scattering area A: pulse width τ and beam width φ.

To calculate the scattering area A with either the pulse width or the beam width, it is determined by the discrimination depth r, which is the oblique distance from the transducer to the outer edge of the scattering surface (Tang et al., 2003), where the following equation expresses r.

$$r = (c\ \tau / 2) \cos\theta / (1 - \cos\theta) \tag{20}$$

Where τ (s) is the pulse width and θ (rad) is the beam angle. When the pulse width is long, i.e., the discrimination depth r is greater than the water depth R, all the seabed within the beam width can be detected because the pulse is extended after the beam edge reaches the seabed (Figure 2-8, a). Therefore, the scattering area A can be calculated from the beam width φ and expressed by the following equation.

$$dA = \pi\ [R^2\ (\tan\theta)^2]\ d\varphi / 2\ \pi\ b^4 \tag{21}$$

On the other hand, if the pulse width is short, i.e., the discrimination depth r is less than the water depth R, the pulse width is cut off before the beam end reaches the seabed (Figure 2-8, b). Therefore, the scattering area A must be calculated from the pulse width. The radius of the reflection area that the pulse width can detect is x, which can be calculated from the three-square theorem as follows:

$$x = \sqrt{(R + c\,\tau / 2)^2 - R^2} \qquad (22)$$

Calculating the scattering area A using equation (21) yields the following equation.

$$dA = \pi\,[(R + c\,\tau/2)^2 - R^2]\; d\varphi / 2\,\pi\, b^4$$

$$\cong\; c\,\tau / 2\; R\; d\varphi\; b^4 \qquad (23)$$

Integrating equation (23) yields the following equation.

$$A = \Gamma\, R\, c\, \tau / 2 \qquad (24)$$

$$\Gamma = \int_{2\pi} b^4\, d\varphi \qquad (25)$$

where Γ is the equivalent beam width of the surface scattering. Substituting equation (24) into equation (19), the sound pressure P_{ss} of the surface return scattered wave is given by:

$$P_{ss}^{\,2} = P_o^{\,2}\, R^{-3} \exp(-4\,\alpha\, R)\,(\Gamma\, c\,\tau / 2)\; ss \qquad (26)$$

The distance term in equation (26) is TVG processed to obtain the following distance properties.

$$30 \log R + 2\,\alpha\, R \qquad (27)$$

Using this TVG correction of 30 log R+2 α R, SS can be calculated using the following formula.

$$SS = EL - (SL + ME + RG) + 30 \log R + 2\,\alpha\, R + 10 \log (R / A) \qquad (28)$$

Where SS is 10 log ss, this equation (23) is the basic equation for determining the surface backscattering strength.

2.5 Figures

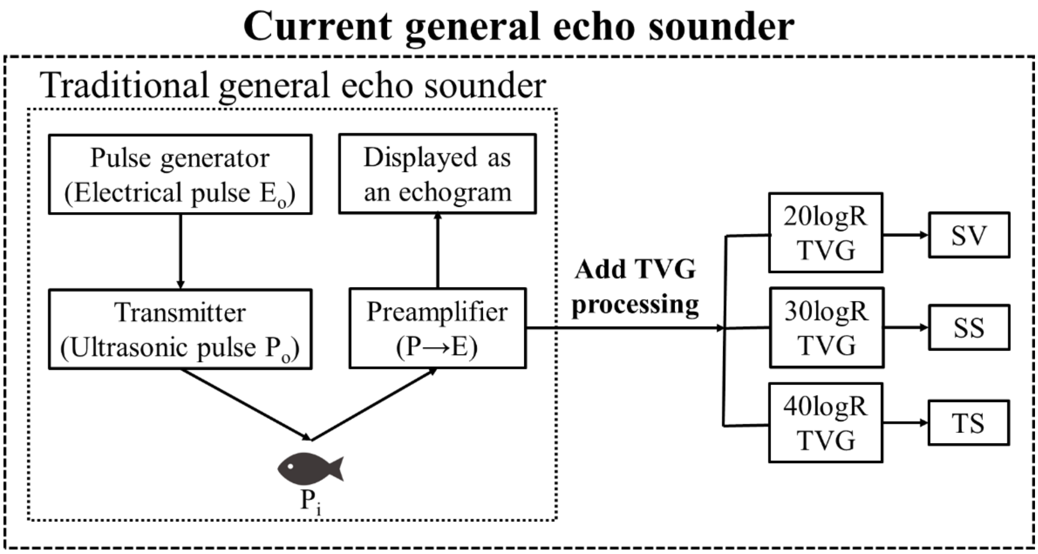

Figure 2-1: Structure diagram of general echo sounders. TVG (time varied gain) processing serves as a distance correction and plays an essential role in the sonar equation. SV is volume backscattering strength; SS is surface backscattering strength; TS is backscattering strength of a single reflector.

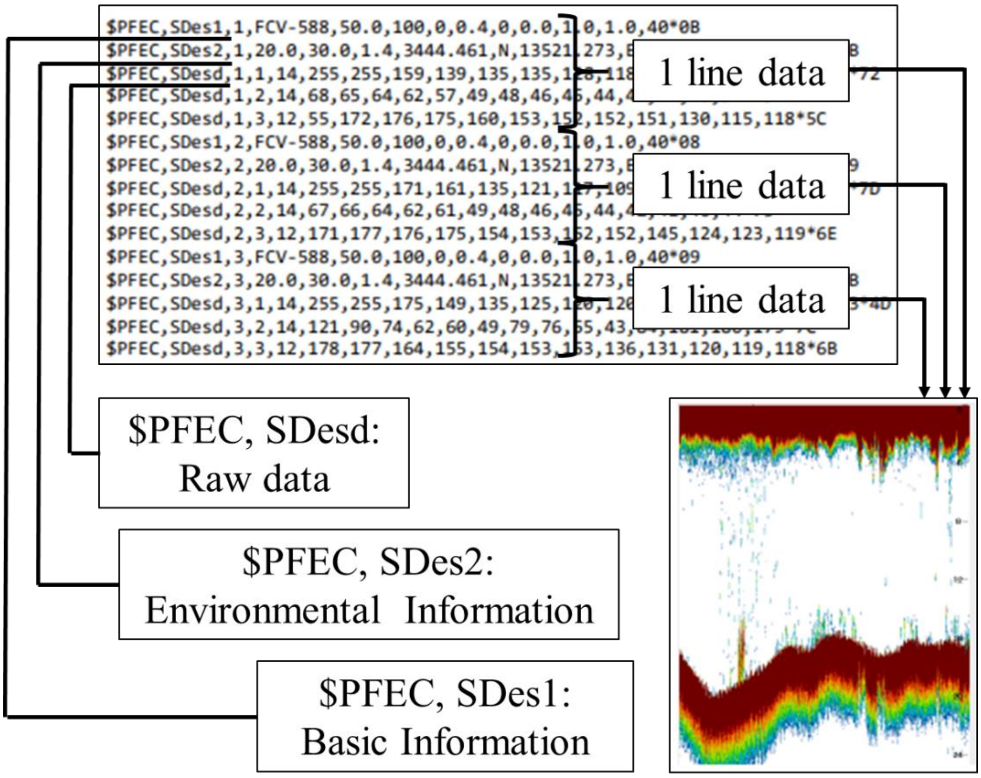

Figure 2-2. A structural description of the raw data from the general echo sounder made by Furuno.

The lower right echogram is an example obtained from general echo sounder.

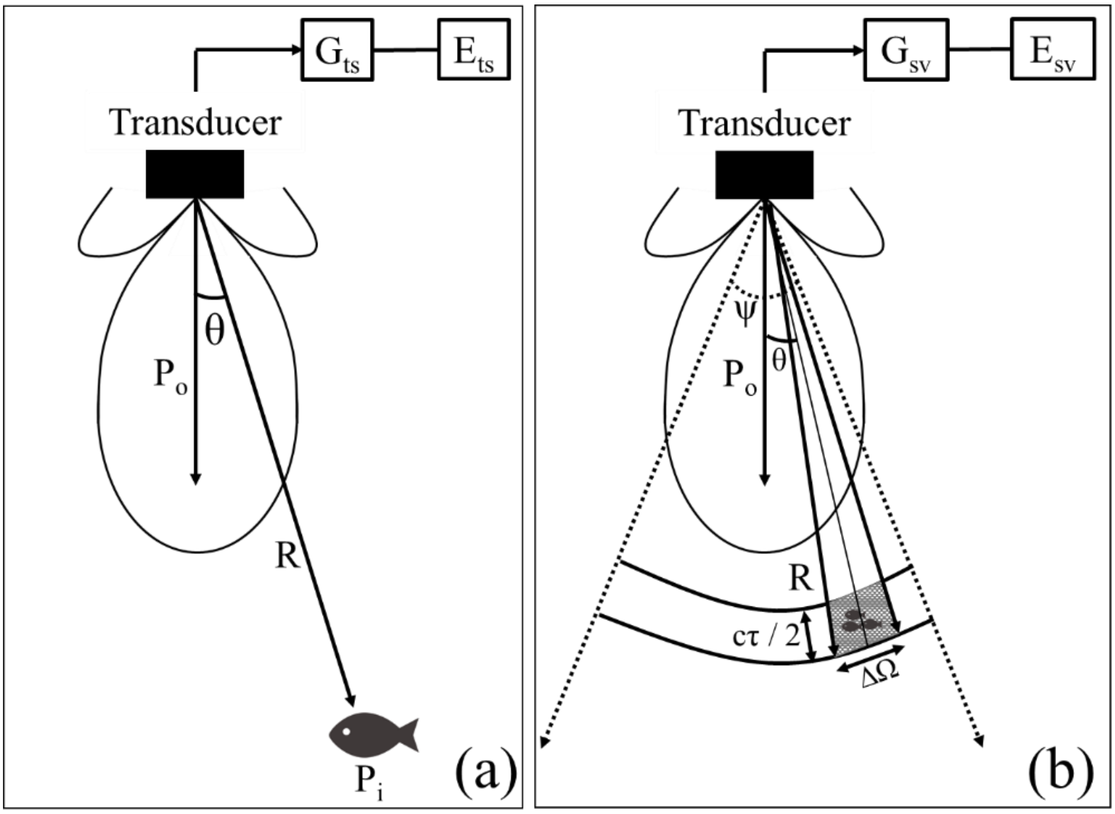

Figure 2-3. Mechanisms of target strength (TS) and volume backscattering strength (SV), (a): explanation of TS, (b): explanation of SV.

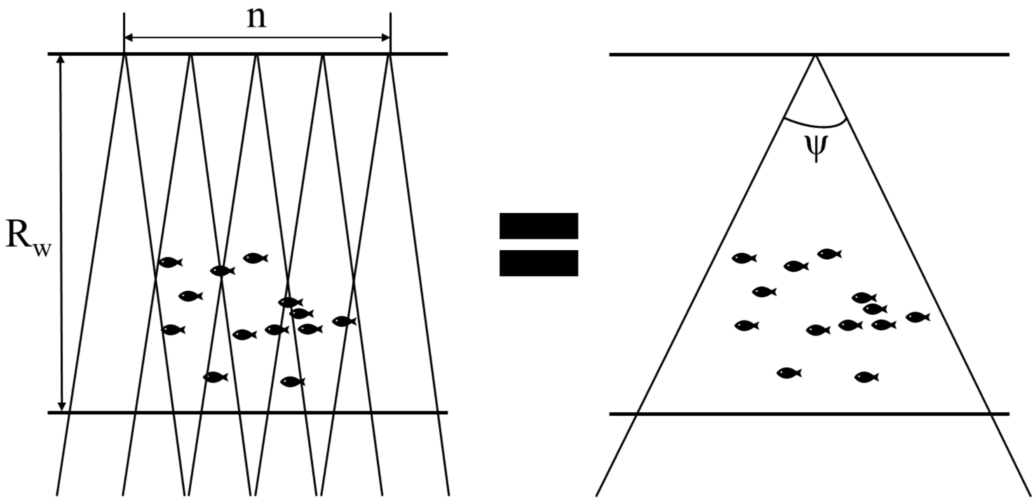

Figure 2-4. Explanation diagram of volume backscattering strength (SV) integrals (integrating over n' echoes in the direction of travel and Rw in the depth direction).

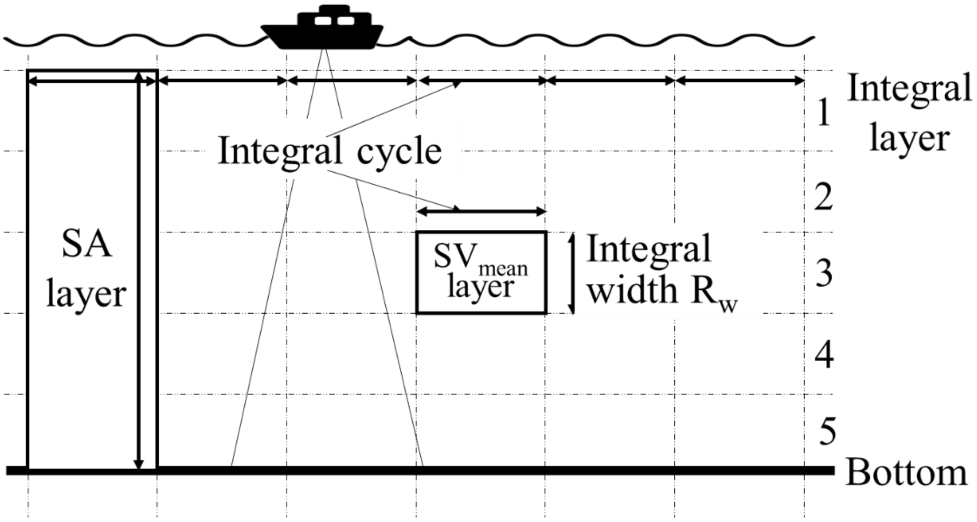

Figure 2-5. Explanation diagram of area backscattering strength (SA) and volume backscattering strength integrals (SV_{mean}).

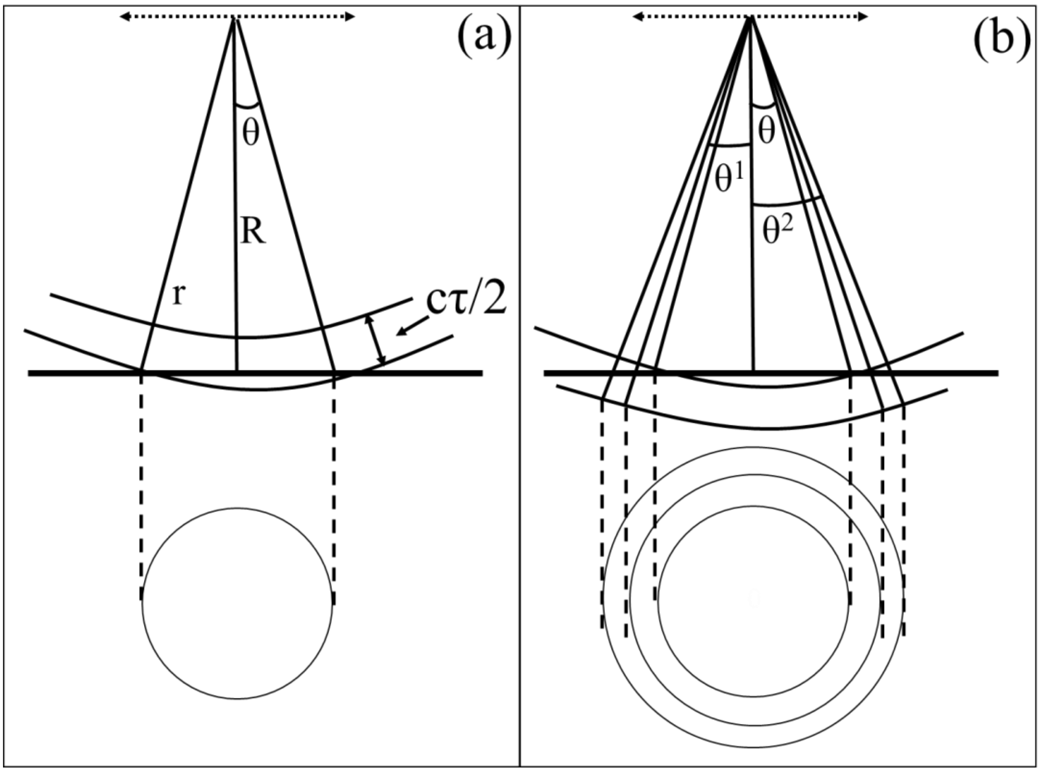

Figure 2-6. Principle of surface scattering strength (SS). The scattering surface broadens from a circle to a ring when the pulse strikes the seabed surface.

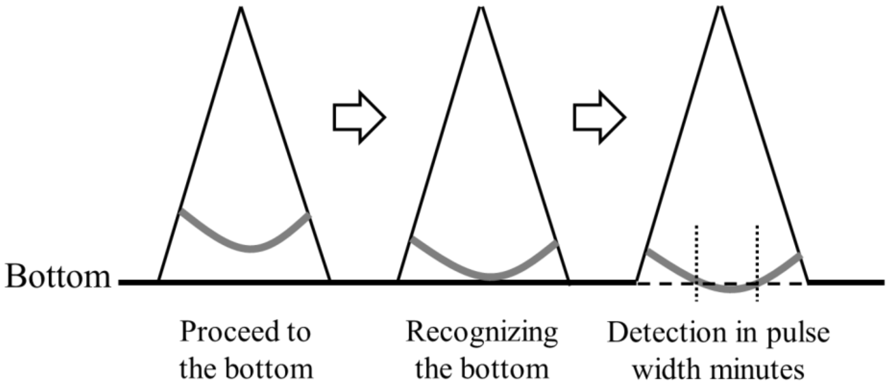

Figure 2-7. Explanatory drawing of the short pulse width case, where the pulse width is cut off before the beam end reaches the seabed.

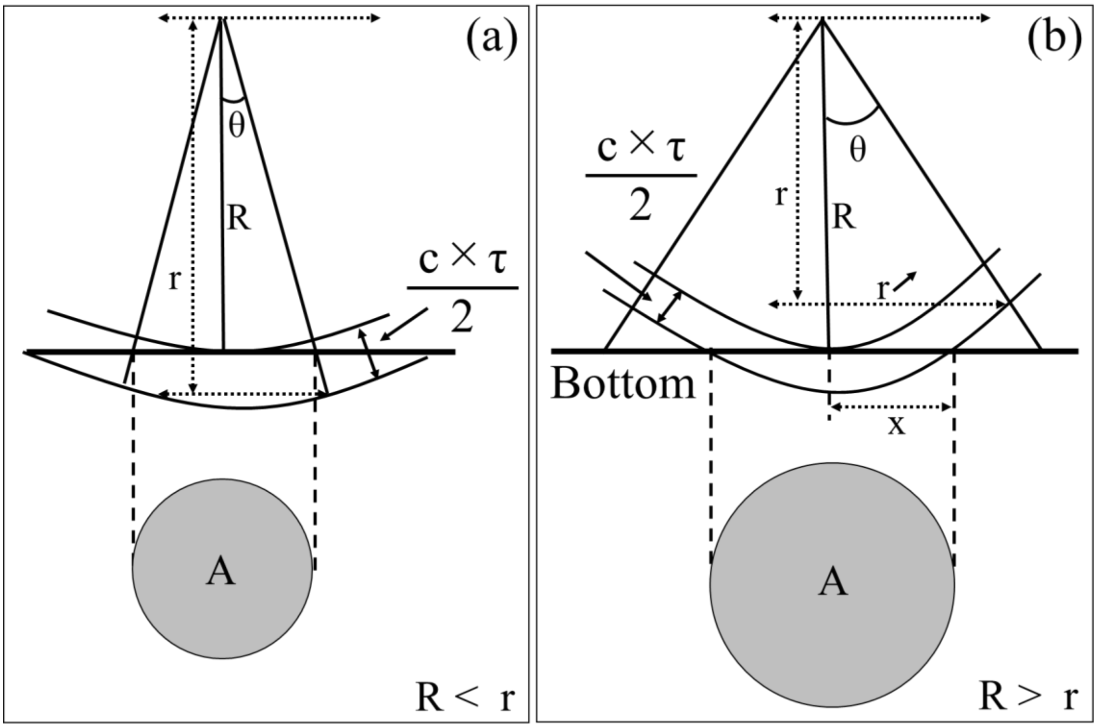

Figure 2-8. Explanatory drawing on calculating the scattering area A by pulse width or beam width. (a): calculated from the beam width φ, (b) calculated from the plus width τ.

3. Calibration for general echo sounders

3.1 Introduction

For general echo sounders, foreign objects such as shells and scales may adhere to the transducer's surface when used in the sea, and these objects may reduce the transducer's sensitivity. In addition, the transducer's sensitivity may also change due to changes in the marine environment, such as temperature and salinity. For example, if the sensitivity changes by -3 dB, the resource conversion is halved or doubled; therefore, the accuracy of the general echo sounders directly affects the resource estimation. From these, it is essential to maintain the accuracy of the general echo sounder by calibrating it periodically to use it for resource assessment.

Although the accuracy of quantification differs between general and quantitative echo sounders, the calibration mechanism is the same. The primary calibration target of an echo sounder is the part that discharges and receives sound, i.e., the transducer, which exchanges electrical and acoustic signals. In the sonar equation, the factor of KTR is the calibration target, and the product of the parameters P_o (sound pressure), M (receiver sensitivity), and GR (gain) is the objective of the overall calibration (Furusawa et al., 1995). If the measured values for calibration do not differ significantly from known theoretical values, the KTR calculated from the measured values can be used. However, if there is a significant difference between the measured and theoretical values, calibration can be carried out by adjusting the KTR to match the theoretical value.

3.2 Calibration using calibration ball

3.2.1 Selection of calibration ball and calculation of theoretical TS

There are various methods of calibrating echo sounders; a method of calibrating transducer using a calibration ball (Figure 3-1), a standard reflector with a known TS, has been used worldwide in recent years (Foote, 1983). Tungsten carbide (WC) balls (Foote and MacLennan, 1984; Miyanohana et al., 1993), which are complex and nearly rigid, or copper balls, which provide pure material, are used as the calibration ball (Foote, 1982). The size and material of the recommended calibration ball depend on the frequency used (Table 3-1). When a political calibration ball is selected, the TS of the calibration ball fluctuates very little due to environmental factors such as water temperature, and there is almost no directivity of the reflections. Therefore, it is essential to determine the calibration ball according to the frequency during calibration.

The theoretical TS of the calibration ball can be obtained by the following equation (Furusawa, 1995).

$$TS = 20 \log (a_1 F / 2) \tag{1}$$

Where a_1 is the radius of the calibration ball, and F is the absolute value of scattering amplitude at infinity. F is a factor of approximately one determined by the material, frequency, radius, and sound speed (Miyanohana et al., 1993). The parameter that varies most significantly with the F is the sound speed c, representing changes in water temperature and salinity. The salinity S of the coast in Japan varies from 30 to 35 psu, and the water temperature T from 0 to 30°C. The range of F in brackets was obtained using those parameters, and the F before the brackets was obtained from the median value (Table 3-1). The theoretical TS of the calibration ball shown in Table 3-1 was calculated using the F before the brackets. Therefore, when calibrating along the coast in Japan, a highly accurate calibration can be achieved by using an appropriate calibration ball and utilizing the theoretical TS in Table 3-1.

However, since the frequencies of general echo sounders may not be listed in Table 3-1, it is necessary to correct water temperature and salinity to obtain the theoretical TS at that frequency (Miyanohana et al., 1993). The calibration ball shows the scattering characteristics of an acoustically elastic ball, and F is considered equivalent to the absolute value f_∞ of the shape function. f_∞ is represented by ka, k_1a, k_2a, ρ, ρ_1, where a is the radius of the calibration sphere, k is the velocity of the sound in the surrounding fluid, k_1, k_2 are the compressional waves and shear waves in the calibration ball, and ρ, ρ_1 is the density in water and the calibration ball. k can be calculated by dividing the angular frequency ω by the sound speed c ($k = \omega / c$), and k_1 and k_2 can be calculated by dividing the angular frequency ω by the sound speed c_1 and c_2 in the calibration ball. Therefore, once the frequency f and the calibration ball are determined, ω, c_1, c_2, ρ, ρ_1 are known and can be defined by the frequency-radius product fa (frequency f × radius a of the calibration ball). As the result, F / f_∞ is expressed as a function of c and fa (Figure 3-2).

Many empirical formulas for determining the sound speed c have been reported, and the Mackenzie and Coppens formulas are relatively easy to use (Mackenzie, 1981, Coppens, 1981). However, the automatic sound speed calculation function installed in current quantitative echo sounders is based on the exact formula of Chen (Chen and Millero, 1977). The valid range of this equation is T = 0 - 40 °C, S = 0 - 40 psu, and P’ = 0 - 100 MPa, covering almost the ocean environment. Using the sound speed c and fa function obtained by either equation, the f_∞ is obtained from Figure 3-1 (Miyanohana et al., 1993; Furusawa et al., 1995). Using f_∞, the theoretical TS can be calculated using equation (1).

3.2.2 Calibration of KTR from measured TS

The transducer can be calibrated by using the TS of the calibration ball that comes near the central directional axis and comparing it to the theoretical TS of the known calibration ball. If the measured TS is close to the theoretical TS, using the new KTR obtained from the TS measured in each survey is essential. Since the general echo sounder is not a split beam, it cannot know the position of the calibration ball within the beam. Therefore, it is necessary to change the position of the calibration ball within the beam range, find the peak position, and calculate the KTR from the maximum TS (Furusawa et al., 1995).

KTR can be obtained using the echo voltage of the calibrated ball measured for calibration using following equation.

$$(K_{TR})^2 = E_{ts}^2 / R^{-4} \exp(-4\, \alpha\, R)\, b^4\, ts \tag{2}$$

Where ts is the maximum value of the calibration ball, and R is the depth of the calibration ball at the maximum value. Since the calibration ball is to come to the principal directivity axis, the directivity function b = 1 can be used. Equation (2) is converted to decibels, resulting in the following equation (Yang et al., 2019).

$$KTR = EL - TS + 40 \log R + 2\, \alpha\, R \tag{3}$$

Where KTR is 10 log K_{TR}, EL is 20 log E_{ts}, and TS is 10 log ts.

In addition, since the absorption coefficient α is greatly affected by water temperature and salinity, it is essential to measure it at each sea area. Particularly, high frequencies above 100 kHz are strongly affected by absorption attenuation. Therefore, the absorption attenuation α is generally calculated using the following equation (Schulkin and Marsh, 1962; Fisher and Simmons, 1977; Francois and Garrison, 1982).

$$\alpha = \frac{A' f_1 f^2}{f_1^2 + f^2} + \frac{B' f_2 f^2}{f_2^2 + f^2} + C' f^2 \tag{4}$$

The first and second terms represent the absorption losses due to boric acid and magnesium sulfate in seawater, respectively, and the third term is the absorption coefficient of fresh water. A', B,' and C' are functions of temperature and pressure, respectively, and f_1 and f_2 are frequencies related to the relaxation time of boric acid and magnesium sulfate, respectively.

From the above, for the general echo sounder, the maximum TS of the calibration ball is measured in each sea area. A new KTR can be obtained by using the distance R to the calibration ball and the absorption attenuation α at that time. Using the new KTR, the backscattering strength of the object in the sea area can be calculated, which is considered to be connected to the accuracy of the resource estimation.

3.3 Calibration using seabed backscattering strength

3.3.1 Overview of calibration using seabed

The calibration using a calibration ball is comprehensively recommended; however, this method is not accessible due to sea conditions and weather. It requires working in calm waters with the calibration ball positioned on the sound axis. Moreover, since this method calibrates the data on the sound axis, it cannot directly calibrate the directional characteristics, which is a necessary parameter when measuring the fish population. Therefore, in this study, we considered developing a new method to comprehensively calibrate the directional characteristics, including the equivalent beamwidth, the transducer system, and the processing system, using the backscattering strength from the seabed.

In this method, the seabed backscattering strength measured by a calibrated general echo sounder is used instead of the theoretical value of the calibration ball (Figure 3-3). The surface backscattering strength (SS) or volume backscattering strength (SV) of the seabed over a particular area is measured with a calibrated general echo sounder and used as a standard value for the seabed in that area. At the validation opportunity, the SS or SV in that area is measured similarly. If it is almost equal to the standard value, the system of the general echo sounder can be calibrated relatively free of anomalies. Therefore, by measuring the seabed SS or SV while underway, the overall calibration of the transducer, including the equivalent beam width, can be easily performed. In addition, if multiple ships are in the same sea area, inter-ship calibration is also possible by obtaining standard values in advance for locations frequently used by multiple vessels.

3.3.2 Characteristics of seabed reflection

Sound waves are generally transmitted and reflected at the boundary between the two media when the media changes during propagation (Anderson, 2007). At the water surface, the ratio of the density of water to that of air is so excellent that the energy of sound waves hardly passes through the surface (Patterson, 1967). In contrast, the density of the seabed is about twice that of water (Aoyama et al., 1997), which causes sound waves to be scattered on the seabed surface, and at the same time, sound waves are transmitted to and reflected under the seabed (Figure 3-4).

One crucial factor determining the seabed's backscattering pattern and strength is the sediment's quality or grain size. In addition, the seabed's scattering pattern depends on the seabed surface's roughness, with a rough seabed scattering widely in many directions while a relatively smooth seabed in a more uniform reflection direction (Figure 3-5). Finally, the backscattering strength of the seabed is determined by the reflection coefficient R_p of the sound pressure amplitude, expressed by the following equation.

$$R_p = \frac{z_2\cos\theta_i - z_1\cos\theta_t}{z_2\cos\theta_i + z_1\cos\theta_t} \qquad (5)$$

Where z_1 and z_2 are the intrinsic acoustic impedances of the incident and transmission media, respectively. t and i are the transmission and incident angles, respectively. Since the intrinsic acoustic impedance varies with the medium (Niida et al., 2005), in the calibration using the seabed, it is necessary to categorize the seabed sediment and investigate the difference in seabed backscattering strength due to different seabed sediment. The Wentworth classification table is often used to categorize seabed sediment, roughly classified into gravel, sand, silt, and clay (Wentworth, 1922).

According to Lambert's law, the seabed's surface backscattering coefficient ss ($1 / m^2$) can be expressed by the following equation.

$$ss = \mu \sin^2 \gamma \quad (6)$$

Where μ is the Lambert coefficient, which shows that the surface backscattering strength of the seabed depends on the incident at a different angle (grazing angle γ). Wong and Chesterman (1968) found similar results, with different surface backscattering strengths for the same seabed sediment at different grazing angles). The transducer of the echo sounder is usually mounted on the bottom of a ship, and sound waves are usually emitted directly below the hull. However, in many cases where sound waves enter the seabed from seawater due to hull motion, the grazing-angles change concerning the boundary plane. Such fluctuations occur as long as the seabed is the target, and even in areas where the seabed is considered to have the same sediment, slight changes in the inclination of the hull are expected to change the seabed backscattering strength.

Therefore, obtaining more stable data to average similar seabed echoes over a particular range is necessary. In this case, it is necessary to consider how much range (hereafter referred to as grid) should be averaged.

The ping rate, water depth, and vessel speed influenced the extraction grid. Therefore, many studies were conducted; Siwabessy et al. (2004) and Hamilton (2001) stated that a 10-ping extraction grid was good, while Anderson et al. (2007) stated that a 15-ping extraction grid for 38 kHz single beam echo sounders minimized measurement variability. Furthermore, Ellingsen et al. (2002) used a 5-ping extraction grid for a 50 kHz echo sounder; however, they found that the minimum effective range of the extraction grid was three pings. Therefore, since the best extraction grid differs among echo sounders and surveys, it is essential to investigate the change in seabed backscattering strength due to the extraction grid.

In conclusion, the received echo voltage varies due to seabed sediment, vessel motion, and other factors. Therefore, it is necessary to examine the echo characteristics of each seabed sediment and consider the appropriate standard value when creating a standard map of the seabed backscattering strength.

3.3.3 Primary and secondary reflections of seabed

There are two parameters that acoustically describe the seabed backscattering strength: primary and secondary reflections of the seabed (Burns et al., 1989; Hamilton, 2001). The primary reflection is the direct reflection from the seabed, while the secondary reflection is the reflection from the seabed → water surface → seabed. Therefore, when the water depth is shallow, sound waves discharged from the transducer are immediately received as a primary reflection, and the signal level entering the receiver circuit may reach an unmeasurable level (saturation of backscattering strength) (Murase et al., 2014). Since the lower the frequency, the lower the distance resolution and the weaker the energy decay (Yokoyama et al., 2005), the lower the frequency tends to saturate more easily. Additionally, if the slope of the seabed is not smaller than 1/2 of the beam width, the secondary reflection of the seabed cannot be accurately measured (Voulgaris and Collins, 1990; Anderson, 2007). In particular, it is difficult to obtain secondary seabed reflections in rocky areas where the slope changes abruptly on both sides because the echo amplitude is reduced.

For these reasons, it is desirable to select as flat an area as possible for the creation of the standard map. In addition, if the measured water depth is shallow, it is necessary to consider whether to use primary or secondary reflections from the seabed.

3.4 Figures

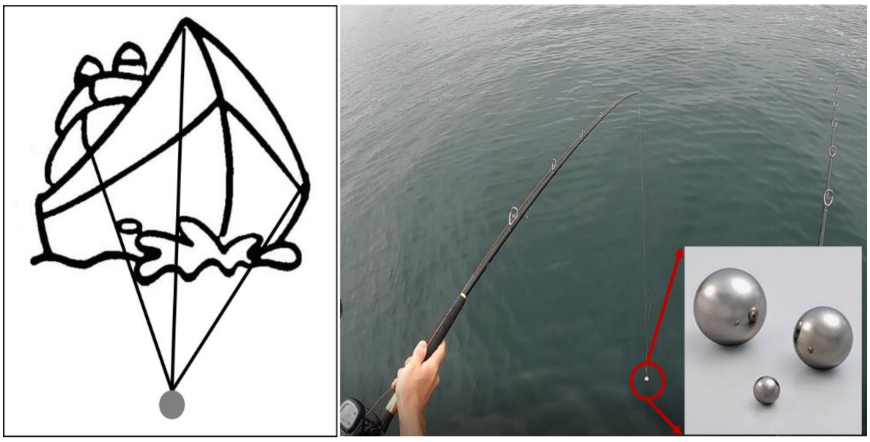

Figure 3-1. Diagram of a calibration survey using a calibration ball. The calibration ball shown in the figure is tungsten carbide (WC) ball.

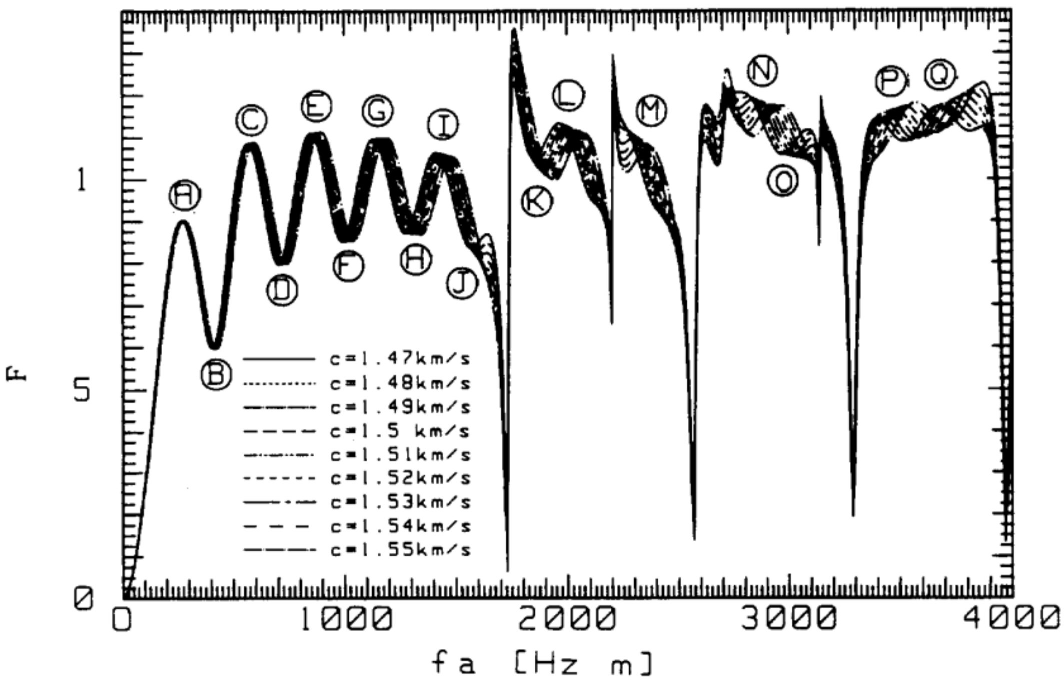

Figure 3-2. Relationship between frequency-radius product fa and the absolute value of scattering amplitude at infinity F obtained at each sound speed (Miyanohana et al., 1993; Furusawa et al., 1995).

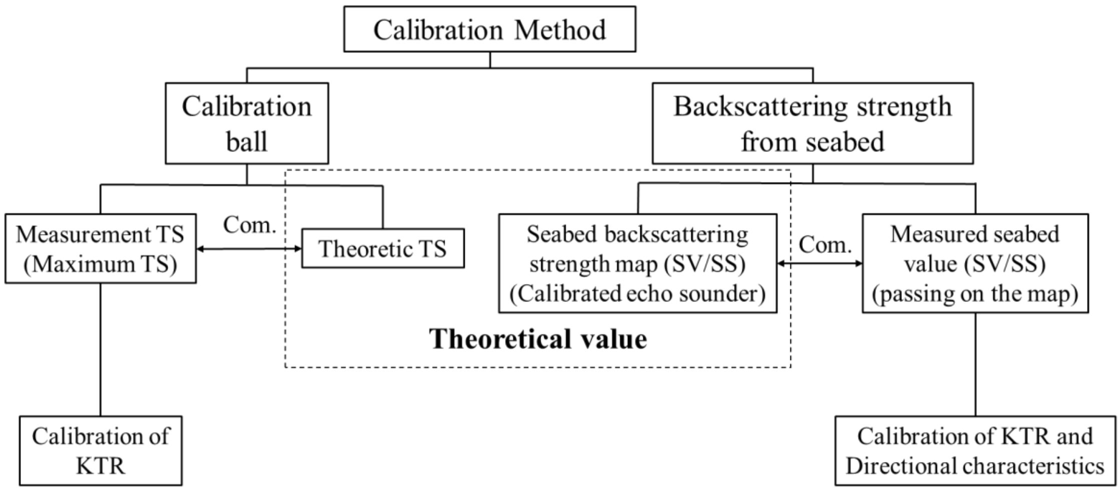

Figure 3-3. Principle of the two calibration methods, using calibration ball and seabed backscattering strength.

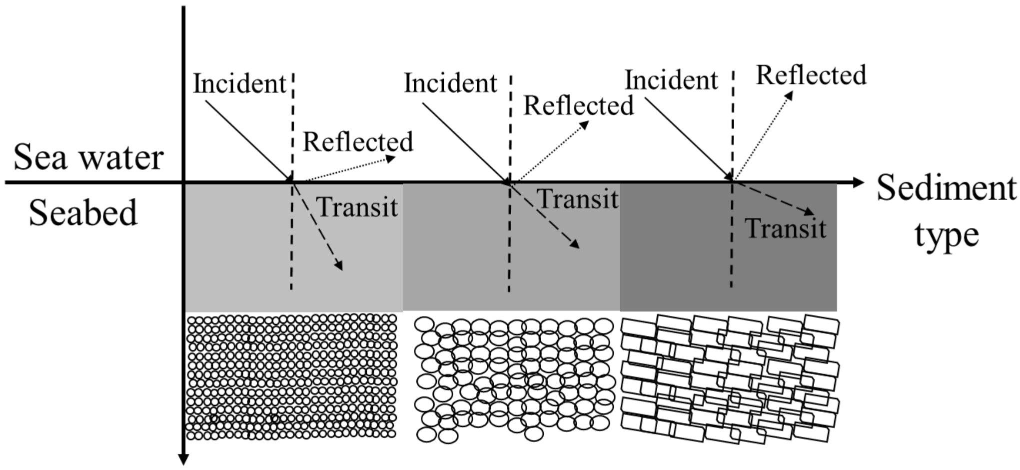

Figure 3-4. The conceptual diagram of transmission and reflection characteristics for different sediment type.

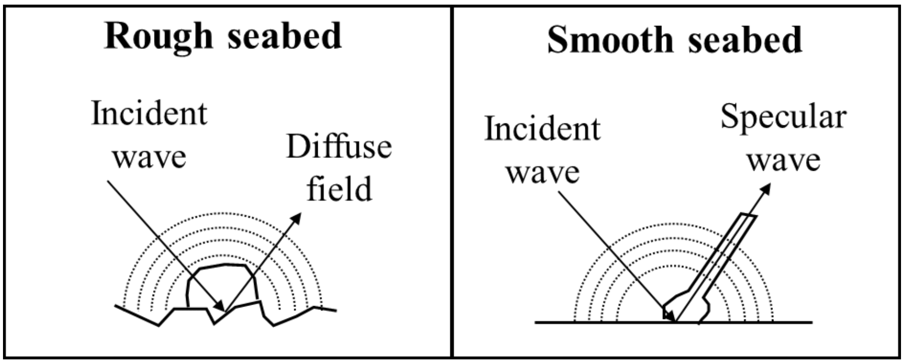

Figure 3-5. Differences in scattering patterns due to the roughness of the seabed (two main types: rough and smooth).

3.5 Tables

Table 3-1. Recommended calibration ball materials and diameters for each frequency and their theoretical TS.

Frequency (kHz)	Material	Diameter (mm)	TS (dB)	F
25	WC	45.0	-38.4 (-38.6 ~ -38.3)	1.065 (1.045~1.085)
38	WC	38.1	-42.3 (-42.4 ~ -42.2)	0.804 (0.759~0.813)
38	Copper	60.0	-33.6 (-33.8 ~ -33.5)	1.388 (1.368~1.048)
50	WC	52.7	-38.6 (-38.8 ~ -38.4)	0.889 (0.867~0.910)
70	WC	41.7	-39.3 (-39.4 ~ -39.1)	1.043 (1.025~1.060)
88	WC	52.7	-37.0 (-37.2 ~ -36.8)	1.075 (1.049~1.101)
100	WC	38.1	-39.9 (-40.3 ~ -39.7)	1.057 (1.010~1.086)
120	WC	38.1	-39.9 (-40.2 ~ -39.5)	1.068 (1.022~1.114)
200	WC	38.1	-39.1 (-39.5 ~ -38.8)	1.161 (1.113~1.209)

4. Determination of calibration using seabed backscattering strength

4.1 Introduction

The calibration survey was conducted using the medium-size purse seine vessel Kakutomaru in the coastal areas of Shimaura Island, Miyazaki, on July 4-5, 2020 (Figure 4-1). The survey area was chosen to be near a fishing port with a maximum depth of about 30 meters. The reason for selecting this area was that, in consideration of the future periodic calibration of multiple general echo sounders, it would be easier to calibrate the standard map at a higher frequency if it were located where many fishing boats often pass by. In addition, in this study, it was decided to use a quantitative echo sounder at the same time to verify the measurement results of the general echo sounder. The two types of echo sounders used were a general echo sounder (FCV-1500L, 15 kHz/200 kHz) manufactured by Furuno, which is equipped on the Kakutomaru, and a quantitative echo sounder (KSE300, 38 kHz/120 kHz) manufactured by Sonic (Table 4-1). The general echo sounder was mounted on the bottom of the vessel, and the quantitative echo sounder was fixed to the port side of the Kakutomaru (Figure 4-2). The echo sounder transducers were set up so that the transducers pointed directly down, with the transducers approximately 1 m below the water's surface.

In the research procedure (Figure 4-3), the general and quantitative echo sounders were calibrated with a calibration ball. The two types of echo sounders were run in a specific sea area where the seabed backscattering strength map was generated, and the backscattering strength of the fish school and the seabed were measured at the same time. In addition to the acoustic data collection, the seabed sediment of the 13 sites was examined using a camera and a mud sampler at the locations indicated on the seabed backscattering strength map.

In the analysis produce (Figure 4-3), to verify the accuracy of the calibrated general echo sounder, the difference between measured TS and theoretical TS was compared at each frequency. In addition, to use the general echo sounder for resource estimation in the future, the accuracy of the calibrated general echo sounder was secondarily verified by comparing the backscattering strength of the same fish school measured by the calibrated general echo sounder and the quantitative echo sounder. Next, the relationship between seabed backscattering strength and sediment obtained from both echo sounders was examined to determine the standard value to be used when creating a seabed backscattering strength map using the data from the calibrated general echo sounder. Finally, we calibrated the non-calibrated general echo sounder with the seabed backscattering strength map. To verify the accuracy of the calibration using the seabed backscattering strength map, the backscattering strength of the same fish group was compared general echo sounder calibrated using a calibration ball and seabed backscattering strength map. Here, two types of data were obtained from the Kakutomaru: data reflecting the calibration value of the calibration ball and raw data without calibration value. The data with calibration values were stored on a personal computer during the survey, while the raw data were downloaded from a server later. The raw data of the Kakutomaru, which did not reflect the calibrated values, was used to calibrate using the seabed backscattering strength map.

4.2 Calibration survey

4.2.1 Calibration of echo sounders with a calibration ball

Calibration area selection and calibration ball preparation Since it was necessary to place the calibration ball directly under the transducer, the survey was conducted in an inner bay where waves, wind, and currents were few, and the seabed was relatively flat. The mean wind speed on the day of the survey was 1.6 m/s on the 4th and 1.8 m/s on the 5th, and the vessel was anchored from the bow and stern to prevent the vessel from being swept away. In addition, if the depth of the calibration ball was shallow enough to make it challenging to guide the ball to the central directional axis, we chose a location with a water depth of at least 30 m. Furthermore, we chose a location with as few organisms and as little vessel traffic as possible to avoid being affected by reactions other than those of the calibration ball during the calibration process.

Since the four frequencies used in this study were 15 kHz, 38 kHz, 120 kHz, and 200 kHz, a calibration ball with a diameter of 38.1 mm WC ball was used for calibration, referring to Table (3-1) in Chapter 3. The calibration ball was wrapped in a coarse net to minimize the effect on the backscattering strength of the calibration ball. To prevent air bubbles from forming on the net, the calibration ball was soaked in a detergent solution before use. During calibration, the calibration ball was hung from three points on the vessel's front, starboard, and port sides with fishing rods so that the calibration ball was directly under the transducer. The calibration ball was positioned at a depth of about 10-15 m where the echoes from the calibration ball could be separated from the seabed, and the beam was sufficiently open at the location of the calibration ball. In addition, the water temperature and salinity used in the calibration were measured in advance. The water temperature T in this study was 21.4 °C, and the salinity S was 30.4 psu.

Calibration of two echo sounders The non-split-beam general echo sounder could not know the position of the calibration ball within the beam. Therefore, after suspending a prepared calibration ball, the position of the calibration ball was varied within the beam range to find the position of the beak. The beam width at low frequency (15 kHz) with a wide beam is 32°, and the beam diameter is approximately 6 m at a water depth of 10 m. The beam width at a high frequency (200 kHz) with a narrow beam is 6°, and the beam diameter is approximately 1 m at a water depth of 10 m. The maximum TS of the calibration ball was checked using a dedicated tool manufactured by Furuno. The echoes of the calibration ball were measured for approximately 5 minutes (Figure 4-4).

Unlike general echo sounders, the quantitative echo sounder is equipped with a calibration mode, a feature unique to quantitative echo sounders. By using the calibration mode, the KTRa is automatically calculated from the TS echoes of the measured calibration ball. The procedure is to measure TS echoes near the central directional axis using the KTRb resulting from the previous calibration. The measured TS echoes are automatically excluded from the measured TS echoes, including those far off the central axis and those that fluctuate due to interference from fish and other echoes. The mean result calculates the measured TS value of the calibration ball, TSm. If the theoretical value of the calibration ball is TSt, KTRa is calculated using the following equation and is reflected as the new KTR.

$$KTRa = KTRb + (TSm - TSt) \quad (1)$$

4.2.2 Measurement of fish school and seabed backscattering strength

The survey area used for the seabed backscattering strength map was chosen to be near the entrance and exit of the island Shimaura, where many vessels frequently pass by (Figure 4-1) so that multiple vessels can calibrate regularly and at the same time. Within this area, the seabed was flat and with no significant sediment changes. Next, the survey lines were established, with each measurement line approximately 1 km in length. The depth of the survey area was approximately 15 m at the shallowest point and 30 m at the deepest point. The survey lines were set to be perpendicular or horizontal to the bare coastline, but there were places where the measurement lines had to be changed to avoid obstructions during the survey.

When measuring the acoustic data of the fish school and the seabed, the vessel speed was kept at 3~5 knots to prevent echo from air bubbles (Simmonds et al., 2006). The positional information was synchronized with the acoustic information and stored in the computer. To compare the backscattering strength of the same fish school and the seabed at the same location, the recording conditions of both echo sounders were standardized with a pulse width of 0.6 ms and a range of 40 m. No sampling was conducted to confirm the fish species in the measured fish school. However, it was assumed to be a school of Japanese anchovy *Engraulis japonicus* with a mean length (L) of 11 cm and a mean weight (W) of 11.4 g, based on information from the purse seine fishery at that time of year.

4.2.3 Collection of seabed sediment

The mud sampling survey was conducted simultaneously with the acoustic survey using a different vessel from that used for the acoustic survey. The sampling points were located on the acoustic measurement line as much as possible, and 13 sites were sampled (Figure 4-5, Table 4-2). The mud sampler was an Ekman Barge-type grab sampler manufactured by RIAGO, the most widely used mud sampler (Figure 4-6). This grab sampler is designed to collect seabed sediments by landing on the seabed with the grab open and closing it with a messenger (Hinokio et al., 2015). The grab sampler is a small, portable, and convenient device that can sample a relatively large area of the seabed (about 10 cm) without disturbing the surface layer of the seabed. However, the number of samples collected using grab sampler may be small when the seabed sediment is hard gravel. Therefore, in this study, when the amount of the collected sample was not large enough, the grab-grabbing device was pulled up a little after landing on the seabed and then dropped suddenly to bite into the seabed for recollection.

4.3 Data analysis

4.3.1 Measured TS and theoretical TS of the calibration ball

In the case of the general echo sounder, the maximum TS of the calibration ball was used and compared to the theoretical TS of the calibration sphere at each frequency in Table (3-1) in Chapter 3 to verify the accuracy of the general echo sounder. In the case of the quantitative echo sounder, the mean TS from multiple calibration ball echoes was used instead of the maximum TS.

In this study, the low frequency of the general echo sounder used is 15 kHz, and the theoretical TS is not given in Table (3-1) in Chapter 3. Therefore, it is necessary to obtain the theoretical TS of 15 kHz. The 15 kHz general echo sounder with a calibration ball depth of 11.3 m, a water temperature of 21.4°C, a salinity of 30.4 psu, and a 38.1 mm WC sphere gives a sound speed c of 1520.2 m /s; the fa function is 285 Hz m. Therefore, the f_{∞} is 0.9 using these parameters based on Figure (3-2) in Chapter 3. With this value, the theoretical TS of the WC ball at a frequency of 15 kHz and 38.1 mm was calculated using Equation (1) in Chapter 3 to be -41.3 dB. This result was validated using NOAA's Standard Sphere Target Strength Calculator (NOAA Southwest Fisheries Science Center) (Foote et al.,1981; MacLennan and Dunn, 1984). Therefore, the theoretical TS of the WC calibration ball at 15 kHz obtained from the NOAA equation was -41.3 dB, which is the same as a result obtained by Equation (1) in Chapter 3 (Figure 4-7).

4.3.2 Extraction of fish school and estimation of biomass

The acoustic data were analyzed using Echoview ver. 12.1 (Sonardata Tasmania Pty Ltd.). Only fish schools were analyzed (Figure 4-8), and area backscattering strength (SA: dB) was used as a measure of fish school density (MacLennan et al., 2002). Parameters for fish school extraction should be specified based on the length or density of the target species (Coetzee, 2000). Since Japanese anchovy was the species caught during the calibration survey period, 3 x 3 m was set as the minimum reaction size height and width for a candidate fish school, considering the school characteristics of sardines (Figure 4-9). In addition, we set the vertical and horizontal distances of 5 x 5 m as the standard for the maximum distance between adjacent reactions to be considered as the same fish school reaction. To eliminate the effects of noise from microorganisms such as plankton and suspended sediments in the sea, the analysis threshold was set at -60 dB (Kang, 2006), and areas of weak reflections below this threshold were treated as not fish schools of interest.

The number of fish per unit area can be calculated from the SA of each fish school obtained at each frequency using the following equation (Abe, 2020).

$$n = SA / TS \quad (1)$$

The TS of Japanese anchovy at 38 kHz is -43.0 dB, at 120 kHz it is -42.9 dB, and at 200 kHz it is -43.5 dB (Amakasu et al., 2010). Since there was no TS for the Japanese anchovy at 15 kHz, the

TS was obtained by a regression equation between general TS and body length (McCartney and Stubbs, 1971).

$$TS = 24.5 * \log L - 4.5 * \log \lambda - 26.4 \quad (2)$$

$$\lambda = c / f \quad (3)$$

Where L (m) is the total length of the fish, λ (m) is the wavelength, c (m / sec) is the speed of sound, and f (Hz) is the frequency. Therefore, 0.1 m λ and -45.0 dB TS were used when calculating the number of Japanese anchovies at 15 kHz. The calculated SA is then multiplied by the area of each fish school to obtain the number of fish in each fish school. In addition, since the weight of the Japanese anchovy identified during the calibration period is approximately 11.4 g, the weight of each fish school can also be calculated.

4.3.3 Calculation of backscattering strength on the seabed

General echo sounder Determining the seabed line is essential to distinguish between echoes in the water column and seabed echoes. The seabed line and the echoes below it is used to calculate the seabed backscattering strength. The maximum echo depth can be considered as the seabed if there are no scatters stronger than the seabed in the ocean (Tanoue et al., 2013). Therefore, since the general echo sounder does not have an automatic seabed detection function, the maximum echo in each ping was used to make the seabed line. The surface backscattering strength (SS) or volume backscattering strength (SV) calculated using the maximum echo was used as an indicator of seabed backscattering strength (see Chapter 2). When determining the seabed secondary reflections, ±1 m from a depth twice the seabed echo was used as the candidate range of secondary reflections. The maximum echo from the candidate range was considered the seabed secondary reflection. However, since the recording rage was 40 m, if the candidate range exceeded 40 m, it was treated as an error and assumed that the seafloor secondary reflection was not taken.

The mean SS (from now on referred to as SS_{mean}) and mean SV (from now on referred to as SV_{mean}) can be obtained by performing echo integration processing on the seabed echoes. The mean value is obtained by averaging over the number of transmissions (from now on referred to as pings) as follows:

$$SS_{mean} = 1/m \ \Sigma^{m} SS \tag{4}$$

$$SV_{mean} = 1/m \ \Sigma^{m} SV \tag{5}$$

Where m is the number of pings to mean, SS_{mean} and SV_{mean} are the integrated means over m pings.

Quantitative echo sounder In the case of the quantitative echo sounder, the seabed echoes were average using the automatic seabed recognition function and the automatic echo integration function since both functions are available. In addition, the integrated echo output is used instead of the echo level, and the TVG output differs from that of the general echo sounder in that both SS and SV use 20 log R (Aoyama, 1999). Therefore, the following equations calculate the SS and

SV voltages in general echo sounder.

$$E_{ss}^2 = (P_o\ M\ G_R)^2\ R^{-2}\ \exp(-4\ \alpha\ R)\ (\Gamma\ c\ \tau / 2)\ ss \quad (6)$$

$$E_{sv}^2 = (P_o\ M\ G_R)^2\ R^{-2}\ \exp(-4\ \alpha\ R)\ (\Psi\ c\ \tau / 2)\ sv \quad (7)$$

Where Γ is the equivalent beam width for surface scattering and Ψ is the equivalent beam width for volume scattering.

When they are integrated over the number of pings (m times) and the distance in the depth direction (R_w layer), the SS_{mean} and SV_{mean} can be obtained with the following equations.

$$SS_{mean} = 1 / m \sum E_{ss}^2 \quad (8)$$

$$SV_{mean} = \int^{Rw} (1 / m \sum E_{sv}^2)\ dR \quad (9)$$

Since quantitative echo sounders use a sharp beam, the equivalent beam width Ψ for volume scattering and the equivalent beam width Γ for surface scattering can be replaced by the following equation (Aoyama et al., 1997).

$$\Gamma = \int \Psi\ dR \quad (10)$$

Therefore, in quantitative echo sounder, SS_{mean} is the product of SV_{mean} and the thickness of the integrating R_w layer and can be obtained by the following equation.

$$SS_{mean} = R_w * SV_{mean} \quad (11)$$

According to a previous study, SS proved to have little effect on the thickness of the integrating layer (Aoyama, 1999). Therefore, in this study, the integral layer was unified to 1 m for all analyses of primary and secondary reflections on the seabed using data from a quantitative echo sounder.

4.3.4 Simple analysis of seabed sediments

The collected sediments were classified using a simple grain size analysis method to determine the sediments' water content ratio and grain size composition. The water content ratio is the weight loss after air-drying the sample and is essential as preliminary information on grain composition (Narita, 2016). For example, it is possible to obtain the water content ratio w (%) using the following equation.

$$w = (ma - mb) / (ma - mc) * 100 \tag{12}$$

Where ma (g) is the total mass of the sample and container before drying, mb (g) is the total mass of the sample and container after drying, and mc (g) is the mass of the container. The sample was approximately 20 to 30 g, and an electronic scale measuring down to 0.01 g was used. First, as a preliminary preparation, the weights mc of the heat-resistant containers were weighed and numbered. Next, 20 to 30 g of each wet sample was placed on each container (Figure 4-10) and spread out with a spatula to avoid bias, and the total mass of the sample and tray before drying, ma, was weighed. The samples were then placed in a thermostatic dryer with their containers and dried at 110 (± 5) °C until a constant mass (fluctuation of less than 1% of the total mass) was achieved (about 3 hours). Since the time required to reach a constant mass varied depending on the sample, drying, and weighing were repeated. Finally, the samples were allowed to stand at room temperature, and the total mass mb of the dried samples and containers was weighed.

According to Wentworth (1922), the grain size of seabed sediments is roughly classified into gravel, sand, silt, and clay, and the grain size boundary of gravel is 2 mm. In Japan, based on the Japanese Industrial Standard, the grain size boundary of gravel is 2 mm, that of sand is 1 / 16 mm, and that of silt is 1 / 256 mm. In this study, silt and clay are collectively referred to as mud, and the seabed sediments are divided into three categories: gravel, sand, and mud. First, the mass of the beaker used to dissolve the sample, md, and the mass of the heat-resistant tray, me, were weighed and numbered. Next, the sample whose moisture content had already been measured was placed in a beaker while still wet (20 to 30 g), and the total mass and the beaker, mf, were weighed. The beggar was then filled with tap water, and the sample was dissolved using a glass rod to avoid lumps. Next, two types of sieves (mesh: 250; aperture size: 2 mm and 62.5 μm) were placed on top of each other, and the dissolved sample was poured onto the sieves and rinsed thoroughly with a wash bottle to avoid any residue on the beggar. The sample remaining on each sieve was then transferred to its tray (Figure 4-11), and the sieves were rinsed with excessive water so that the water falling from the sieves was properly removed (until the water falling from the sieves was clear). Finally, the samples were placed in a thermostatic dryer with their trays and dried at 110 (± 5) °C until a constant mass (fluctuation of less than 1% of the total mass) was achieved (about

2 hours). After drying, the samples were left at room temperature, and the total mass of the gravel and tray, mh, and the total mass of the sand and tray, mi, were weighed. The total mass mg of each sample after drying was determined using the following equation using the moisture content.

$$mg = (mf - md) * w \quad (13)$$

The percentage of each grain size was then calculated using the following equation.

$$Gravel = (mh - me) / mh * 100 \quad (14)$$

$$Sand = (mi - me) / mi * 100 \quad (15)$$

$$Mud = 100 - Gravel - Sand \quad (16)$$

Finally, the sites were grouped using the percentage of each grain size at each sampling site (Yokoyama and Ishii, 2009). Again, KyPlot statistical software was used for grouping. In this study, the following items were used to analyze seabed sediments. (1) Tray for drying samples, (2) Beaker for dissolving samples, (3) Glass rod and spatula for mixing samples, (4) Washing bottle for washing samples, (5) Electronic balance (top plate type), (6) Sieve, (7) Dryer.

4.3.5 Creation of seabed scattering strength map

In this study, there were three main criteria for determining the standard value of seabed scattering strength: First, the parameters used for the seabed scattering strength map were determined. Since seabed reflection can be primary or secondary, each possibility was considered. Second, because differences in seabed scattering strength can be expected even for similar seabed sediment, it was considered necessary to mean the seabed scattering strength over a particular range to obtain more stable data. The ping rate (transmission period) differs depending on the echo sounder used; therefore, when comparing data from different echo sounder types, the parameter used to determine the criterion for the grid is the distance traveled rather than the number of pings. Third, since the seabed backscattering strength varies significantly with different seabed sediment, creating a seabed backscattering strength map is desirable for each seabed sediment.

A seabed backscattering strength map was created from the seabed backscattering strength extracted under the above conditions using the kriging function (ArcGIS 10.1, ESRI), a spatial statistical method. Kriging is a method of spatially predicting values at arbitrary points by structuring spatial correlations of data using the similarity of data from closely spaced stations (Inoue et al., 2009). The predicted value with the lowest predicted variance can be determined for any point in the seabed backscattering strength map created from the measurements. Using these measured and predicted values, non-calibrated general echo sounders passing on the seabed backscattering strength map can be calibrated.

4.4 Results

4.4.1 TS of the calibration ball and estimated KTR

General echo sounder At 15 kHz, the maximum value of the calibration ball was -41.3 dB, measured at a depth of 11.3 m. The theoretical TS of the 15 kHz is -41.3 dB, with no difference between the measured and theoretical values. At 200 kHz, the maximum value of the calibration ball was -38.8 dB, measured at a depth of 11.5 m (Table 4-3). The theoretical TS of the 200 kHz is -39.1 dB, and the difference between the measured and theoretical values was as small as 0.3 dB. Then, the maximum TS of the calibrated ball, the distance R to the maximum TS, and the absorption attenuation α were used in equation (5) $KTR = EL - TS + 40 \log R + 2 \alpha R$ in Chapter 3 to obtain the new KTR at each frequency. The absorption attenuation α was calculated using equation (4) in Chapter 3, resulting in a value of 1.4 dB / km at 15 kHz and 7.5 dB / km at 200 kHz. Therefore, using the above parameters, the new KTR for each frequency was calculated to be 16.7 dB at 15 kHz and 30.5 dB at 200 kHz. These new KTRs were reflected in general echo sounder and used to calculate the backscattering strength.

Quantitative echo sounder The mean TS of the calibrated ball measured in this study was -42.4 dB at 38 kHz. Since the theoretical TS of the 38 kHz is -42.3 dB, there was little difference between the measured and theoretical values (Table 4-3). At 120 kHz, the mean TS of the measured calibration ball was -39.8 dB. Again, the theoretical TS of the 120 kHz is -39.9 dB, indicating that there was little difference between the measured and theoretical values at 120 kHz. Using these measurements, the new KTRs were automatically calculated and reflected.

4.4.2 SA and estimated biomass of the fish school

Forty-five fish groups were extracted as Japanese anchovy groups in the study area. The SA of each fish group differed depending on the frequency (Table 4-4). For example, the SA obtained from the general echo sounder was -27.8 ~ -18.2 dB at 15 kHz and -23.0 ~ -13.2 dB at 200 kHz. For the quantitative echo sounder, the SA was -34.6 ~ -21.5 dB at 38 kHz and -39.5 ~ -23.5 dB at 120 kHz. The number and weight obtained from each SA also differed between frequencies for the same Japanese anchovy group.

On the other hand, the SA_{mean} obtained from all extracted fish groups was -22.3 dB at 15 kHz, -17.6 dB at 200 kHz, -27.0 dB at 38 kHz, and -29.9 dB at 120 kHz (Table 4-5). The number and weight of all fish were calculated using these SA_{mean} values to be 300,319 fish and 3,424 kg at 15 kHz, 461,581 fish and 5,262 kg at 200 kHz in general echo sounder. For the quantitative echo sounder, the estimated biomass at 38 kHz was 305,522 fish and 3,483 kg; at 120 kHz, it was 102,200 fish and 1,165 kg.

4.4.3 Seabed scattering strength obtained from general echo sounder

The water depth in the study area was 3 m at the shallowest point and 40 m at the deepest point. The echo number of the primary reflection of the seabed extracted at one ping was 4608, and the

SS calculated from these echoes was -30.0 to -27.2 dB at 15 kHz, -23.8 to -22.7 dB at 200 kHz, showing only a slight change in SS at both frequencies (Figure 4-12, Table 4-6). The SV at each ping was -17.4 to -14.9 dB at 15 kHz and -3.0 to -1.9 dB at 200 kHz, showing no significant change in both frequencies and SS. Thus, in the study area, the backscattering strength of primary reflections on the seabed was saturated despite the change in water depth.

The number of echoes for secondary reflections on the seabed extracted at one ping was lower than that for primary reflections, at 1,523. Since the measurement range of the acoustic data is 40 m, and the primary reflections on the seabed exceed 20 m, i.e., the depth of the secondary reflections exceeding 40 m, are treated as error data. Using those echoes to calculate the backscattering strength of seabed secondary reflections, SS was -93.0 ~ -27.5 dB at 15 kHz and -80.7 ~ -47.5 dB at 200 kHz, SV was -82.3 ~ -16.8 dB at 15 kHz and -59.9 ~ -25.5 dB at 200 kHz (Figure 4-13, Table 4-6). The results of SS and SV show that the backscattering strength of secondary reflection on the seabed varies with the seabed sediment or depth.

In addition, the SS_{mean} and SV_{mean} calculated for each grid using the secondary reflections from the seabed varied with frequency and grid range. In SS_{mean}, the maximum value at 15 kHz did not vary among the analysis grids and was -27.5 dB. In contrast, the minimum value was approximately -90 dB for grids up to 10 m and approximately -66.4 dB for grids with a broader range (Table 4-7). Similarly, at 200 kHz, the maximum SS_{mean} was -47.5 dB for all analyzed grids, while the minimum was approximately -80 dB for grids up to 10 m and approximately -70 dB for grids above 50 m. Averaging the SS_{mean} values for each grid (Table 4-8), the mean SS_{mean} obtained from the 1 m, 5 m, and 10 m grids at 15 kHz were -51.1 ~ -47.9 dB, while the mean SS_{mean} calculated from the 50 m, 100 m, and 500 m grids were -42.8 ~ -40.9 dB. At 200 kHz, as at 15 kHz, the mean SS_{mean} averaged from the 50 m grid varied significantly, with the mean SS_{mean} obtained from grids up to 10 m being -66.8 ~ -64.5 dB and the mean SS_{mean} calculated from the 50 m grid being -60.8 ~-58.6 dB.

In SV_{mean}, the maximum value of SV_{mean} for both frequencies did not vary with the analysis grid, while the minimum value was bordered by 10 m (Table 4-7). The maximum value of SV_{mean} was -16.8 dB at 15 kHz and 25.5 dB at 200 kHz, while the minimum value of SV_{mean} was -82.3 ~ -80.2 dB from grids up to 10 m and approximately -55.5 dB of the grids from 50 m at 15 kHz. At 200 kHz, the SV_{mean} obtained from the grid up to 10 m was approximately -60 dB, and the grids from 50 m were -50.1 ~ -47.8 dB. The mean SV_{mean} obtained for each frequency was -40.3 ~ -30.2 dB at 15 kHz and -45.4 ~ -37.2 dB at 200 kHz (Table 4-8). The mean SV_{mean} also changed abruptly and significantly from the 50 m grid at both frequencies.

4.4.4 Seabed scattering strength obtained from quantitative echo sounder

Only at locations where echoes of secondary reflections could be obtained using the general echo sounder analysis was conducted using the quantitative echo sounder. The primary and secondary reflections on the seabed were extracted for each ping, and both showed changes in backscattering strength with changes in the seabed sediments. For the primary reflection, SS was -32.5 ~ -3.5 dB at 38 kHz and -32.0 ~ -2.9 dB at 120 kHz, while SV was -32.4 ~ -3.4 dB at 38 kHz and -32.0 ~ -3.0 dB at 120 kHz. For the secondary reflection, SS was -61.6 ~ -11.9 dB at 38 kHz and -73.2 ~ -23.3 dB at 120 kHz, while SV was -61.5 ~ -12.0 dB at 38 kHz and -73.2 ~ -23.2 dB at 120 kHz (Table 4-6). For the quantitative echo sounder, SS and SV results were not significantly different for both primary and secondary reflections on the seabed.

Additionally, the secondary reflections on the seabed were calculated for each grid using SS and SV, and no sudden and significant changes in the backscattering strength on the seabed were found for different grids. For example, at 38 kHz, the maximum value calculated from SS_{mean} and SV_{mean} was -26.2 ~ -11.9 dB, and the minimum was -58.4 ~ -46.4 dB (Table 4-7). At 120 kHz, the maximum value calculated from SS_{mean} and SV_{mean} was -35.2 ~ -25.1 dB, and the minimum value was -70.1 ~ -55.9 dB. Furthermore, the mean SS_{mean} and SV_{mean} calculated from these values did not vary significantly by a grid, approximately -35 dB at 38 kHz and -44 dB at 120 kHz (Table 4-8).

4.4.5 Grain size composition of sediments

Of the 13 seabed sediment sites sampled, ten sites were mapped on the seabed backscattering strength map (Figure 4-5). The seabed sediment of these ten sites was classified into four major groups (Figure 4-14). The sandy sediments were generally high, ranging from 35% to nearly 97% of the total (Table 4-9). In particular, sandy sediments dominated at five sites (496, 498, 500, 502, and 504), with a percentage of more than 90%. Sites 490, 492, and 506 were sandy, with sandy content ranging from 68 to 76% and gravelly content ranging from 22 to 27%, indicating that they were sandy mixed with gravelly material. On the other hand, sites 488 and 494 were dominated by gravelly materials, accounting for more than 60%. In addition, site 494 had the highest percentage of gravelly material, containing 95% gravelly material.

In summary, the seabed sediment collected in the middle of the survey line (496, 498, 500, 502, and 504) is sandy (hereafter referred to as S), with sandy material accounting for more than 90%. The other sampling points are at the edge of the survey line, and the percentage of gravelly material is higher than in the middle of the survey line. Sites 490, 492, and 506 were found to be sandy-gravelly (hereafter referred to as SG), site 488 was gravelly-sandy (hereafter referred to as GS), and site 494 was mostly gravelly (hereafter referred to as G).

4.4.6 Backscattering strength of seabed secondary reflections in each sediment

The SS and SV of the seabed secondary reflections at each sampling site are summarized in Table 9. At 15 kHz with the general echo sounder, the SS of S was -49.7 ~ -37.5 dB, the SS of SG was -40.3 ~ -31.7 dB, the SS of GS was -40.8 dB, and the SS of G was -38.2 dB, indicating that there were no characteristics of SS depending on the seabed sediment. The SV was -39.1 ~ -26.8

dB for S, -30.2 ~ -20.4 dB for SG, -30.7 dB for GS, and -41.1 dB for G, also showing no characteristics by seabed sediment. The same trend was observed at 200 kHz for the general Echo sounder and both frequencies for the quantitative echo sounder, and SS and SV did not vary significantly with seabed sediment.

Comparing the results of the general echo sounder and quantitative echo sounder (Table 4-9), the mean difference of SS between the two echo sounders at low frequency was 4.8 dB, and at high frequency was 13.6 dB. On the other hand, the mean difference in SV between the two echo sounders at low frequency was 5.7 dB, and at high frequency was 7.6 dB, indicating that the difference in the SV between the two echo sounders was smaller than that of the SS.

4.5 Discussion

4.5.1 Accuracy verification of calibrated general echo sounder

A comparison of the measured and theoretical values of the calibration ball showed that the difference between the measured and theoretical values was less than 0.3 dB at both frequencies for the general echo sounder and the quantitative echo sounder. Considering that slight changes in the measured values of the calibration ball due to changes in the ocean environment can be assumed and that the accuracy of calibration using the current calibration ball is about 0.5 dB at maximum (Aoyama, 1999), the results of this study are very positive. Therefore, since the measured and theoretical values of the calibration ball are in good agreement, the general echo sounder, reflecting the parameters obtained from the measurements of the calibration ball, can be used for stock assessment.

In addition, there was a large difference between the SA of the same fish group measured by the calibrated general echo sounder and the quantitative echo sounder and the biomass calculated from the SA (Table 4-4). This is thought to be due to the difference in beam width and distance attenuation at the frequencies used. The higher the frequency, the narrower the beam spread and the stronger the attenuation. Therefore, it can be assumed that there is a slight difference in the SA of the same fish school depending on the frequency, since there is a difference in the area measured and the backscattering strength depending on the frequency. However, when it came to the biomass calculated from the SA of the entire study area, the differences between frequencies were smaller (Table 4-5). The frequency often used for resource assessment is the low frequency of 38 kHz in the case of the quantitative echo sounder, because high frequencies have a wider beam spread and stronger backscattering strength from the fish school than low frequencies. From 38 kHz, the estimated biomass was 3,483 kg for the entire study area. The total biomass estimated from 15 kHz by the general echo sounder was 3,424 kg, showing little difference from that of the quantitative echo sounder. On the other hand, the biomass in the study area calculated from 200 kHz was 5,262 kg, which may be an overestimation for use in stock assessment. Therefore, when using a general echo sounder to assess abundance, it is expected that a lower frequency can be used to calculate biomass more accurately than a higher frequency.

4.5.2 relationship between sediments and seabed scattering strength

In this study, we could not identify seabed sediment using the backscattering strength of seabed echoes obtained from general echo sounders. Therefore, we could not examine seabed backscattering strength maps for each seabed sediment. Seabed reflection property can be described using the intrinsic acoustic impedance, which expresses the seabed material's acoustic hardness. Since sand particles are sufficiently smaller than the wavelength of sound in water, the reflection of sound waves on the seabed is close to specular reflection. However, the diffuse reflection will occur when discharged on a seabed with gravel particles more significantly than the wavelength of sound in water (Niida et al., 2005). Therefore, the maximum backscattering strength of seabed due to differences in acoustic impedance is considered to be greater in sandy than in gravelly sediments.

However, in addition to acoustic impedance, the convergence time of the echoes also varies with the sediment. For sand, the maximum value is higher than gravel due to the difference in acoustic impedance, but the convergence time tends to be longer for gravel (Tao and Motooka, 2005). When considering the characteristics of seabed reflections, it is necessary to simultaneously consider two factors: the maximum backscattering strength of the echo and the convergence time due to diffuse reflection. However, there is a large overlap between the distribution of the reflection signal from gravel, which has a long convergence time due to diffuse reflection, and the distribution of the reflection signal from sand, which has a high peak value and a short convergence time. Therefore, in some cases, the distribution of seabed backscattering strength overlaps, making it difficult to characterize the characteristics of seabed backscattering strength due to different seabed sediment. Therefore, this study examined the reference value for the seabed backscattering strength map without classifying the seabed sediment.

4.5.3 Determination of values to be used for standard map

Use of seabed secondary reflections The primary reflection of the seabed was calculated using SS and SV with a general echo sounder, and the backscattering strength of the seabed was saturated at both frequencies (Figure 4-12). Reflection saturation is a state in which there is no change in backscattering strength in response to physical changes such as the object's size or the depth of the water. Generally, sound waves attenuate with the distance they are carried in the ocean (Fujii and Nogi, 2018); however, if the sound waves are strong and the water depth is shallow, the sound waves may already be reflected before they attenuate. In such cases, the sound waves are reflected as strongly as when discharged, often resulting in the same acoustic reflection level despite changes in the object and depth. In the case of a quantitative echo sounder, TVG processing, a function to compensate for propagation attenuation that increases in proportion to distance, is installed to avoid data saturation even at shallow survey depths (Aoyama and Matsumoto, 2009). However, unlike the quantitative echo sounder, TVG processing is not automatically executed as a function in the general echo sounder but is manually added to the recorded data. Therefore, when a general echo sounder records data, the backscattering strength tends to be nonlinear and saturated at shallow survey depths.

Considering the above, the location of the seabed scattering strength map where several general echo sounders can be calibrated periodically should be where many fishing boats pass by daily without causing any hassle to the fishermen. Therefore, the locations tend to be near the entrances and exits of fishing ports, where the water depth tends to be shallow. In this study, considering the above situation, the reference value used for the seabed scattering strength map is not the primary reflection of the seabed but the secondary reflection.

Use of acoustic indicator SV The mean SS of the seabed secondary reflections extracted at one ping each were compared between the general and quantitative echo sounders. The difference between the two echo sounders was 13.9 dB at low frequencies and 21.7 dB at high frequencies (Table 4-6). Mean SV was also compared with the same parameters, and the results showed that at low frequencies, the difference between the two echo sounders was 3 dB, and at high frequencies, the difference was 0.3 dB. The results calculated for each ping from the two acoustic indicators show that the difference between the general and quantitative echo sounders in the backscattering strength of the seabed secondary reflection was significant for the SS and trim for the SV. In addition, the mean SS_{mean} and SV_{mean} obtained for each grid were compared for both echo sounders, and similar results were obtained (Table 4-8). At low frequencies, the difference in mean SS_{mean} was 5.6 ~ 14.3 dB, and the difference in mean SV_{mean} was 1.5 ~ 4.1 dB. At higher frequencies, the mean SS_{mean} difference was 14.8 ~ 22.1 dB, and the mean SV_{mean} difference was 0.4 ~ 6.4 dB. Regardless of the analysis grid, the difference between the general and quantitative echo sounders tends to be smaller for the mean SV_{mean} than for the mean SS_{mean}. Therefore, we considered SV to be a more appropriate acoustic indicator to be used for seabed backscattering strength maps than SS.

In this study, the TVG process used to calculate SS for the general echo sounder and the quantitative echo sounder was different, with 30 log R for the general echo sounder and 20 log R for the quantitative echo sounder. Therefore, it is natural that there would be a significant difference in SS. According to a previous study, the theoretical SS of the primary reflection from the seabed obtained from the same general echo sounder was approximately -22.6 dB at 15 kHz and approximately -19.3 dB at 40 kHz when the seabed sediment was SG. The angle of incidence was 10 ~ 70°, a difference of approximately 3 dB (Jackson, 1994). Therefore, it is considered that the difference in SS will be slight when the TVG process used is the same. Although 30 log R should be used for calculating SS by the general echo sounder, the difference in backscattering strength due to differences in TVG processing will become an unavoidable problem when comparing general echo sounder and quantitative echo sounder in the future. In this study, the validity of SV was verified when comparing seabed backscattering strength between both echo sounders. Therefore, using SV instead of the conventional SS is considered adequate when comparing the future seabed backscattering strength of the two types of echo sounders.

Calculation with 50 m grid The maximum and minimum values of SV_{mean} calculated for each grid at both frequencies for the general echo sounder showed that the grid below 10 m tended to show a significant variation. The grid above 50 m showed a minor variation (Table 4-7). Therefore, it is considered better to use a wide-range grid with less variation in SV_{mean} than a narrow-range analysis grid to avoid the influence of different seabed sediment as much as possible.

However, the length of a single survey line is 1 km, and too extensive an analysis range reduces the number of reference values used in the seabed backscattering strength map, making it difficult to obtain a highly accurate map. Therefore, a 50 m grid, which has a relatively wide analysis range, was used to create a seabed backscattering strength map in this study.

Based on the above, the reference values used for the seabed backscattering strength map in this study are extracted using the following parameters: (1) Secondary reflection on the seabed was used, (2) Acoustic indicator SV was used to calculate the backscattering strength, and (3) The analysis range is 50 m grid (Figure 4-15).

4.6 Calibration with seabed scattering strength map and accuracy verification

The SV_{mean} extracted from the seabed secondary reflection of the non-calibrated general echo sounder on a 50 m grid had a maximum value of -8.3 dB, a minimum value of -47.1 dB, and a mean value of -23.6 dB at 15 kHz and a maximum value of -59.5 dB, a minimum value of -84.3 dB, and a mean value of -73.5 dB at 200 kHz (Table 4-10). On the other hand, the mean value of the seabed backscattering strength map created using SV_{mean} on a 50 m grid was -32.1 dB at 15 kHz and -39.4 dB at 200 kHz. A comparison using both means showed a difference of 8.5 dB at 15 kHz and a very large difference of 34.1 dB at 200 kHz. Therefore, in this study, the non-calibrated general echo sounder was calibrated using the seabed backscattering strength map, and the raw data at 15 kHz had to be lowered by 8.5 dB. In comparison, at 200 kHz, the raw data had to be raised by 34.1 dB.

The accuracy of the seabed backscattering strength map was verified by comparing the extracted SA of Japanese anchovy groups from the general echo sounder calibrated with the above results and the general echo sounder calibrated with the calibration ball. The SA_{mean} of all fish schools extracted from the general echo sounder calibrated by the seabed backscattering strength map was -22.1 dB at 15 kHz and -16.9 dB at 200 kHz, while the SA_{mean} of all fish schools extracted from the general echo sounder calibrated by the calibration ball was -22.3 dB at 15 kHz and -17.6 dB at 200 kHz (Table 4-11). At both frequencies, the difference between the two echo sounders was less than 0.7 dB, which is very small. In addition, the SV of the seabed secondary reflection at the same sediment sampling point was compared between the general echo sounder calibrated with the seabed backscattering strength map and the calibration ball. The difference between the two echo sounders at all sampling points was less than 0.5 dB for both frequencies, which was in excellent agreement (Table 4-12).

From above, the results obtained from the general echo sounder calibrated by the seabed backscattering strength map and the one calibrated by the calibration ball did not differ significantly. Therefore, the general echo sounder calibrated by seabed backscattering strength can be used for stock assessment. This study's calibration method using the seabed backscattering strength map was proven effective.

4.7 Summary

A calibration method using the echo integral output of the seabed for a quantitative echo sounder has already been verified (Aoyama, 1999). However, since a general echo sounder cannot directly output the echo integral, it is necessary to reexamine the calibration method using the echo level of the seabed. In this study, the practicality of a new calibration method using the volume backscattering strength obtained from the reflected echo level of the seabed obtained from a general echo sounder was verified. If this method is adapted to inter-ship calibration, multiple echo sounders in the same sea area will have the same level. It may be possible to evaluate biomass more quantitatively.

It was also suggested that fishing vessels establish a survey system because surveys by research vessels cannot be conducted frequently due to budgetary and workforce constraints (Furusawa, 2019). Therefore, developing a simple, inexpensive "quasi" quantitative echo sounder that can be mounted on fishing vessels is considered necessary. Applying the calibration method for general echo sounders using the seabed backscattering strength map proposed in this study, the general echo sounders installed on all fishing vessels can resemble quantitative echo sounders. In the future, it is expected that a system of stock assessment centered on fishing vessels will be established using inexpensive and widely used general echo sounders instead of a small number of expensive quantitative echo sounders.

4.8 Figures

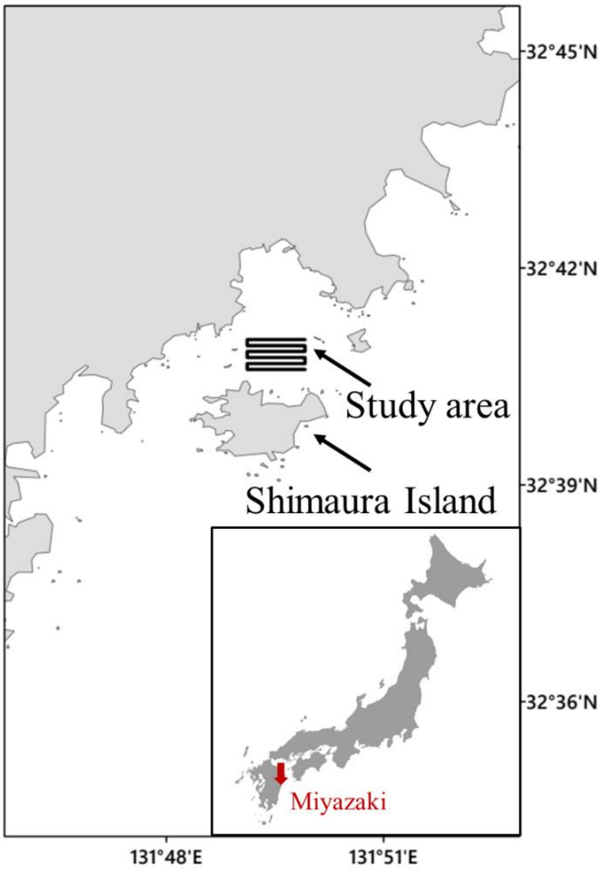

Figure 4-1. Study area, coastal areas of Shimaura Island, Miyazaki, Japan. The black line indicates the survey line.

Figure 4-2. Kakutomaru, a purse seine fishing vessel used for the survey, and the installation location of an external quantitative echo sounder.

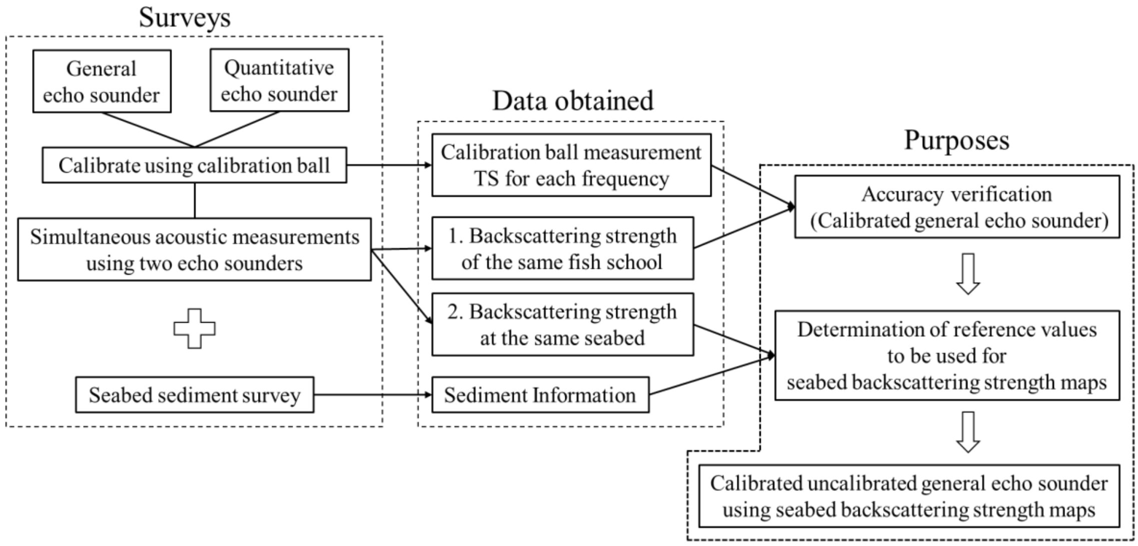

Figure 4-3. Illustration on the mechanism of calibration survey using general echo sounder and quantitative echo sounder.

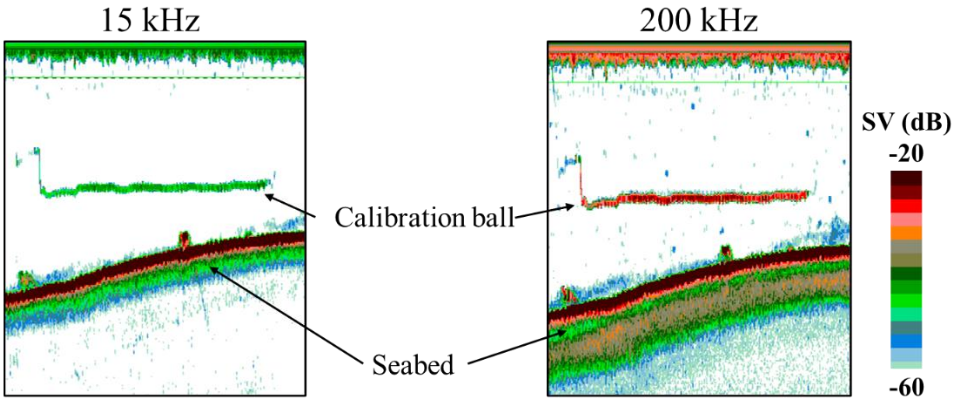

Figure 4-4. Echograms of calibration ball in general echo sounder (these echograms reflect the calibration values of the calibration ball).

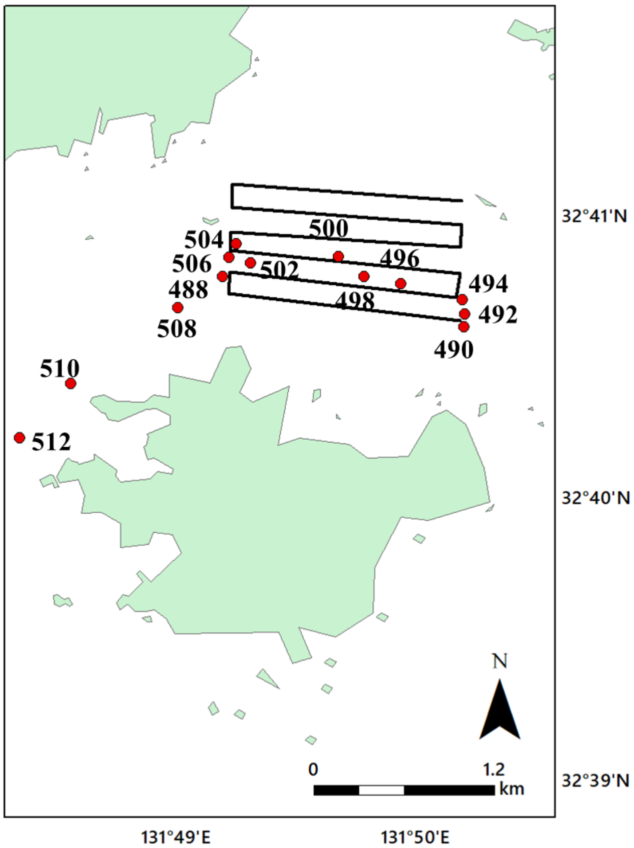

Figure 4-5. Survey lines and locations where seabed sediments were sampled. The red circle indicates the location of the mud sampling, and the number indicates the GPS number.

Figure 4-6. An Ekman Barge-type grab sampler manufactured by RIAGO was used to sample the seabed sediments.

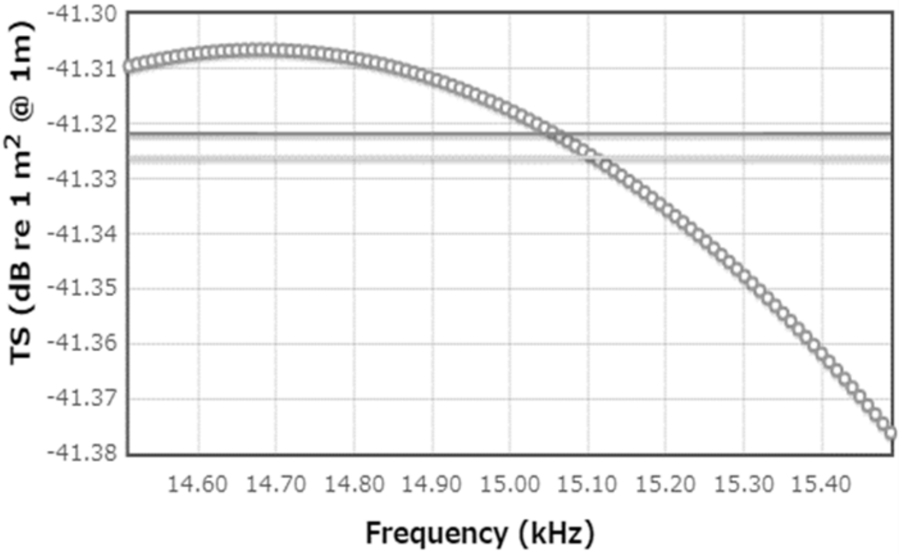

Figure 4-7. The theoretical TS of the WC calibration ball at 15 kHz was obtained from NOAA's Standard Sphere Target Strength Calculator (NOAA Southwest Fisheries Science Center).

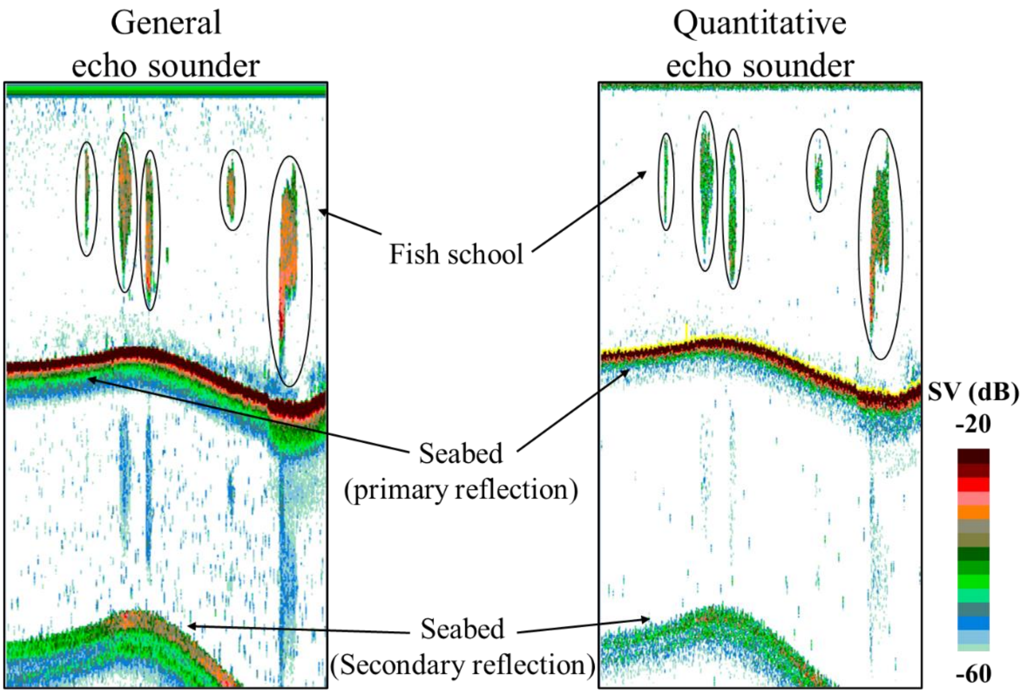

Figure 4-8. Echograms of fish schools, primary and secondary reflections on the seabed in general echo sounder and quantitative echo sounder.

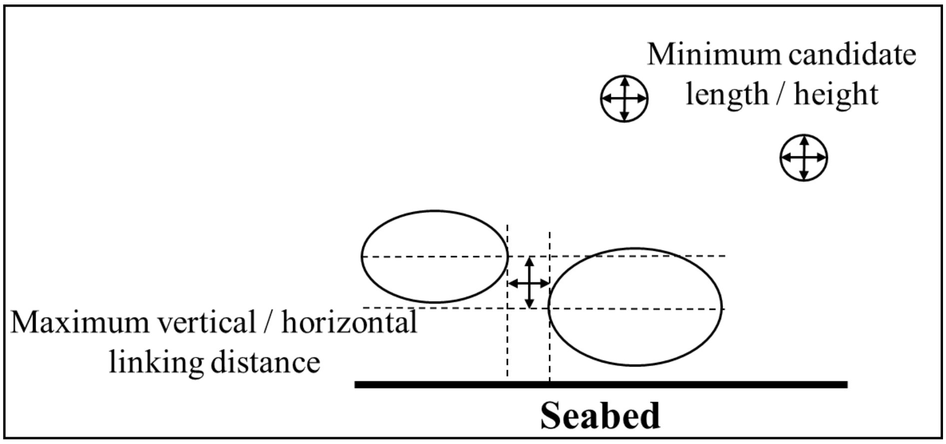

Figure 4-9. Diagram of fish school detection in Echoview. Two main detection conditions: the size of the fish group to be considered as a fish group, and the distance at which neighboring fish groups are recognized as the same fish group.

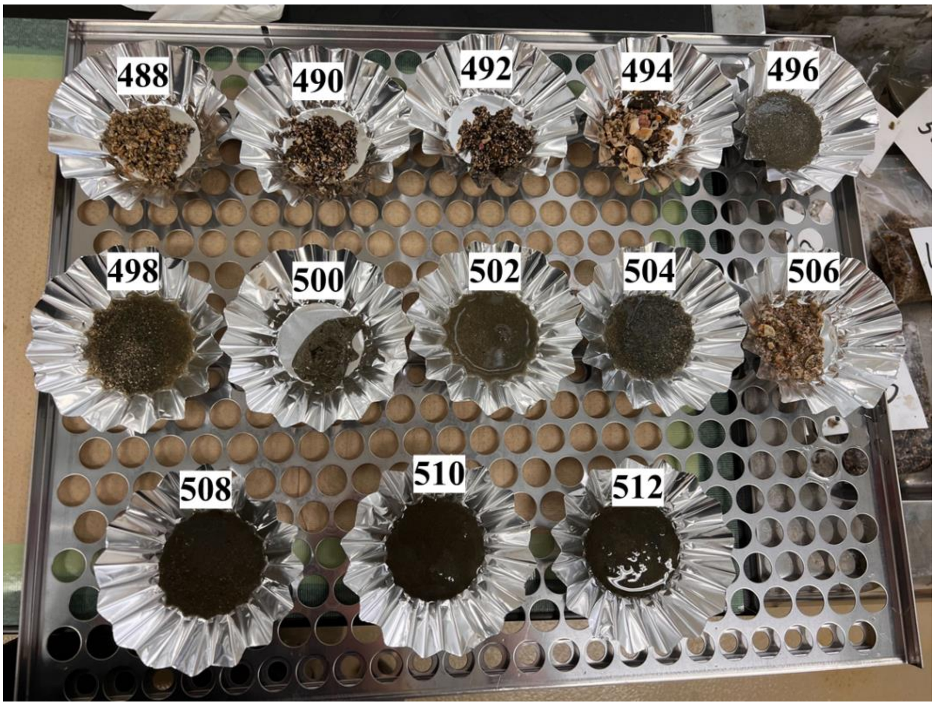

Figure 4-10. Seabed sediments at each sampling point divided around 30g. The number indicates the GPS number.

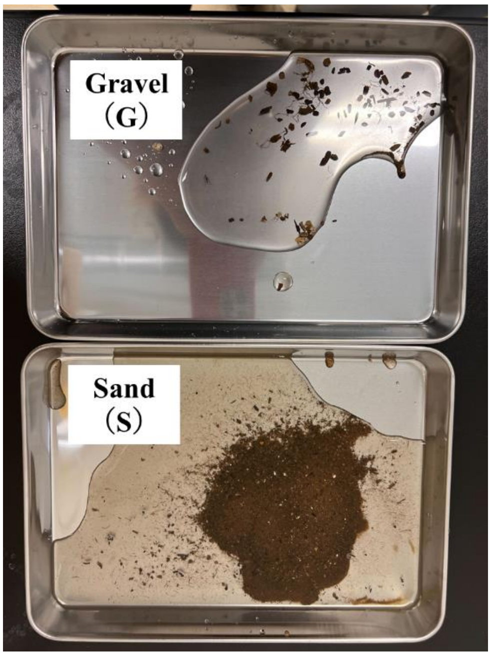

Figure 4-11. Example of using a sieve to separate grain size. Gravel and sand were left on each sieve, and mud was washed off the sieve.

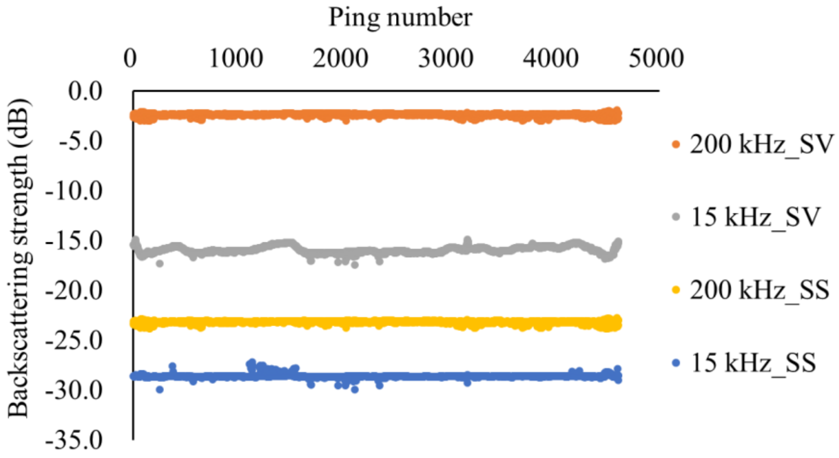

Figure 4-12. SS and SV of the seabed primary reflections were extracted for each ping from the general echo sounder data.

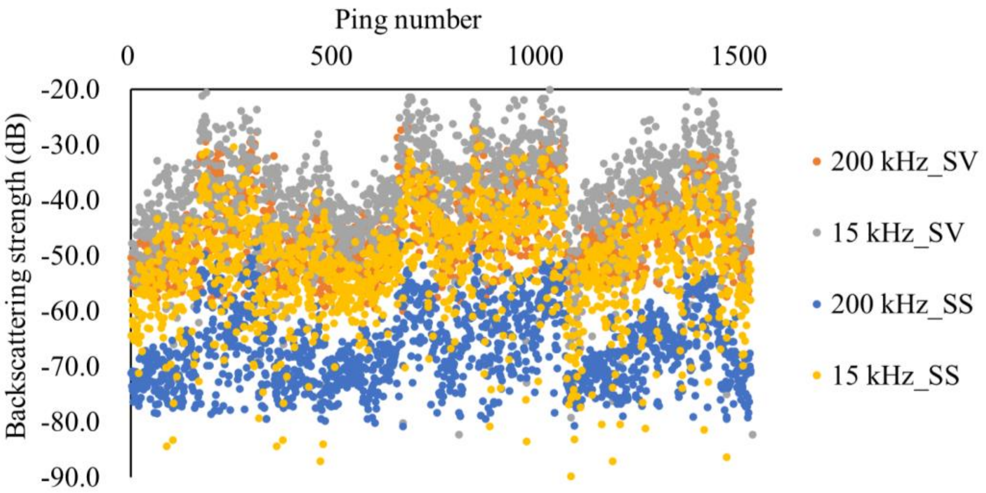

Figure 4-13. SS and SV of the seabed secondary reflections were extracted for each ping from the general echo sounder data.

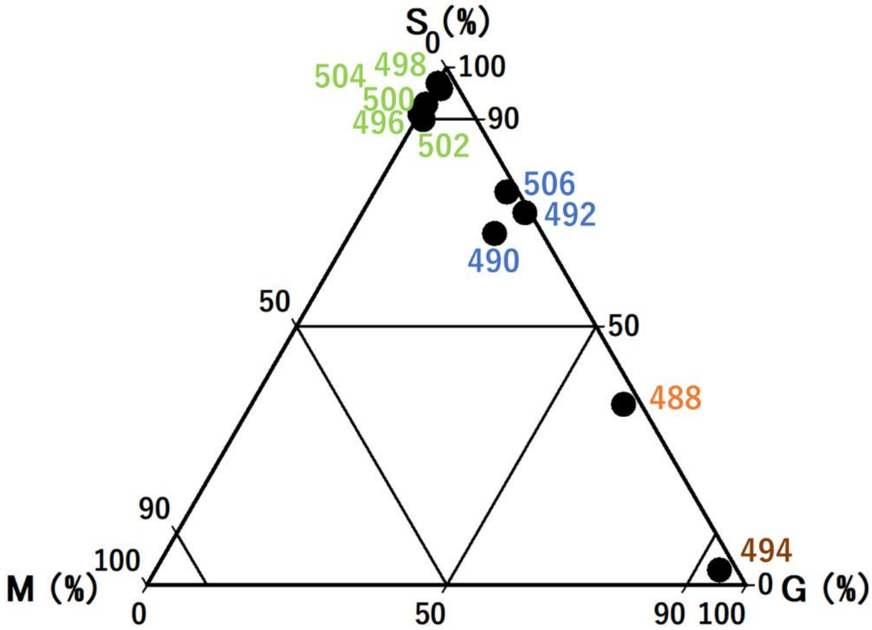

Figure 4-14. The result of seabed sediments was classified using KyPlot statistical software. The green numbers represent sandy (S), blue numbers represent sandy-gravelly (SG), orange number represents gravelly-sandy (GS) and brown number represents gravelly (G).

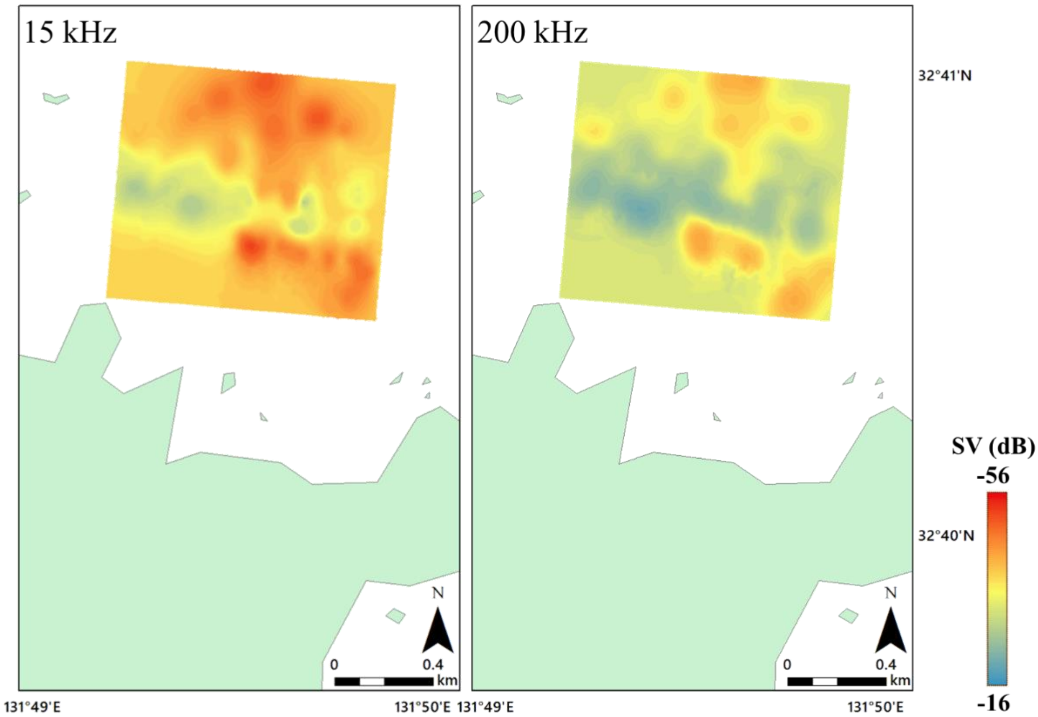

Figure 4-15. Created seabed backscattering strength map using the following parameters: (1) secondary reflection on seabed, (2) acoustic indicator SV, and (3) analysis range of 50 m grid.

4.9 Tables

Table 4-1. Setting for general echo sounder and quantitative echo sounder used in study survey.

	Specification			
	General echo sounder		Quantitative echo sounder	
Transducer	FCV-1500L		T-178	T-182
Frequency(kHz)	15	200	38	120
Beam type	Single		Split	
Pulse width(ms)	0.6		0.6	
Ping rate(s)	1.4		0.2	

Table 4-2. GPS data and water depth of sampling locations for seabed sediments (13 sampling points in total).

GPS number	LAT (°N)	LON (°E)	Depth (m)
488	32.67798	131.81690	8
490	32.67625	131.83407	24
492	32.67700	131.83402	18
494	32.67787	131.83378	16
496	32.67845	131.82937	19
498	32.67872	131.82675	17
500	32.67977	131.82485	16
502	32.67893	131.81878	18
504	32.67997	131.81765	16
506	32.67917	131.81727	15
508	32.67590	131.81400	24
510	32.67088	131.80698	27
513	32.66742	131.80373	28

Table 4-3. Measured and theoretical TS of the calibration ball at each frequency in general and quantitative echo sounder.

		Measured TS (dB)	Theoretical TS (dB)
General echo sounder	15 kHz	-41.3	-41.3
	200 kHz	-38.8	-39.1
Quantitative echo sounder	38 kHz	-42.4	-42.3
	120 kHz	-39.8	-39.9

Table 4-4. SA of each fish group, and estimated number and weight from SA at eachl frequency.

	General echo sounder						Quantitative echo sounder					
	15 kHz			200 kHz			38 kHz			120 kHz		
Fish school	SA (dB)	n	W (kg)	SA (dB)	n	W (kg)	SA (dB)	n	W (kg)	SA (dB)	n	W (kg)
1	-18.2	28,051	320	-13.8	62,917	717	-25.2	27,254	311	-27.8	10,909	124
2	-21.6	7,931	90	-14.5	35,075	400	-26.7	10,282	117	-27.9	7,054	80
3	-22.5	6,123	70	-15.6	25,279	288	-28.5	7,229	82	-30.8	3,085	35
4	-21.9	4,921	56	-18.9	5,887	67	-25.0	12,806	146	-27.7	4,833	55
5	-23.6	4,408	50	-17.7	9,461	108	-27.3	6,938	79	-30.2	2,489	28
6	-27.5	773	9	-22.9	2,020	23	-27.3	5,099	58	-32.0	1,484	17
7	-22.7	3,467	40	-19.0	6,510	74	-27.0	7,719	88	-31.5	1,419	16
8	-22.7	6,224	71	-16.0	16,077	183	-23.7	19,974	228	-26.3	7,085	81
9	-20.1	5,137	59	-13.5	18,857	215	-26.9	2,696	31	-28.7	927	11
10	-20.5	29,268	334	-16.1	57,386	654	-24.1	45,183	515	-25.9	24,389	278
11	-18.2	11,711	134	-13.5	29,111	332	-21.5	27,331	312	-23.5	16,867	192
12	-27.8	487	6	-22.6	1,210	14	-33.0	673	8	-36.6	160	2
13	-22.1	8,042	92	-18.6	12,104	138	-25.3	16,109	184	-28.4	4,014	46
14	-23.1	1,970	22	-17.9	2,554	29	-30.2	1,220	14	-33.6	164	2
15	-24.6	2,465	28	-20.2	5,305	60	-32.3	876	10	-36.0	281	3
16	-22.2	5,983	68	-18.9	11,223	128	-27.7	6,006	68	-31.7	1,957	22
17	-21.3	2,631	30	-17.4	5,674	65	-28.4	1,846	21	-30.9	888	10
18	-21.3	5,046	58	-16.9	8,042	92	-23.6	8,062	92	-27.6	1,883	21
19	-25.1	4,992	57	-20.1	6,687	76	-34.6	1,095	12	-39.5	140	2
20	-25.4	2,415	28	-20.7	3,615	41	-32.0	1,169	13	-37.1	182	2
21	-24.9	2,813	32	-20.2	3,770	43	-29.5	2,604	30	-34.0	426	5
22	-26.2	1,225	14	-20.9	2,272	26	-32.9	663	8	-37.7	70	1
23	-24.5	2,747	31	-19.3	5,270	60	-28.4	3,640	41	-32.8	524	6
24	-24.5	655	7	-19.9	967	11	-29.6	782	9	-34.4	197	2
25	-20.8	4,070	46	-17.1	20,229	231	-26.5	11,865	135	-30.3	3,318	38
26	-26.0	1,715	20	-20.2	4,982	57	-31.4	1,472	17	-35.3	464	5
27	-24.5	3,746	43	-18.7	7,636	87	-32.2	1,753	20	-38.1	104	1
28	-22.0	3,548	40	-17.1	7,953	91	-29.3	2,045	23	-34.6	266	3
29	-19.7	11,786	134	-14.6	34,030	388	-24.7	13,267	151	-27.0	5,673	65
30	-20.9	2,784	32	-18.4	3,986	45	-25.1	2,507	29	-26.5	1,763	20
31	-19.7	6,260	71	-14.1	12,634	144	-23.3	9,177	105	-26.5	4,644	53
32	-21.5	5,950	68	-15.7	16,465	188	-27.5	6,187	71	-33.8	973	11
33	-24.4	777	9	-21.4	729	8	-28.6	1,171	13	-32.2	458	5
34	-26.4	272	3	-21.4	891	10	-28.3	1,068	12	-29.3	760	9
35	-24.1	2,436	28	-18.3	7,132	81	-29.8	2,809	32	-34.7	564	6
36	-26.3	1,787	20	-20.4	4,713	54	-33.1	1,284	15	-37.2	175	2
37	-23.4	1,177	13	-19.6	2,349	27	-29.6	1,021	12	-34.2	284	3
38	-21.9	5,026	57	-17.1	7,438	85	-29.5	2,698	31	-33.8	556	6
39	-24.8	1,170	13	-20.8	1,781	20	-29.6	1,382	16	-33.9	252	3
40	-26.4	434	5	-20.7	256	3	-25.7	11,548	132	-27.8	6,362	73
41	-21.2	15,047	172	-17.2	18,664	213	-26.3	15,672	179	-31.2	2,354	27
42	-25.0	2,085	24	-20.0	4,664	53	-34.2	328	4	-36.0	160	2
43	-23.0	10,790	123	-18.4	23,607	269	-29.3	8,332	95	-33.7	1,978	23
44	-19.2	17,358	198	-15.2	33,803	385	-22.8	31,469	359	-26.0	15,164	173
45	-19.8	32,685	373	-15.7	50,694	578	-26.5	25,546	291	-31.0	5,195	59

Table 4-5. SA_{mean} obtained from the average all fish school data, number and weight estimated using SA_{mean} at each frequency.

		SA_{mean} (dB)	n_area	W_area (kg)
General echo sounder	15 kHz	-22.3	300,319	3,424
	200 kHz	-17.6	461,581	5,262
Quantitative echo sounder	38 kHz	-27.0	305,522	3,483
	120 kHz	-29.9	102,200	1,165

Table 4-6. SS & SV of the seabed primary and secondary reflections extracted one ping each from the general echo sounder and quantitative echo sounder, and the difference between the two echo sounders.

		Primary Reflection					
		SS			SV		
		Max.	Min.	Mean	Max.	Min.	Mean
General echo sounder	15 kHz	-27.2	-30.0	-28.6	-14.9	-17.4	-15.9
	200 kHz	-22.7	-23.8	-23.1	-1.9	-3.0	-2.3
Quantitative echo sounder	38 kHz	-3.5	-32.5	-10.2	-3.4	-32.4	-10.2
	120 kHz	-2.9	-32.0	-11.9	-3.0	-32.0	-11.9
		Secondary Reflection					
		SS			SV		
		Max.	Min.	Mean	Max.	Min.	Mean
General echo sounder	15 kHz	-27.5	-93.0	-51.1	-16.8	-82.3	-40.3
	200 kHz	-47.5	-80.7	-66.8	-25.5	-59.9	-45.4
Quantitative echo sounder	38 kHz	-11.9	-61.6	-37.2	-12.0	-61.5	-37.2
	120 kHz	-23.3	-73.2	-45.1	-23.2	-73.2	-45.1
General echo sounder - Quantitative echo sounder	15 kHz - 38 kHz	15.6	31.4	13.9	4.8	20.8	3.1
	200 kHz - 120 kHz	24.2	7.5	21.7	2.3	13.3	0.3

Table 4-7. maximum and minimum values of SS_{mean} and SV_{mean} calculated for each grid using backscattering strength of seabed secondary reflections.

SS_{mean}								
	General echo sounder				Quantitative echo sounder			
	15 kHz		200 kHz		38 kHz		120 kHz	
Grid	Max.	Min.	Max.	Min.	Max.	Min.	Max.	Min.
1m	-27.5	-93.0	-47.5	-80.7	-11.9	-58.4	-25.1	-70.1
5m	-27.5	-93.0	-47.5	-80.7	-17.8	-51.9	-29.1	-60.0
10m	-27.5	-91.6	-47.5	-79.4	-20.2	-49.7	-30.5	-58.4
50m	-27.5	-66.4	-47.5	-71.7	-23.1	-48.5	-33.2	-56.9
100m	-27.5	-66.4	-47.5	-71.2	-24.4	-47.6	-33.3	-56.8
500m	-27.5	-66.4	-47.5	-68.6	-26.2	-46.4	-35.2	-55.9

SV_{mean}								
	General echo sounder				Quantitative echo sounder			
	15 kHz		200 kHz		38 kHz		120 kHz	
Grid	Max.	Min.	Max.	Min.	Max.	Min.	Max.	Min.
1m	-16.8	-82.3	-25.5	-59.9	-12.0	-58.3	-25.0	-70.1
5m	-16.8	-82.3	-25.5	-59.9	-17.7	-51.8	-29.1	-60.1
10m	-16.8	-80.2	-25.5	-58.6	-20.2	-49.7	-30.5	-58.4
50m	-16.8	-55.5	-25.5	-50.1	-23.1	-48.5	-33.2	-56.9
100m	-16.8	-55.5	-25.5	-50.0	-24.4	-47.6	-33.3	-56.8
500m	-16.8	-55.5	-25.5	-47.8	-26.2	-46.4	-35.2	-55.9

Table 4-8. mean SS_{mean} & mean SV_{mean} calculated for each grid using seabed secondary reflections and the difference between the two echo sounders.

	mean SS_{mean}				Δmean SS_{mean}	
	General echo sounder		Quantitative echo sounder		General echo sounder - Quantitative echo sounder	
Grid	15 kHz	200 kHz	38 kHz	120 kHz	15 kHz - 38 kHz	200 kHz - 120 kHz
1m	-51.1	-66.8	-36.9	-45.1	14.2	21.7
5m	-50.2	-66.3	-35.9	-44.3	14.3	22.1
10m	-47.9	-64.5	-35.6	-44.1	12.3	20.3
50m	-42.8	-60.8	-35.4	-44.0	7.4	16.8
100m	-42.1	-59.9	-35.4	-44.0	6.7	16.0
500m	-40.9	-58.6	-35.4	-43.8	5.6	14.8
	mean SV_{mean}				Δmean SV_{mean}	
	General echo sounder		Quantitative echo sounder		General echo sounder - Quantitative echo sounder	
Grid	15 kHz	200 kHz	38 kHz	120 kHz	15 kHz - 38 kHz	200 kHz - 120 kHz
1m	-40.3	-45.4	-36.9	-45.1	3.4	0.4
5m	-39.4	-45.0	-35.9	-44.3	3.5	0.7
10m	-37.1	-43.1	-35.6	-44.1	1.5	1.0
50m	-32.1	-39.4	-35.4	-44.0	3.3	4.5
100m	-31.3	-38.5	-35.4	-44.0	4.1	5.4
500m	-30.2	-37.2	-35.2	-43.6	5.0	6.4

Table 4-9. Grain size composition, SS & SV of seabed secondary reflections, and the difference between two echo sounders at each sampling site. The green numbers represent sandy (S), blue numbers represent sandy-gravelly (SG), orange number represents gravelly-sandy (GS) and brown number represents gravelly (G).

				SS (dB)				ΔSS (dB)	
				General echo sounder		Quantitative echo sounder		General echo sounder - Quantitative echo sounder	
GPS number	G (%)	S (%)	M (%)	15 kHz	200 kHz	38kHz	120 kHz	15 kHz - 38 kHz	200 kHz - 120 kHz
488	62	35	3	-40.8	-60.5	-36.8	-45.5	-4.1	-15.0
490	24	68	8	-40.3	-54.4	-32.8	-39.8	-7.5	-14.6
492	22	76	2	-38.2	-60.3	-35.4	-45.5	-2.8	-14.8
494	95	3	3	-51.3	-62.8	-41.8	-52.8	-9.5	-10.0
496	0	91	9	-40.5	-57.4	-34.5	-40.9	-5.9	-16.6
498	0	97	3	-40.2	-57.1	-35.0	-44.0	-5.2	-13.2
500	0	93	7	-37.5	-62.4	-35.1	-45.1	-2.4	-17.3
502	1	90	9	-49.7	-65.7	-43.0	-51.3	-6.7	-14.5
504	1	96	3	-41.5	-56.2	-40.8	-49.2	-0.7	-6.9
506	27	72	1	-31.7	-49.4	-28.1	-36.4	-3.5	-13.0
				SV (dB)				ΔSV (dB)	
				General echo sounder		Quantitative echo sounder		General echo sounder - Quantitative echo sounder	
GPS number	G (%)	S (%)	M (%)	15 kHz	200 kHz	38kHz	120 kHz	15 kHz - 38 kHz	200 kHz - 120 kHz
488	62	35	3	-30.7	-39.7	-36.8	-45.5	6.1	5.8
490	24	68	8	-30.2	-33.6	-32.8	-39.8	2.6	6.2
492	22	76	2	-28.0	-39.5	-35.4	-45.5	7.4	6.0
494	95	3	3	-41.1	-40.8	-41.8	-52.8	0.7	12.0
496	0	91	9	-30.1	-36.6	-34.4	-40.8	4.4	4.1
498	0	97	3	-29.5	-36.3	-35.0	-44.0	5.5	7.6
500	0	93	7	-26.8	-41.6	-35.1	-45.1	8.3	3.5
502	1	90	9	-39.1	-44.9	-43.0	-51.3	3.9	6.3
504	1	96	3	-30.4	-34.1	-40.8	-49.2	10.4	15.1
506	27	72	1	-20.4	-27.4	-28.1	-36.4	7.7	9.0

Table 4-10. SV_{mean} extracted on a 50 m grid from the seabed secondary reflections of the non-calibrated general echo sounder, and the correction values to be used for the non-calibrated general echo sounder.

	SV_{mean} (dB) Raw data		
	Max.	Min.	Mean
15 kHz	-8.3	-47.1	-23.6
200 kHz	-59.5	-84.3	-73.5
	SV_{mean} (dB) Seabed backscattering strength map		
	Mean		
15 kHz	-32.1		
200 kHz	-39.4		
	Correction value (dB) Raw data - Seabed backscattering strength map		
	Δmean		
15 kHz	-8.5		
200 kHz	34.1		

Table 4-11. SA_{mean}, estimated number, and weight of all fish groups obtained from the general echo sounder calibrated with the calibration ball and the general echo sounder calibrated with the seabed backscattering strength map.

	SA_{mean}_area (dB)	n_area	W_area (kg)
15 kHz (Cal. using calibration ball)	-22.3	300,319	3,424
200 kHz (Cal. using calibration ball)	-17.6	461,581	5,262
15 kHz (Cal. using seabed map)	-22.1	298,308	3,401
200 kHz (Cal. using seabed map)	-16.9	571,236	6,512
Δ15 kHz (Calibration ball - Seabed map)	0.2	2,011	23
Δ200 kHz (Calibration ball - Seabed map)	0.7	109,655	1,250

Table 4-12. SVs of seabed secondary reflections extracted from a general echo sounder calibrated with a calibration ball and a general echo sounder calibrated with the seabed backscattering strength map at the same sediment sampling site and the difference between the two.

GPS number	488	490	492	494	496	498	500	502	504	506
	SV (dB)									
15 kHz (Cal. using calibration ball)	-30.7	-30.2	-28.0	-41.1	-30.1	-29.5	-26.8	-39.1	-30.4	-20.4
200 kHz (Cal. using calibration ball)	-39.7	-33.6	-39.5	-40.8	-36.6	-36.3	-41.6	-44.9	-34.1	-27.4
15 kHz (Cal. using seabed map)	-30.3	-29.8	-27.6	-40.8	-29.9	-29.5	-26.8	-39.0	-30.6	-20.7
200 kHz (Cal. using seabed map)	-40.0	-33.8	-39.7	-41.0	-36.8	-36.4	-41.7	-45.0	-34.1	-27.4
Δ15 kHz (Calibration ball - Seabed map)	0.4	0.4	0.4	0.3	0.2	0.0	0.0	0.1	0.2	0.3
Δ200 kHz (Calibration ball - Seabed map)	0.3	0.2	0.2	0.2	0.2	0.1	0.1	0.1	0.0	0.0

5. Resource assessment of Hyuga-nada using multiple fishing vessels

5.1 Introduction

The coast of Miyazaki's Hyuga-nada, influenced by the Kuroshio Current moving northward offshore, the inflow of river water, and the Bungo Channel, are reasonable fishing grounds for small pelagic fish such as mackerel, sardines, and horse mackerels. Therefore, many fisheries have flourished because of the great fishing grounds. However, in recent years, many fisheries have faced challenging conditions due to declining fish stocks, low fish prices, increased operating costs such as fuel oil, and declining consumption caused by COVID-19. Many coastal fisheries are therefore considering the creation of highly profitable models and are making efforts to shift to highly profitable/performance fisheries.

The purse seine fishery, the mainstay of Miyazaki Prefecture, is also involved in this initiative. The Kitaura and Shimaura town fishing cooperatives, whose primary industry is purse seine fishery, have tried to reduce operational costs and increase profits by building new vessels, refurbishing used vessels, and introducing new equipment. The Miyazaki Prefecture purse seine fishery mainly targets pelagic fish such as mackerel, sardines, and horse mackerel (Fukuda, 2013). Each fleet consists of four vessels (one net vessel, one fish carrier, and two searching/gathering vessels). Fish schools are searched for by echo sounder installed on purse seiners vessels, and when detected, the searching/gathering boat collects the fish, and the net boat casts a fishing net to catch them. Therefore, for purse seine fishery, information on these pelagic fishes' resources and fishing conditions is essential for planning management and operational efficiency.

Based on the above, it is considered that the acoustic data collected from general echo sounders on board all purse seiners vessels help estimate resource levels and assess fishing grounds on the coast of the Hyuga-nada. For example, the Kitaura and the Shimaura Town Fishing Cooperative have dozens of purse seiners vessels. Using the acoustic data from the general echo sounders on all these vessels, it would be possible to quickly obtain basic information (catch, fish distribution, fish species composition) on the operation days of multiple fishing vessels, enabling comprehensive coverage of the Hyuga-nada. However, as explained in Chapter 4, the data measured by conventional general echo sounders are not quantifiable; therefore, quantification of general echo sounders is necessary for resource assessment. In this study, only one vessel (Kakutomaru) was surveyed for calibration due to the influence of the spread of COVID-19 infection. Therefore, in Chapter 5, only the data from the Kakutomaru, calibrated with the seabed scattering strength map, was used for acoustic analysis, and combined with fish catch data to estimate the abundance index and evaluate the fishing grounds on the Hyuga-nada.

5.2 Methods

5.2.1 Catch data of purse seine

Daily (January 2019-December 2020) catches by species, and target size of 24 purse seine vessels (including the Kakutomaru) belonging to the Kitaura and the Shimaura Town Fisheries Cooperative Association were used to analyze fish species composition. Data on catch target size was divided into only three groups: small size, medium size, and large size. The fishing season for each species was defined as the period during which the sum of consecutive monthly catches accounted for more than 20% of the total.

5.2.2 Extraction of acoustic data

Based on the results obtained in Chapter 4, only the low frequency (15 kHz) of the calibrated Kakutomaru from 2019-2020 was used in this chapter because the low frequency of the general echo sounder was more suitable than the high frequency for biomass estimation. However, since data were available due to storage server problems in June 2019, acoustic data from July 2019 to December 2020 were used. For the analysis, to remove the effects of noise from microorganisms such as phytoplankton and zooplankton and suspended solids in the ocean, a threshold of -60 dB was used in this study (Kang, 2006), and regions of weak reflection below this threshold were treated as not being the fish school. In addition, since the inclusion of data when the fish were being collected with a purse seine would likely result in overestimation of the fish abundance and bias in the fish distribution, the data used in the analysis were only those obtained while the Kakutomaru was running, and locations with a speed of 3 knots or less were excluded from the scope of the analysis. Furthermore, since the extreme backscattering strength of bubbles emitted from under the vessel and the seabed, data up to 5 m from the surface and data 1 m from the seabed were treated as insufficient data. In this study, the range of the recording data was set to 155 m, so if the seabed was deeper than 155 m, the seabed was uniformly set to 155 m.

The area backscattering strength (SA: dB), the backscattering strength per unit area, and the volume backscattering strength (SV: dB), the backscattering strength per unit volume, were extracted as indicators of the extracted fish school density (MacLennan et al., 2002). SA_{mean} averaged SA at 1000 m intervals horizontally, and SV_{mean} averaged SV at 1000 m intervals horizontally and 10 m intervals vertically. Echoview ver. 12.1 (Sonardata Tasmania Pty Ltd.) was used as the analysis software. The software was then integrated with the geographic information system ArcGIS ver. 10.2 (Esri Inc.) technology to visualize fish school location information based on space.

5.2.3 Estimation of fish distribution

To understand the fish school distribution trend, the fish school's horizontal and vertical structures were clarified using the extracted SA_{mean} and SV_{mean}. First, the obtained SA_{mean} was represented on a map using ArcGIS in the horizontal structure, and the distance from the shore L

(m) to the SA_{mean} cell was calculated. After then, the horizontal structure was statistically estimated using the Generalized Additive Model (GAM), which assumes a normal distribution of the SA_{mean} and the calculated distance from the shore L (Pinilla, 2010). The GAM is not restricted to linear relationships and has flexibility in the statistical distribution of data (Murase, 2009). In addition, in the vertical structure, the relationship between the SV_{mean} and the central depth of the SV_{mean} cell D (m) and the relationship between the SV_{mean} and the distance of the SV_{mean} cell from the seabed Db (m) were estimated using the programming language for building models for General Algebraic Modeling System (GAMs) (Ginsburgh and Keyzer, 1997; Harrison et al., 2000; Fossati and Wiegard, 2002). Note that GAM and GAMs were run in R ver. 3.5.0 (R Core Team 2017), and the package was "mgcv" functions. Gaussian distributions were used for the error structure in all models, and the link function was identity; the summary statistic for GAM and GAMs, the practical degrees of freedom (edf), was used to quantify the strength of non-linearity of the driver strength relationship (Hunsicker et al., 2016).

5.2.4 Estimated abundance index

To estimate the fish abundance index migrating to the study area, the average SA_{mean} of the study area (hereafter: $AreaSA_{mean}$) and the catch composition of the purse seine during the study period were used. If the catch composition of the purse seine can represent the fish species composition of the study area, the fish abundance index N in the study area was calculated using the following equation.

$$\sum n_k = \frac{\text{AreaSAmean}}{\sum ts_k * P_k} \tag{1}$$

$$N = \text{Area} * \sum n_k \tag{2}$$

Where n_k, ts_k, and p_k are the mean density per unit area of fish species k, target strength per kg, and percentage of the total catch, respectively, and $AreaSA_{mean}$ and Area are the estimated mean SA and area of the assessment area, respectively. TS_k used in this study is mackerel - 30.8 dB, sardines - 34.6 dB, horse mackerel - 39.3 dB, and other fish species - 31 dB (Aoki et al., 1988).

5.3 Results and Discussion I: Catch and abundance index

5.3.1 Catch and species composition

Figure 5-1 shows the annual catches of each species and their proportion of the total catches based on the two years of purse seine catches. In 2019, mackerel and round herring (*Etrumeus micropus*) were the main species caught in the Hyuga-nada, accounting for more than 50% of the total catches at 28,496 tons. In 2020, mackerel and round herring stayed the same; however, Japanese sardine (*Sardinops melanostictus*) was also caught in large numbers, and the annual catch of these three species was 39,494 tons, making them the mainstay.

Additionally, Figure 5-2 shows the monthly changes in catch by species. In 2019, the total catch in January was 2,507 tons, and the catch was mainly mackerel and horse mackerel; from February to May, most of the catch was mackerel, with a peak in March when the monthly catch was 6,707 tons. From June, mackerel continued to decrease, and sardines such as round herring and Japanese sardines began to be caught, and this phenomenon continued until September. The monthly catch continued to decline from March; in September, it was one-third of the March figure at 2,159 tons. In October, Amberfish (*Decapterus maruadsi*) dominated the fishery, and the monthly catch dropped sharply to 980 tons; in November, Round herring was again caught in large numbers, and the monthly catch increased momentarily to 2,391 tons. December saw the lowest monthly catch, with only 805 tons.

In 2020, the catch in January and February was low, less than 1,100 tons; in March, mackerel were caught in large numbers, amounting to 8,865 tons and accounting for 16 % of the annual catch. From June, sardines were the main species caught, such as round herring and Japanese sardine, which continued to be caught in large quantities until December, with no significant change in catch from June to December, approximately 6,000 tons. In addition to sardines, horse mackerels, such as Japanese horse mackerel (*Trachurus japonicus*) and Amberfish, were caught in October and November.

5.3.2 Abundance index estimated from acoustic data

The monthly abundance index was calculated using the $AreaSA_{mean}$ for each month and the percentage of catch from the purse seine (Table 5-1). In 2019, the estimated abundance index tended to increase, with a high percentage of mackerel and sardines caught from July to September (Figure 5-3). In October, most of the catch was horse mackerels, and the estimated monthly abundance index was 9,957 tons, the highest in 2019. Conversely, the estimated abundance index declined sharply from November, reaching 3,027 tons in December.

In 2020, the estimated abundance index was lower in January, with only 3,033 tons (Table 5-1; Figure 5-3); it tended to increase from February to March, with March having the highest estimated abundance index in 2020. In March, mackerel were the main species, with an estimated monthly abundance index of 13,989 tons; from April, the estimated abundance index decreased, falling to 1,927 tons in May; from June to December, the catch was dominated by sardines, with the estimated abundance index remaining essentially unchanged until August. The estimated abundance index was high in September and October, over 10,000 tons; however, it began to decline from November, reaching 4,311 tons in December.

5.3.3 Correlation between catch and estimated abundance index

To compare the catch of purse seine and the abundance index estimated from acoustic data, the data from July 2019 to December 2020, when both results were available, was used. In terms of purse seine catch, the highest month in 2019 was July, and the lowest was December (Figure 5-4); in 2020, the catch was highest in March but lowest in February. The abundance index estimated from acoustic data showed a different trend from the catch in 2019, with the highest abundance index in October and the lowest in December. In 2020, the estimated abundance index was highest in March, close to the catch, but lowest in May, which was different from the catch. Thus, the monthly catch and abundance index estimates showed the same trend in some cases and differed in others. This discrepancy is likely due to each month's different areas of the assessment sea area. Since the abundance indices estimated in this study were calculated from the areas where purse seine fishing was conducted each month, there may be an effect on the area of the assessment area.

Considering the above reason, since the survey area for each month was different, the area-standardized abundance index was used compared to the catch. The overall correlation between catch and area-standardized abundance index estimates across all data showed a positive correlation ($R^2 = 0.53$; $P < 0.05$). Furthermore, the estimated abundance index increased as the catch increased (Figure 5-5). The abundance index estimated by acoustic data and the purse seine catch showed the same overall fluctuation trend. Therefore, it is possible to quantify abundance index that conventional general echo sounders could not capture, and it can be said that the acoustic information obtained by fishing vessels represents the abundance index on the Hyuga-nada.

This study has established a method for quantifying the abundance index by combining one month's acoustic data from one general echo sounder (one fishing vessel). In the future, fish school information can be easily obtained over a wider area and at a higher frequency using all purse seiner vessels. This will enable us to cover the entire area of the Hyuga-nada and grasp the daily fluctuations in biological information. Furthermore, by accumulating this information monthly and yearly and continuing to monitor it, it will be able to estimate the abundance index of the entire Hyuga-nada more accurately.

5.4 Results and Discussion II: Visualization of fish distribution variation

5.4.1 Monthly distribution trends in 2019

In this study, detailed information on the distribution and fluctuation of fish schools in the Hyuga-nada was obtained by combining one month of consecutive acoustic data collected by a single fishing vessel. In July, 861 SAs were obtained, with only 5 SAs having a solid strength of -30 dB or greater, and the most frequent SA was in the -40 dB to -30 dB range (Table 5-2). The distribution trends of those SAs were examined, and there was little significant change in acoustic strength with distance from shore (Figure 5-6-a, Figure 5-7-a, Table 5-3). In August, 882 SAs were obtained, 41 of which showed an intense strength of -30 dB or greater and 668 of which showed a strength of -40 to -30 dB, indicating a more significant number of solid strengths than in July. These fish schools were more abundant in waters up to 20,000 m from shore and tended to be more assertive near 20,000 m from shore than on the shoreside (Figure 5-6-b, Figure 5-7-b). In September, the number of points where SA was obtained increased to 1298. Most of the SAs were stronger than -40 dB, and more than 80 % of the total SAs were observed at 1080 stations. The distribution area was more expansive than in July and August; however, it is still concentrated in waters up to 20,000 m from shore, as was the case in July and August (Figure 5-6-c, Figure 5-7-c). In October, solid acoustic strength decreased, with only one point showing a strong response of -30 dB or more significant. The fish distribution ranges also became smaller and were concentrated on the shoreside (Figure 5-6-d, Figure 5-7-d). Similarly, no muscular strength was observed in November, and SA tended to be distributed primarily on waters up to 20,000 m from shore (Figure 5-6-e, Figure 5-7-e). 1137 SAs were obtained in December, most of which were weaker than -40 dB. These fish groups were also concentrated in waters up to 20,000 m from shore; their distribution range was the widest in 2019 (Figure 5-6-f). In addition, the horizontal distribution trend of these fish schools by GAM showed that the SA did not change significantly with distance from shore (Figure 5-7-f). Therefore, the fish school in December was found to be small-scale and widely distributed in the Hyuga-nada.

5.4.2 Monthly distribution trends in 2020

In January and February, approximately 680 SAs were obtained, most of which were within the -50 dB to -30 dB strength range (Table 5-2). In January, fish schools were distributed mainly within 20,000 m from shore and tended stronger offshore than onshore (Figure 5-8-a, Figure 5-9-a, Table 5-3). Similar results were obtained in February, with a stronger fish school strength observed in the area beyond 15,000 m from the shore than on the shoreside (Figure 5-8-b, Figure 5-9-b). In March and April, the number of points where SA was obtained increased to approximately 1300 points. Of these, strong strength of -30 dB or higher was observed at about 140 points, and more than 50% of the points where fish school strength was observed had a strength of -40 dB or higher. The fish school was more abundantly distributed offshore than on shore, especially in the area from 20,000 m to 50,000 m from shore in March (Figure 5-8-c, Figure 5-8-d, Figure 5-9-c, Figure 5-9-d). In May, the strength of the fish school decreased, and most were observed in the strength range from -50 dB to -40 dB. Fish schools in May tended to be widely distributed along the coastal side of the Hyuga-nada (Figure 5-8-e, Figure 5-9-e). In June, SA was obtained at fewer points. Additionally, the fish schools were concentrated in waters up to about 20,000 m from shore, and their distribution range was much smaller than in May (Figure 5-8-f, Figure 5-9-f). In July 1173 SAs were obtained, and 548 points showed strong fish school strength above -40 dB, more than in June. Most fish schools were distributed within 20,000 m of shore and were more abundant offshore than on the shoreside (Figure 5-8-g, Figure 5-9-g). In August, 888 SAs were acquired, more than 60% within the -40 dB to -30 dB strength range. As in July, most fish schools were distributed within 20,000 m of the shore, with slight significant variation in SA with distance from shore (Figure 5-8-h, Figure 5-9-h). From September to December, the fish strength was stronger than in August, and the distribution range was narrower than in August. (Figures 5-8-i ~ Figure 5-8-l). In all months except October, most fish schools tended to be distributed within 20,000 m from shore (Figure 5-9-i, Figure 5-9-k ~ Figure 5-9-l); however, in October, the fish school was observed as far as 30,000 m from shore (Figure 5-9-j).

5.4.3 Dominant fish species per month over two years

Fish species composition showed slight differences between the two years (Figure 5-2). In 2019, from January to May, the dominant species were mackerel, and from June to September, the dominant species in the area were mackerel and sardines, mainly round herring; in October, most of the catch was Amberfish, and from November, the catch of Round herring increased again.

In 2020, catches were low in January and February, and unlike in 2019, mackerel were rarely caught; in March and April, mackerel became the dominant species, with most catches being mackerel (Figure 5-2). From June, sardines began to be caught, similar to 2019. However, the dominant species differed from 2019, with both round herring and Japanese sardine being caught in 2020, with Japanese sardine being caught in huge numbers. This phenomenon continued until December, with sardines, mainly Japanese sardines, being the dominant species from June to December. Furthermore, as in 2019, horse mackerels were caught in October; however, the dominant species in 2020 was not Amberfish but Japanese horse mackerel.

5.4.4 Relationships between distributional characteristics and dominant species

From July to December 2019, most of the fish school was distributed within 20,000 m and in waters with slight depth variation; in 2020, most of the fish school was distributed within 20,000 m from shore in all months except March, April, and October. In March and April 2020, the number of fish schools was higher than in other months, and the distribution range of fish schools was considerably more comprehensive. Many fish schools are distributed from the shore side to the offshore side, with an extreme strong fish school strength on the offshore side from 15,000 m from the shore. In October, the distribution range was narrower than in March and April; fish schools were also found on the offshore side from 20,000 m from the shore.

The seabed topography of the Hyuga-nada is that the continental shelf extends 20,000 - 30,000 m offshore, and the water depths are shallower than 200 m. Offshore from it, a continental slope deepens abruptly (Tokkeshi et al., 2020). In March and April 2020, most of the catch was adult mackerel. Since mackerel are characterized by their abundance in the 200 m isobaths and offshore (Nozu, 1980), it is likely that during months when mackerel are caught in large numbers, the fish school will be more extraordinary offshore than 20,000 m from the shore. In October 2020, in addition to sardines, Japanese horse mackerels were caught in large numbers, and the catch in October accounted for 50 % of the annual catch of Japanese horse mackerels. In the Hyuga-nada, it has been suggested that most Japanese horse mackerel caught in October are age-0 fish (Fukuda, 2010). It is also pointed out that Japanese horse mackerel is a species that does not migrate widely (Tsukamoto, 2007). Juvenile fish distributed in the frontal area of the Kuroshio migrate to the coastal area due to warm water spillover (Uehara and Mitani, 2007). Therefore, it is considered that an increase in the recruitment of age-0 Japanese horse mackerels from the offshore area in October 2020 will lead to an increase in the fish school on the offshore side of the Hyuga-nada.

In months other than these three, most of the catch is sardines, including round herring and Japanese sardines. However, in 2019, the main catch was dominated by round herring, while in

2020, Japanese sardine was the main catch. In general, the phenomenon of species shifts between Japanese anchovy (*Engraulis japonica*) and Japanese sardine is often cited (Sugimoto, 2008; Takasuga, 2007); however, in the Hyuga-nada, such shifts have also been observed between round herring and Japanese sardine (Fukuda, 2012). It has been suggested that Japanese sardines prefer to mix with schools of round herring because they have a similar life history (Takasuga, 2007). Juveniles of both species are distributed in shallow coastal waters from February to April, and in June and July, they tend to move offshore on the continental shelf around 20,000 m from the shore. Therefore, it is considered that in months when round herring and Japanese sardine were the dominant fish species, the distribution area may have been near the continental shelf up to 20,000 m from shore in Hyuga-nada.

In summary, the distributional characteristics of the fish school for each month of the year obtained in this study were in good agreement with the ecology of each dominant fish species. Therefore, the differences in the distribution of fish schools may reflect the ecology of different dominant fish species. In addition, this study examined the monthly relationship between fish distribution and dominant fish species using acoustic data from a single fishing vessel. However, more detailed information on fish distribution and abundance can be obtained using acoustic data from multiple fishing vessels. Therefore, the general echo sounder equipment on board fishing vessels can efficiently collect fish school distribution information in three dimensions, enabling the visualization of biological information, which has become the most critical issue in fisheries resource assessment. Furthermore, suppose this information is used effectively. In that case, it will enable us to visualize biological information in more detail and accuracy and evaluate resource amounts using an accurate database in the future.

5.5 Results and Discussion III: Fishing ground characteristics

Figure 5-10 shows the fishing seasons of mackerel, sardines, and horse mackerels in the Hyuga-nada. Two species of mackerel inhabit the Hyuga-nada: Chub mackerel and Blue mackerel (*Scomber australasicus*). In this study, since separating the species based on catch was impossible, they were collectively referred to as mackerel. In 2019, large adult mackerel were caught during the peak season from March to April, and in 2020, large adult mackerel were caught mainly in March. In addition, the most frequently caught sardines were round herring, and Japanese sardines were often caught as bycatch. Medium-sized round herrings were caught mainly in November 2019 and 2020, while small-sized round herrings were caught in large numbers in July 2019 and August 2020. Japanese sardines were rarely caught in 2019, but in 2020, small Japanese sardines were caught most frequently from June to August, and giant Japanese sardines were caught most frequently from September to December. Furthermore, there were two types of horse mackerels in Hyuga-nada: Japanese horse mackerels and Amberfish. In 2019, few Japanese horse mackerels were caught, but in 2020, many small Japanese horse mackerels were caught in October. In 2020, the catch of Amberfish was smaller than in 2019, and more adult Amberfish were caught, mainly in January. Therefore, in this study, mackerel caught in large numbers from March to April was considered the adult mackerel group. The large numbers of round herring and Japanese sardines caught from September to December were considered adult sardine groups, and the small ones caught from May to August were considered small sardine groups. The Amberfish caught in January were considered the adult Amberfish group. In their peak season in October, the Japanese horse mackerels and Amberfish were considered the small horse mackerel group.

In addition, to examine the distributional characteristics of each fish group, acoustic data from the month with the highest catch of each fish group during the two years were used. For adult mackerel, the catch was high in March in both years; however, since the acoustic data in March 2019 were unavailable, acoustic data in March 2020 were used. Adult Round herrings were caught more in November 2019, and small round herrings were caught more in July 2019. Therefore, acoustic data in November 2019 were used for adult round herrings, and in July 2019 were used for small round herrings in the analysis. Similarly, for the Japanese sardine, acoustic data in September 2020 were used for adult fish, and acoustic data in July 2020 were used for small fish. For Amberfish, the acoustic data in January 2020 was used for the adult fish, while the acoustic data in October 2019 was used for small fish. No month accounted for most of the total catch of Japanese horse mackerels; however, since much small Japanese horse mackerel were caught in October 2020, the acoustic data in October 2020 was used to examine the distribution characteristics of small Japanese horse mackerel. Echograms of each fish group are shown in Figure 5-11.

5.5.1 Fishing ground characteristics of mackerels

Adult mackerel tended to be distributed more offshore than on the shore in Hyuga-nada (Figure 5-12-a). In addition, the horizontal distribution trend by GAM showed that the fish school strength became more robust as they moved offshore (Figure 5-13, Table 5-4). On the other hand, the vertical distribution trend did not show any significant change in the fish school strength with depth; however, the strength was more muscular at deeper depths than at shallower depths. Thus, the distribution characteristics of adult mackerel were characterized by a more excellent distribution offshore than on the shoreside and across all depth zones.

According to a previous study, mackerel caught mainly in March ~ April in the Hyuga-nada are likely to be mature mackerel (2 years old or older) (Fukuda, 2010). In addition, mackerel fishing grounds older than two years are often formed in the Bungo Channel and the northern part of the Hyuga-nada, off Tsuno and Tosakibana, suggesting that they tend to migrate as large groups with strong offshore characteristics (Fukuda, 2010). In this study, adult mackerel were found off Tsuno and in the northern part of the Hyuga-nada, consistent with previous studies results.

5.5.2 Fishing ground characteristics of sardines

Adult sardines group GAM analysis of the horizontal distribution trend revealed that the fish school was concentrated in an area up to 25,000 m from the shore (Figure 5-13). The vertical distribution trend with a tendency to be evenly distributed from the surface to 150 m. Like Round herring, adult Japanese sardines were abundantly distributed in an area up to 20,000 m from the shore and shallow layer (Figure 5-12-c). Thus, the distribution trend of adult Japanese sardines in September was similar to that of adult round herring in November, with the fish school concentrated in waters up to 20,000 m from shore and more abundantly distributed in the shallow depth zone than in the deep zone.

It has been suggested that adult round herring and Japanese sardines tend to be distributed around the northern boundary between Bungo Channel and Hyuga-nada and on the continental shelf and its margins from north to south of Hyuga-nada (Fukuda, 2013). In the Hyuga-nada, there are 200 m isobaths of the continental shelf at about 20,000 m from the shore. Therefore, round herring and Japanese sardines tended to be distributed up to 20,000 m from the shore in this study, similar to the distribution characteristics observed in the previous study.

Small sardines group Small Round herring tended to be distributed evenly in the area from the shoreside to 18,000 m, regardless of the distance from the shore (Figure 5-12-f). The horizontal distribution trend of these fish schools found that the fish school strength did not change significantly with distance from the shore (Figure 5-13). Vertically, the fish school strength was most substantial at depths up to 30 m and tended to decrease with depth below that depth. In addition, from the distance from the seabed, the most muscular strength was observed in the depth zone from the bottom to 30 m. This result indicates that small round herrings are relatively abundant in shallow waters near the shore. On the other hand, small Japanese sardines showed a slightly different distribution trend from small round herrings. Small Japanese sardines were distributed in waters up to 18,000 m from the shoreside; however, they tended to be distributed more offshore (Figure 5-12-g). The statistically calculated horizontal distribution trend also showed a similar trend, with increased fish school strength more than 10,000 m from the shore (Figure 5-13). The vertical distribution trend showed that the fish school strength was more robust in the deeper depth zone than in the shallower depth zone.

It has been reported that small-sized fish of round herring and Japanese sardines tend to form mainly on the continental shelf around the central part of the Hyuga-nada (Fukuda, 2013). However, although the distribution areas of juveniles of both species are similar, the distribution areas become different when they grow to a specific size. Japanese sardines join shallow coastal waters from February to April, migrate onto the continental shelf from June to July, and then move further offshore and disperse from the fishing grounds (Fukuda, 2012). On the other hand, after moving onto the continental shelf in June ~ July, Round herring tends to be distributed mainly in the marginal area of the continental shelf from August to October, then moves to the offshore area from November and tends to be displaced from the fishing grounds. Therefore, the distribution areas of the two species are considered to differ from around July. In this study, we found that in July, small-sized round herring and Japanese sardines were distributed mainly in the area from shore to 18,000 m. However, round herring was the dominant species, they were distributed mainly on the shoreside, and when Japanese sardine was the dominant species, they were distributed mainly on the offshore side. This difference in distribution characteristics may reflect the different ecology of both species.

5.5.3 Fishing ground characteristics of horse mackerels

Adult Amberfish group Adult Amberfish was distributed mainly within 20,000 m from shore (Figure 5-12-d). GAM analysis of these fish schools revealed that the horizontal distribution trend showed increased in fish school strength offshore from 10,000 m from the shore (Figure 5-13). Vertical distribution showed that the most muscular strength was observed at depths of 50 m and 150 m from the surface, and the most muscular strength was observed in the depth zone from the bottom to 70 m. From the above results, Amberfish were distributed closer to the bottom than mackerel and sardines.

It has been suggested that Amberfish grow in shallow waters and tend to move offshore after one year (Doiuchi and Takeda, 2010). In addition, speculating on the characteristics of the fishing grounds for Amberfish by purse seine in the outer Kii Channel, it has been observed that the fishing grounds of adult Amberfish tend to gradually expand from the shoreside to the continental shelf from spring to summer (Harada and Takeda, 2014). Since the Kii Channel is located south of the Hyuga-nada, it is considered that the migration period of Amberfish in the Hyuga-nada is earlier than that in the outer Kii Channel. Therefore, in this study, it is considered that a large number of adult Amberfish distributed in the offshore area in January reflects the migratory behavior of Amberfish due to their growth stage. In addition, since the ecological characteristics of the Amberfish are close to those of the Japanese horse mackerel, the habitat of adult fish shifts to the bottom layer (Ito et al., 1985). Therefore, it is considered that the distributional characteristics of the adult Amberfish obtained in this study, which is closer to the bottom layer, reflect the ecology of adult Amberfish.

Small horse mackerel group In October, small Amberfish were distributed within 20,000 m from the shore, while small Japanese horse mackerels were found in waters up to 30,000 m from shore (Figure 5-13). In the horizontal distribution trends of the two species, the Amberfish tended to be distributed closer to shore than the Japanese horse mackerel. In the vertical distribution trends, the most significant number of Amberfish were found in the depth zone from the surface to 100 m and from the bottom to 100 m, indicating that fish school was most abundant in the area up to 100 m depth. On the other hand, Japanese horse mackerel showed a muscular school strength from the surface to depths deeper than 50 m, and the most robust school strength was observed near the bottom. Therefore, Japanese horse mackerels were more abundantly distributed in the deep offshore zone than Amberfish.

In the Hyuga-nada, Amberfish eggs and fry appear in June ~ November (Matsuda, 1969), and age-0 Japanese horse mackerel are caught in October ~ November (Fukuda, 2010). In addition, Amberfish are more coastal than Japanese horse mackerels (Harada et al., 2015), and small fish are characterized by aggregation in shallow water areas (Takeda, 2002). On the other hand, juvenile Japanese horse mackerels live together with other juvenile fish in association with flow algae (Yosho et al., 1984), and it has been reported that fishing grounds tend to be formed mainly on the continental shelf around the Bungo Channel ~ north side of the Hyuga-nada (Fukuda, 2013). Based on these facts, it is logical that differences in distribution areas can be observed because of the different ecology of small-sized Amberfish and small-sized Japanese horse mackerels.

5.5.4 Future challenges for fishing ground assessment

In the Hyuga-nada, adult mackerel, including Chub mackerel and Blue mackerel, tended to be distributed mainly in the waters off Tsuno. However, it has been reported that the two species' migratory status differs yearly (Goto, 2020). The Blue mackerel is more offshore than the Chub mackerel, with somewhat different spawning grounds and distribution areas for the two species (Yukami et al., 2008; Goto, 2020). Therefore, it is considered necessary to understand each species' abundance of migration and distribution characteristics to assess the fishing ground characteristics of the two species more accurately in the future. Additionally, the distribution of sardines was more shoreward than mackerel, and their fishing grounds were mainly located on the continental shelf to the continental shelf margin. However, while the distribution areas of adult round herring and Japanese sardine were similar, there were some differences in the distribution areas of smaller fish. Compared to other migratory fish, round herring is relatively more localized and moves to offshore areas as it grows; however, it tends to move later than Japanese sardines (Asami, 1974). Therefore, differences in the distribution areas of the two species depending on their growth stages need to be examined in more detail. Furthermore, regardless of growth stage, Horse mackerel, mackerel, and Japanese sardine are migratory fish that come to the Hyuga-nada to spawn. On the other hand, Round herring mainly fish in the coastal areas between Hyuga-nada and Kumano-nada and have more regional characteristics than other migratory fish. Therefore, it will be necessary to consider each fish's migratory ecology when evaluating its future fishing grounds.

In this study, we could efficiently understand the actual conditions of fish distribution in three dimensions using multiple acoustic data. As a result, the characteristics of fishing grounds for pelagic fishes in 2019-2020 were clarified. It is considered that acoustic information will be used in conjunction with fishermen's experience to improve the efficiency of planned management and operations. On the other hand, pelagic fishes are species with highly variable abundance and are known to change their distribution areas depending on the abundance and environmental factors (Goto, 2020). In the mackerel, it has been reported that Blue mackerel is in warmer water than Chub mackerel and that Blue mackerel forms fishing grounds under conditions of 13-23 °C (Hirai,

1999) and Chub mackerel under conditions of 16-20 °C (Okabe et al., 2009). In sardines, Japanese sardines are more adapted to cold temperatures than round herring (Matsuoka, 2001, Kano and Kunimori, 2018). In addition, it is reported that a crucial oceanic condition for both species is the northward movement of the Kuroshio front during summer and autumn (Kondo, 1988). Moreover, juvenile Japanese horse mackerels are characterized by their habitat associated with flow algae (Yosho et al., 1984). The distribution of flow algae in the Hyuga-nada fluctuates greatly depending on the Kuroshio Current. The above results suggest that the fluctuations in sea conditions associated with the Kuroshio Current significantly impact the formation of fishing grounds for mackerel, sardines, and horse mackerels in the Hyuga-nada. In the future, it is expected that the analysis of sea conditions will be added to the analysis of fish distribution and abundance to understand the amount and timing of migratory fish and the formation of fishing grounds more precisely.

5.6 Summary

In this study, multiple acoustic data were used to efficiently determine the actual condition of the fish school in three dimensions, enabling direct visualization underwater. Conventionally, most acoustic survey surveys on fishery resources have used research vessels (Hamano, 2019; Shida, 2019; Zhu al., 2021). However, the number of surveys has been limited due to the time required and economic costs, and the essential information used to assess fishery resources needs to be increased. In particular, the abundance of pelagic fishes such as horse mackerel, mackerel, and sardines fluctuate greatly depending on the season and year (Nishioka et al., 2019; Kono, 2020); therefore, more basic information is needed for fishery assessment for these pelagic fishes. In this study, acoustic information obtained from a calibrated general echo sounder installed on the fishing vessels made it possible to collect continuous biological information. In the future, applying it to multiple fishing vessels makes it possible to obtain acoustic data from multiple fishing vessels on the same day of operation, making it easier to obtain a broader range and a more significant number of basic information. Even for fish species whose abundance fluctuates rapidly, it is thought that the mechanism of the fluctuation can be understood by accumulating a vast amount of primary data over a long period.

In addition, it is considered that the influence of global-scale environmental changes occurring water environment is a very significant factor in the fluctuation of fishery resources (Tokeshi et al., 2021; Goto, 2022). Therefore, long-term monitoring of fish fisheries obtained by fishing vessels, in addition to environmental information, is expected to lead to the prediction of fishing grounds and elucidation of the mechanism of fishery fluctuation. Furthermore, by accumulating monthly and yearly data and monitoring continuously, changes from the past can be understood, enabling us to predict the future and find clues to improve the current situation. Thus, by scientifically clarifying the mechanism of fisheries resource fluctuations, we can contribute to the sustainable conservation of fisheries resources in the future without overfishing or human-caused destruction of resources.

5.7 Figures

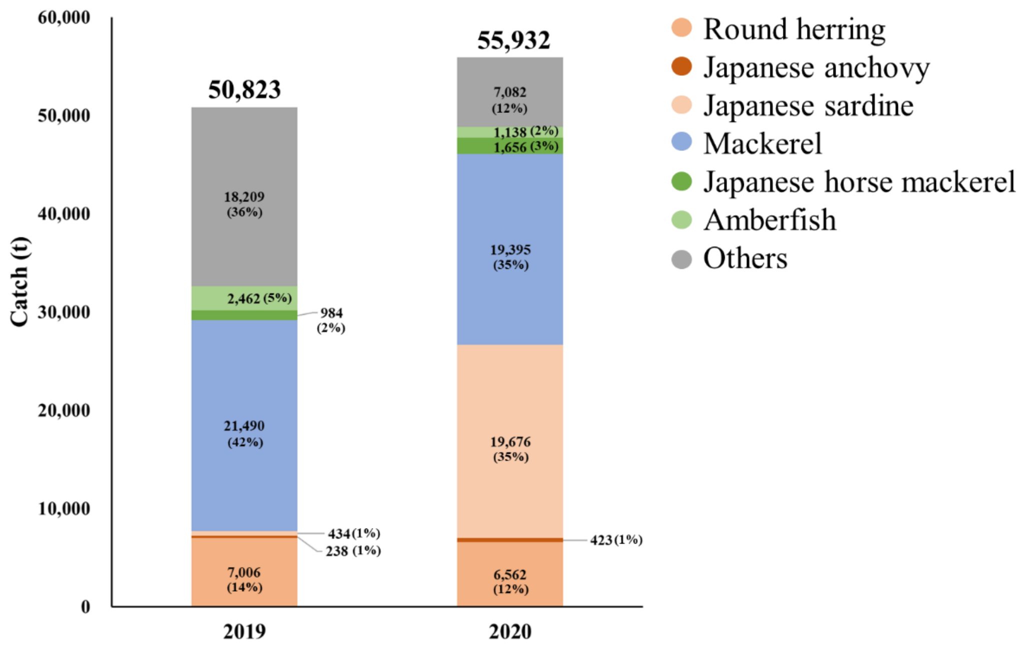

Figure 5-1. Annual catch by fish species for purse seine fishery in 2019 and 2020 (for 24 vessels).

The percentage is the ratio of each species' catch to the total annual catch.

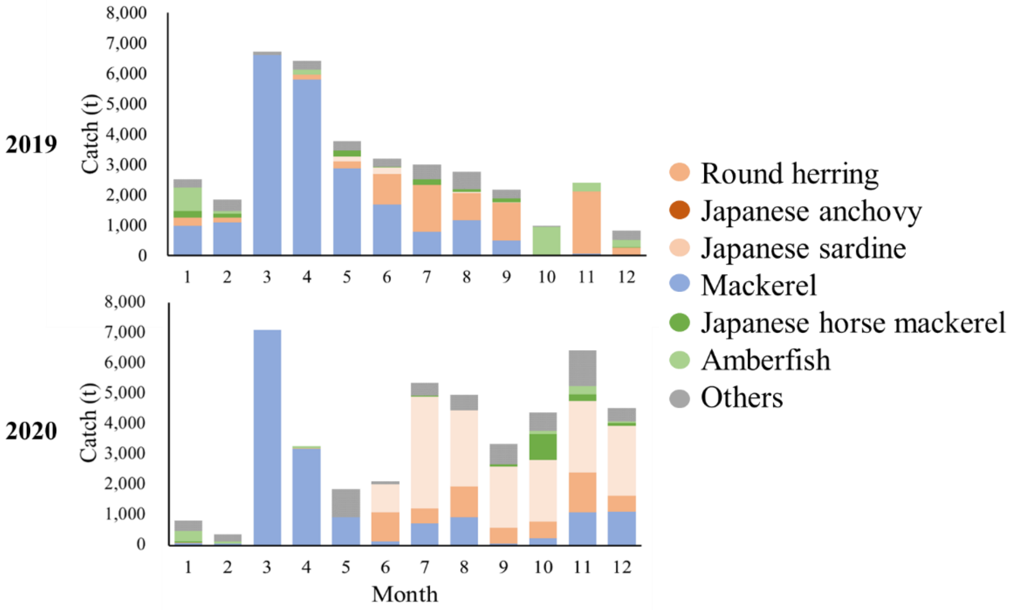

Figure 5-2. Monthly catch of each species in the purse seine fishery in 2019 and 2020 (for 24 vessels).

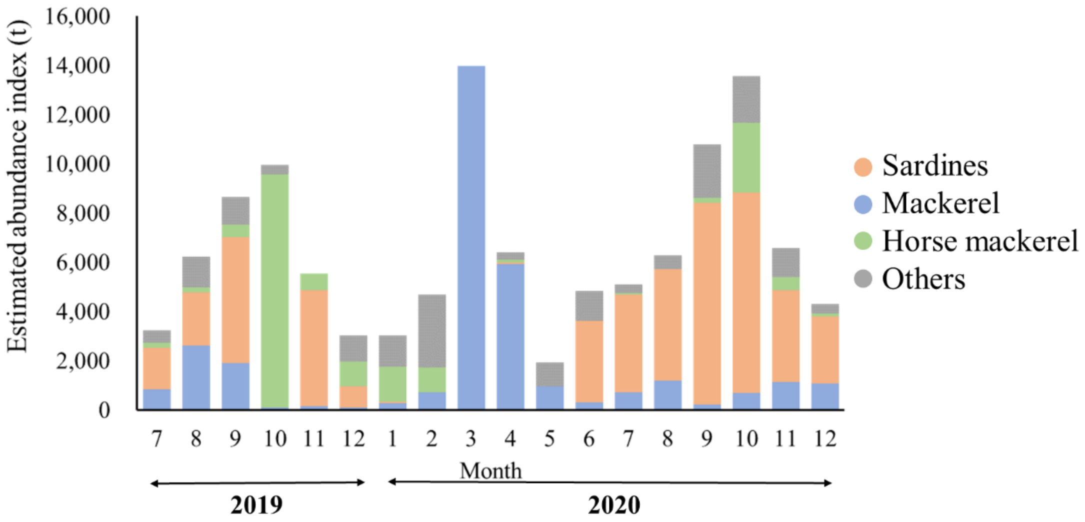

Figure 5-3. Abundance index of each fish species by month estimated using the percentage of purse seine catch and acoustic information ($AreaSA_{mean}$) for each month.

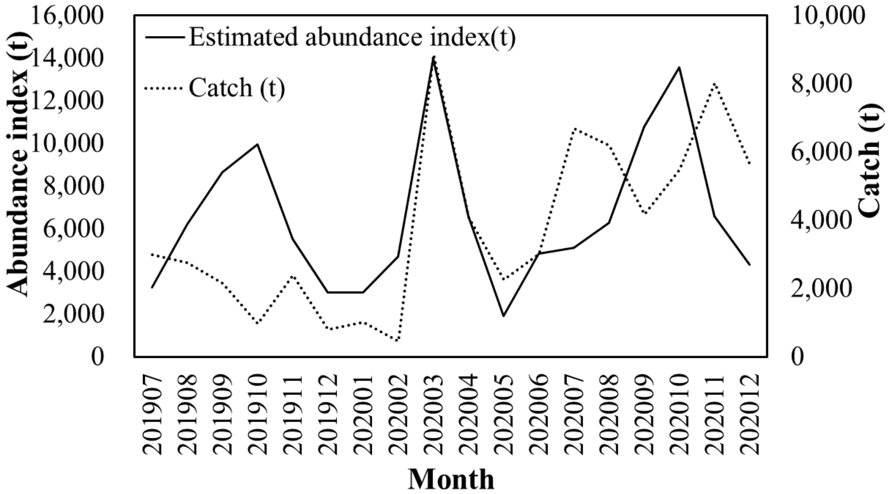

Figure 5-4. Trends in the monthly catch of purse seines fishery and monthly abundance index estimated from acoustic information. The solid line shows the estimated abundance index, and the dotted line shows the catch.

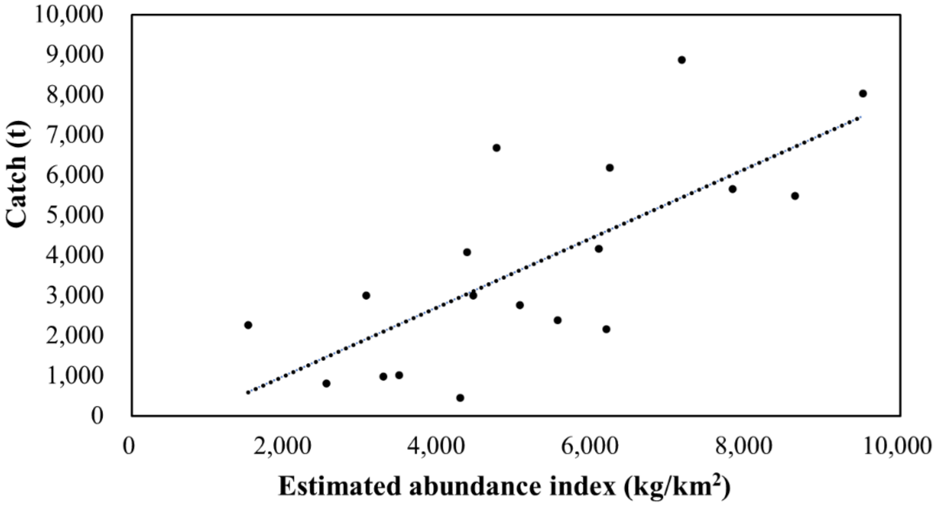

Figure 5-5. Correlation between the monthly catch of purse seines fishery and monthly abundance index estimated from acoustic information. The estimated abundance index was the area-standardized abundance index.

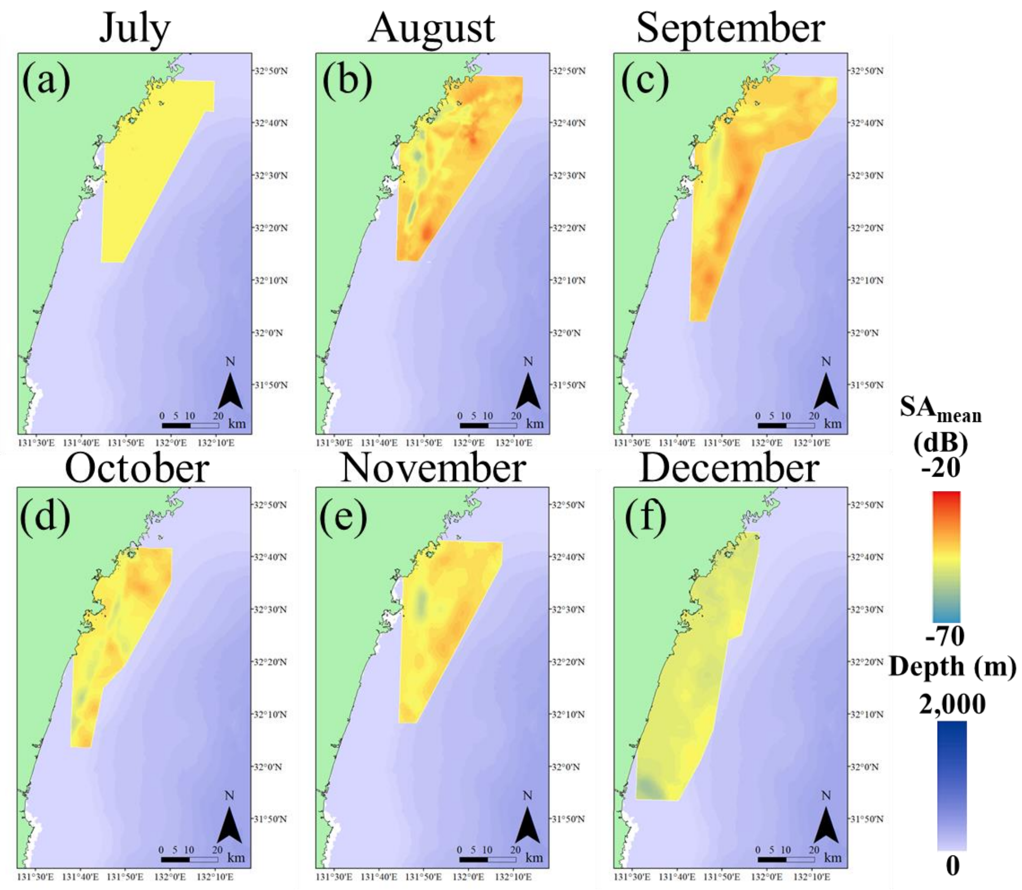

Figure 5-6. Fish distribution map showing fish distribution characteristic trends in 2019 using acoustic data SA_{mean} and created using the kriging function of ArcGIS. The SA_{mean} was calculated averaged SA at 1000 m intervals horizontally. The blue-only color bar indicates the depth of the Hyuga-nada, while the red-blue color bar indicates the change in SA_{mean}.

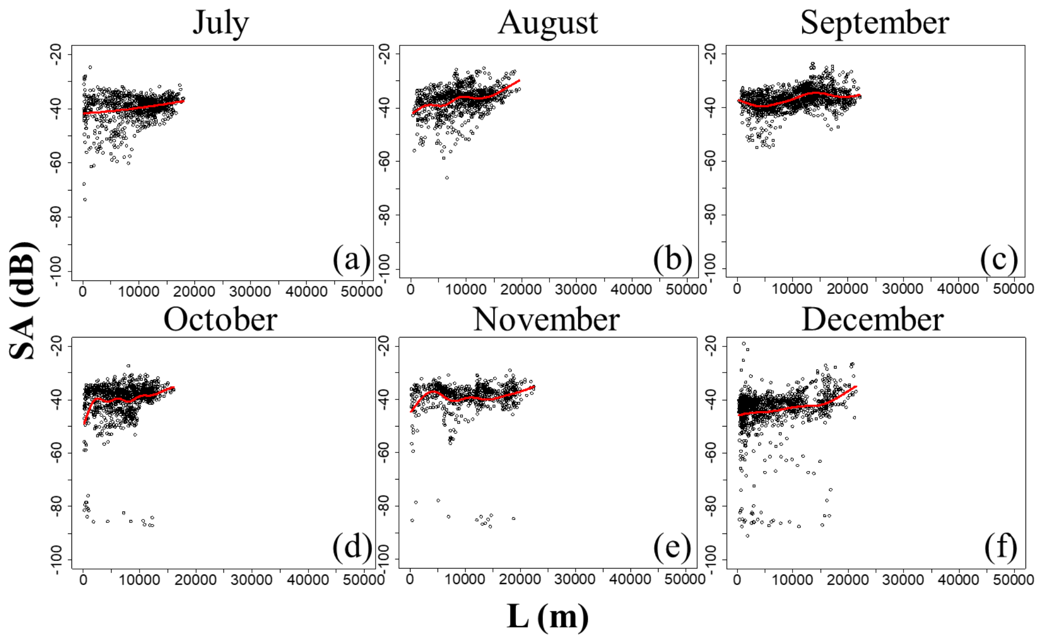

Figure 5-7. Seasonal variation of fish distribution in 2019 in horizontal structure expressed as the relationship between SA_{mean} and distance from shore L based on GAM. The solid red line shows the estimated line of fish distribution, and the circles show the measured value of SA_{mean}.

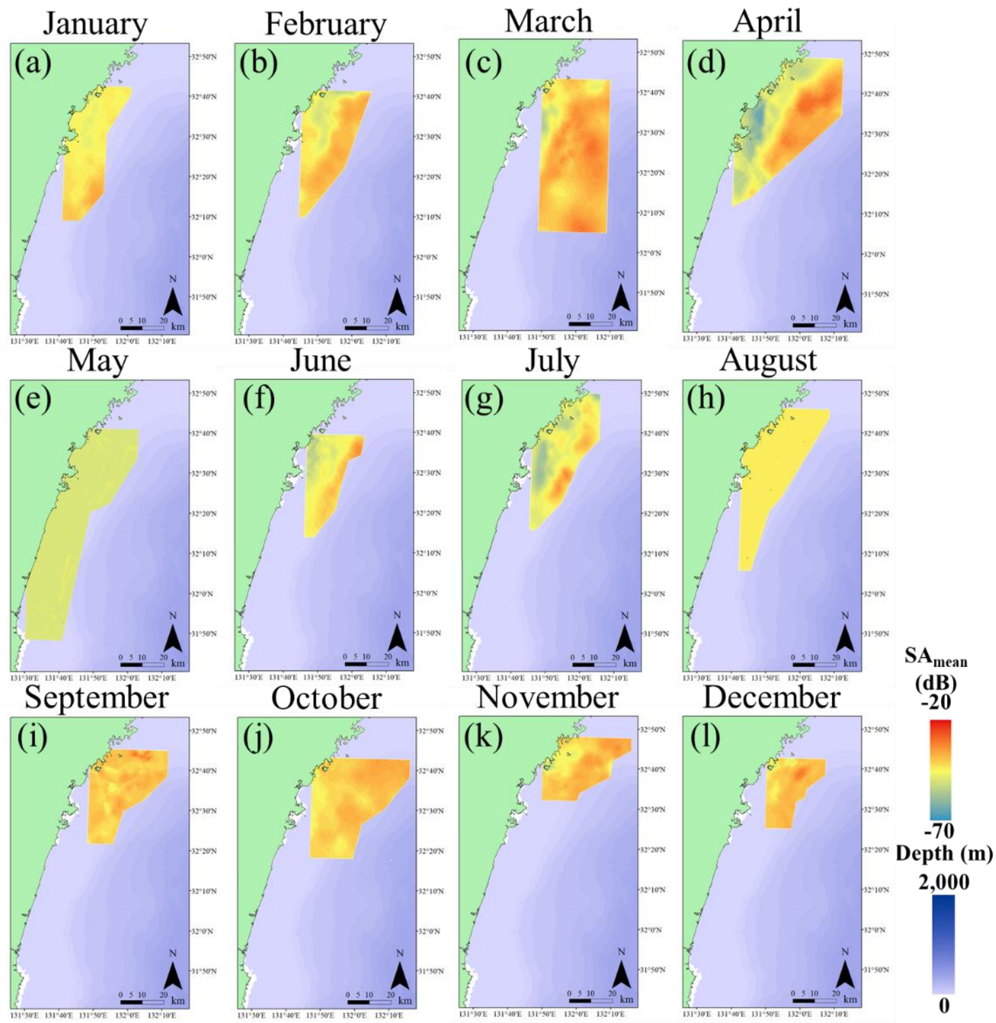

Figure 5-8. Fish distribution map showing fish distribution characteristic trends in 2020 using acoustic data SA_{mean} and created using the kriging function of ArcGIS. The SA_{mean} was calculated averaged SA at 1000 m intervals horizontally. The blue-only color bar indicates the depth of the Hyuga-nada, while the red-blue color bar indicates the change in SA_{mean}.

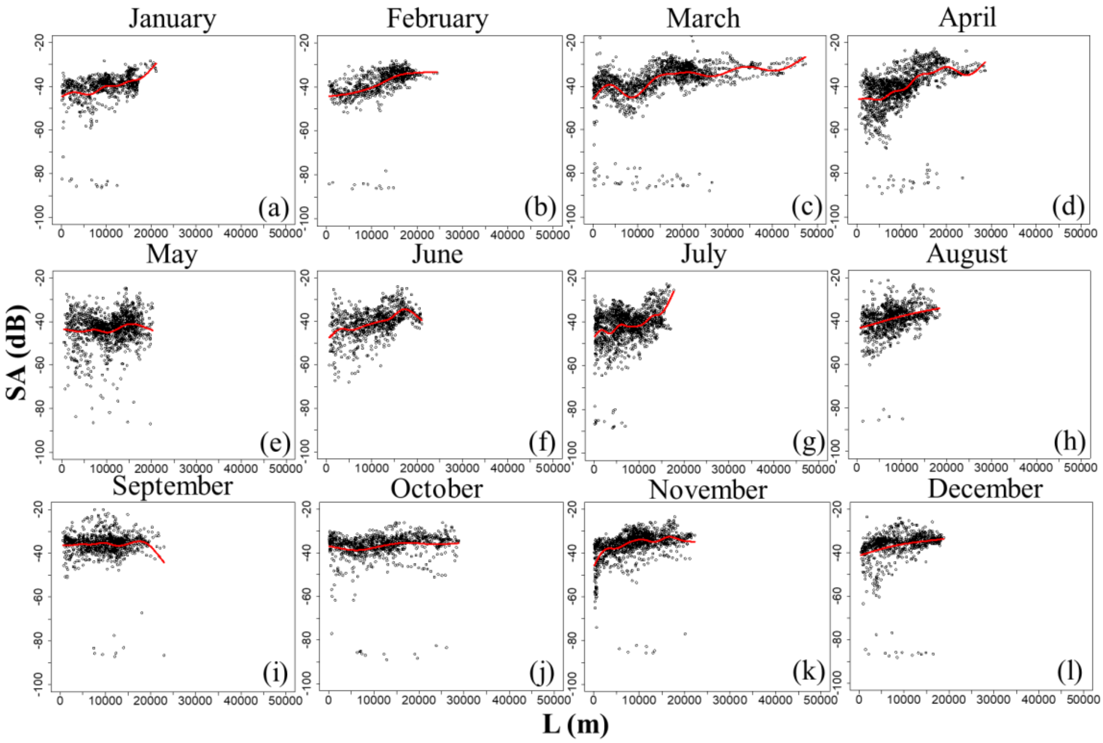

Figure 5-9. Seasonal variation of fish distribution in 2020 in horizontal structure expressed as the relationship between SA_{mean} and distance from shore L based on GAM. The solid red line shows the estimated line of fish distribution, and the circles show the measured value of SA_{mean}.

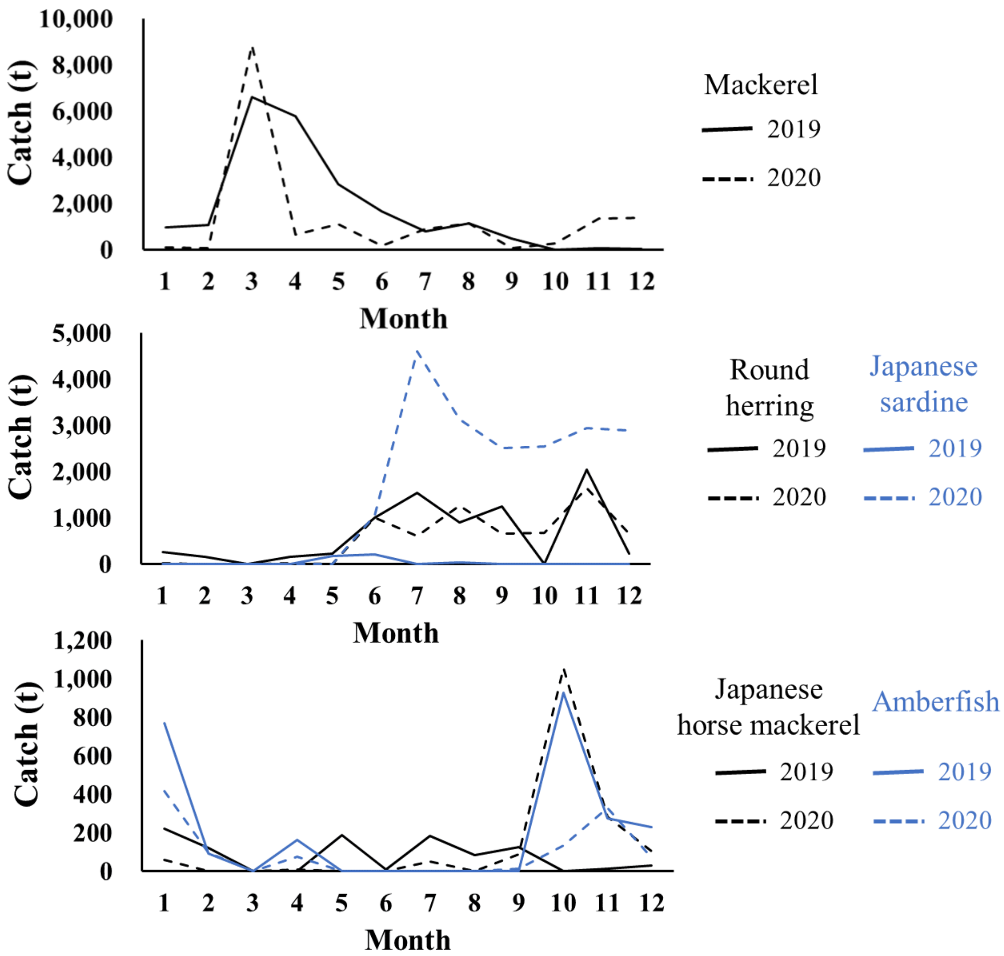

Figure 5-10. Monthly catches of purse seine fishery in 2019 and 2020 for each dominant fish species (for 24 vessels).

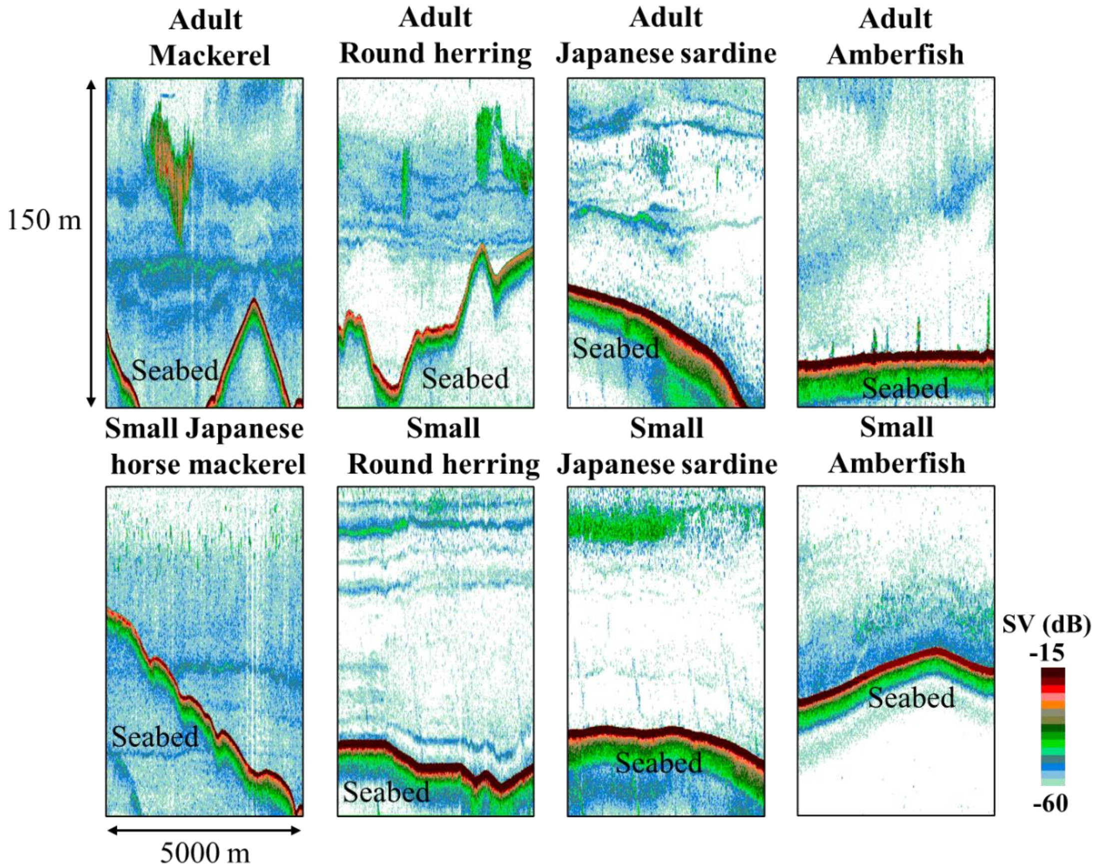

Figure 5-11. Echograms of the analysis month for each fish group. The color bar shows the change of SV (Each echogram is an example of a portion of that month).

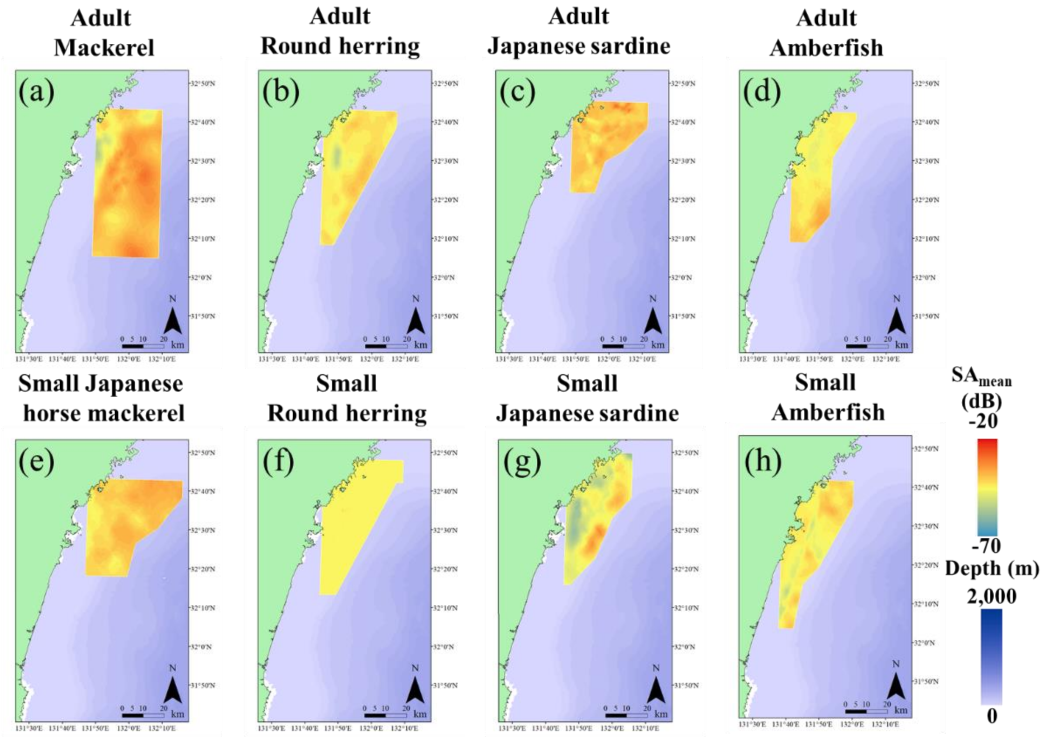

Figure 5-12. Horizontal structure in fish distribution for each fish group from the ArcGIS kriging function expressed as the SA_{mean} and distance from shore L. The blue-only color bar indicates the depth of the Hyuga-nada, while the red-blue color bar indicates the change in SA_{mean}.

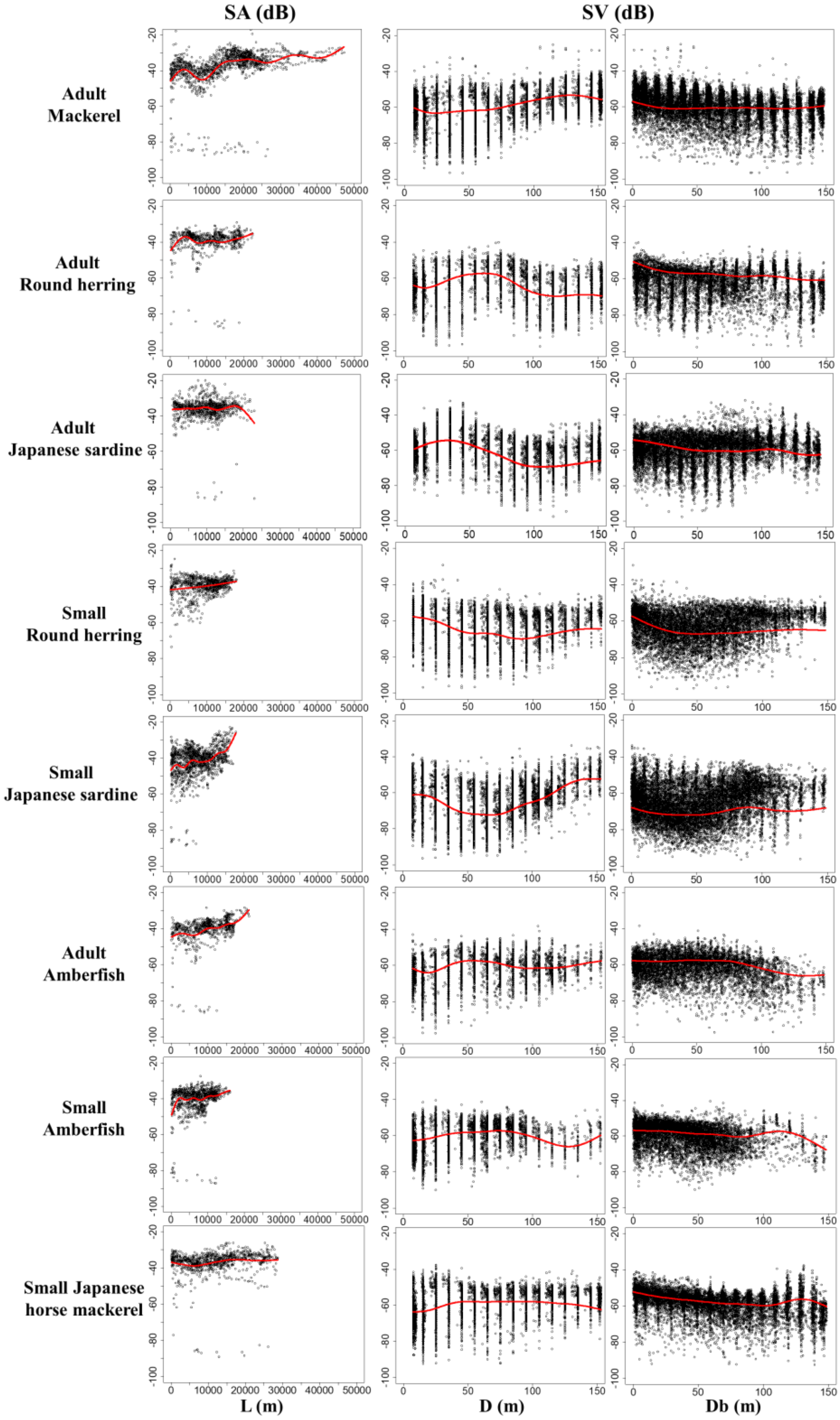

Figure 5-13. Fish distribution in horizontal and vertical structures based on GAM. The solid red line shows the estimated trend, and the circles show the measured value.

5.8 Tables

Table 5-1. Measured $AreaSA_{mean}$, assessment area and estimated abundance index of each month in Hyuga-nada.

	Month	$AreaSA_{mean}$ (dB)	Survey area (km^2)	Estimated abundance index (t)
2019	7	-37.9	1062	3,243
	8	-35.0	1229	6,214
	9	-35.1	1401	8,653
	10	-37.7	883	9,957
	11	-37.3	999	5,540
	12	-39.5	1194	3,027
2020	1	-37.9	871	3,033
	2	-35.6	1099	4,694
	3	-32.3	1955	13,989
	4	-34.6	1515	6,604
	5	-39.1	1274	1,927
	6	-36.6	1089	4,837
	7	-36.8	1076	5,107
	8	-35.3	1012	6,292
	9	-33.2	1000	10,784
	10	-34.8	1572	13,566
	11	-33.3	691	6,580
	12	-34.1	551	4,311

Table 5-2. Monthly total data points of SA_{mean} and data points of SA_{mean} within each backscattering strength ranged in 2019 and 2020.

		Number of Samean (A number of days)	SA_{mean}			
			~ -50dB	-50dB ~ -40dB	-40dB ~ -30dB	-30dB ~ -20dB
2019	201907	861 (15)	46	284	526	5
	201908	882 (14)	20	153	668	41
	201909	1298 (17)	18	200	1034	46
	201910	954 (12)	47	265	641	1
	201911	652 (10)	28	135	488	1
	201912	1137 (21)	97	794	236	10
2020	202001	685 (11)	38	234	408	5
	202002	683 (13)	16	207	446	14
	202003	1321 (21)	69	265	830	157
	202004	1287 (21)	171	452	526	138
	202005	1258 (21)	143	750	347	18
	202006	854 (20)	62	343	417	32
	202007	1173 (23)	125	500	505	43
	202008	888 (18)	38	273	536	41
	202009	877 (18)	12	99	696	70
	202010	909 (15)	24	115	740	30
	202011	1127 (19)	34	140	850	103
	202012	794 (20)	41	74	638	41

Table 5-3. Statistical results of the relationship between SA_{mean} and distance from shore L in 2019 and 2020.

2019												
	January	February	March	April	May	June	July	August	September	October	November	December
Estimate	-	-	-	-	-	-	-39.9	-37.1	-36.9	-40.1	-39.3	-44.0
edf	-	-	-	-	-	-	1.65	6.88	6.46	7.63	6.71	4.37
p-value	-	-	-	-	-	-	<0.05	<0.05	<0.05	<0.05	<0.05	<0.05
Adjusted r^2	-	-	-	-	-	-	0.05	0.14	0.21	0.08	0.04	0.04
Deviance explained (%)	-	-	-	-	-	-	4.8	14.9	21.4	8.7	5.0	4.7
GCV score	-	-	-	-	-	-	24.49	20.49	12.84	53.01	51.37	71.03
2020												
	January	February	March	April	May	June	July	August	September	October	November	December
Estimate	-40.5	-38.3	-37.6	-41.1	-43.3	-40.3	-41.7	-39.0	-36.0	-37.0	-36.1	-37.0
edf	6.66	3.83	8.77	8.27	6.04	7.75	8.26	1.87	6.50	4.34	8.01	1.89
p-value	<0.05	<0.05	<0.05	<0.05	<0.05	<0.05	<0.05	<0.05	<0.05	<0.05	<0.05	<0.05
Adjusted r^2	0.12	0.22	0.19	0.22	0.04	0.23	0.12	0.11	0.02	0.03	0.21	0.06
Deviance explained (%)	12.5	22.2	19.9	22.7	4.1	23.2	13.0	11.0	2.4	3.4	21.1	6.4
GCV score	50.79	46.84	78.97	80.53	51.20	31.95	59.79	38.24	39.64	49.14	36.89	64.67

Table 5-4. Statistical results of the relationship between SA_{mean} and distance from shore L, SV_{mean} and depth D, SV_{mean} and distance from seabed Db in each fish group.

	Adult Mackerel			Adult Round herring			Adult Japanese sardine			Adult Amberfish		
	SA	SV		SA	SV		SA	SV		SA	SV	
	s(L)	s(D)	s(D_b)	s(L)	s(D)	s(D_b)	s(L)	s(D)	s(D_b)	s(L)	s(D)	s(D_b)
Estimate	-37.6	-58.8		-39.3	-62.8		-36.0	-59.7		-40.5	-61.7	
edf	8.77	8.51	6.56	6.71	8.60	7.37	6.50	7.85	8.32	6.66	8.44	7.16
p -value	<0.05	<0.05	<0.05	<0.05	<0.05	<0.05	<0.05	<0.05	<0.05	<0.05	<0.05	<0.05
Adjusted r^2	0.19	0.24		0.04	0.27		0.02	0.35		0.12	0.20	
Deviance explained (%)	19.9	24.2		5.0	27.6		2.4	34.7		12.5	19.9	
GCV score	78.97	45.71		51.37	50.58		39.64	41.86		50.79	45.47	
	Small Japanese horse mackerel			Small Round herring			Small Japanese sardine			Small Amberfish		
	SA	SV		SA	SV		SA	SV		SA	SV	
	s(L)	s(D)	s(D_b)	s(L)	s(D)	s(D_b)	s(L)	s(D)	s(D_b)	s(L)	s(D)	s(D_b)
Estimate	-37.0	-58.4		-39.9	-62.4		-41.7	-64.6		-40.1	-59.5	
edf	4.34	8.26	8.92	1.65	8.07	6.19	8.26	8.66	7.50	7.63	8.30	8.11
p -value	<0.05	<0.05	<0.05	<0.05	<0.05	<0.05	<0.05	<0.05	<0.05	<0.05	<0.05	<0.05
Adjusted r^2	0.03	0.20		0.05	0.27		0.12	0.33		0.08	0.18	
Deviance explained (%)	3.4	19.6		4.8	27.6		13.0	33.5		8.7	18.3	
GCV score	49.14	37.05		24.49	50.01		59.79	64.02		53.01	37.15	

6. General Discussion

6.1 Adaptation of calibration methods using the seabed

This study established a method for quantifying acoustic information captured by a general echo sounder on a fishing vessel. This method enables us to efficiently grasp the actual conditions of fish schools in three dimensions using multiple acoustic data and to realize direct underwater visualization.

The appropriate sea area for the calibration method established in this study is a sandy area with slight variation in seabed topography. Since most of the seabed in these conditions is located near fishing ports, making site selection is very easy. Creating a standard map of the seabed backscattering strength, including the calibration of a general echo sounder, can be performed in a short time, at least three days. In the future, the calibration of general eco sounders will be performed automatically by passing over the reference map. Once a seabed backscattering strength standard map is created, calibration can be easily performed within a few years. From above, the calibration method using the seabed established in this study can be easily adapted to various sea areas and various fishing vessels.

On the other hand, because the characteristics vary depending on the frequency, differences in backscattering strength are observed between frequencies even for the same object (same seabed). Therefore, when calibrating a general echo sounder using a seabed backscattering strength standard map, it is necessary to create a standard map for each frequency. In addition, since the seabed quality and the range of the standard map vary depending on the sea area, it is essential to determine the optimal parameters for calculating the standard map values for each sea area. With these two points in mind, the calibration method using the seabed backscattering strength can be easily adapted to any fishing vessel in any sea area.

For example, in the whitebait (fry of sardines) fishery in the Shizuoka Prefecture, a system has been constructed to inform fishermen on the location and quantity of whitebait fish schools in operation using general echo sounder order to realize efficient operations (Kobayashi et al., 2021). However, at the present stage, due to the quantitative nature of the acoustic data obtained by general echo sounders, the system has only reached the point where the cross-sectional area of the fish school is expressed in three levels as biomass information. Therefore, it will be possible to quantify the information obtained from the general echo sounder by introducing the calibration method established in this study to the whitebait fishing vessels. In the future, it is expected to be possible to estimate the abundance index and distribution trend of fish schools rather than the cross-sectional area and to assess and manage fishing grounds and resources more accurately.

6.2 Utilization of acoustic information obtained from general echo sounders

It is considered most important for the current Japanese fisheries to scientifically assess fishery resources, maintain the marine ecosystem, and prevent the depletion of fishery resources. Conventionally, the assessment of fishery resources has been conducted by collecting necessary data through oceanographic observations and catch surveys by research vessels, as well as by using fishery catch information (Katayama, 2020). Thus, the base of the fishery assessment is the catch, and it currently needs to be determined whether it represents the true fish abundance or not. In this study, we could visualize fish resource information using multiple acoustic data from a single vessel. In the future, this system will significantly improve the current resource management system by collecting real-time data at fishing sites and using information from multiple vessels to visually grasp fish resource information over a wider area and at higher frequencies.

However, analyzing these vast amounts of primary data is time-consuming and workforce intensive. For example, acoustic data obtained from an echo sounder is analyzed using dedicated analysis software to extract values used for resource estimation. However, this analysis takes much time, making it challenging to analyze the vast amount of data acquired quickly. The most time-consuming part of the process is the primary processing of backland noise, which leads to an overestimation of the number of resources. In the future, by combining these vast amounts of primary data with artificial intelligence (AI) technology, we can expect to automatically analyze vast amounts of data obtained from multiple fishing vessels daily.

Additionally, in the current Japanese fisheries industry, management by total allowable catch (TAC) is based on the individual quota (IQ) method. TAC is allocated to individual fishermen or fishing vessels, and the fishermen are prohibited from fishing more than their quotas. Therefore, sustainable, and efficient fishing is vital for fishermen. Therefore, it is necessary to establish a system that stores biological information obtained from multiple general echo sounders at research institutions and makes it available to fishermen through information and communication technology (ICT). Fishermen can visually grasp the distance from the port to the fishing grounds and the fish abundance present in the fishing grounds by using the fish resource information. This will enable fishermen to search for more efficient fishing grounds or select fishing grounds based on the ratio of the cost of fishing to the amount of fish landed. It is expected to contribute to ensuring the profitability of fishermen and maintaining and improving their income. It is also expected that the fishery will smoothly shift from a fishery based on intuition and experience to a data-based fishery by utilizing primary data rather than operating based on experience and intuition alone.

Finally, the calibration methods established in this study can be used to obtain data quickly and accurately, no matter who conducts the surveys. Therefore, training personnel to use these measuring instruments is accessible, and any generation of researchers and fishermen can easily handle them. In light of the above, the results of this research will promote the fisheries that can realize accurate resource assessment and efficient operation in the future and will significantly advance conventional resource assessment and management.

Acknowledgements

I express my sincere gratitude to my supervisor, Professor Kazushi Miyashita, for providing me with this precious study opportunity as a Ph.D. student in his laboratory. I especially want to express my most profound appreciation to my supervisor, Associate Professor Kenji Minami, for his elaborated guidance, considerable encouragement, and invaluable discussion that made my outstanding research achievement and study life unforgettable. I also appreciate the two-vice advisor, Professor Masahiro Nakaoka, and Tsutomu Tokeshi, for their helpful discussions and comments on this manuscript.

I would like to thank Yoshihiro Nishiyama and Akinori Kasai, who works in FURUNO ELECTRIC CO., LTD., for advice on analysis. I am also grateful for the assistance of the Miyazaki Prefectural Fisheries Experiment Station, Kitaura town fishing cooperatives, and Shimaura town fishing cooperatives in Miyazaki. I also thank Dr. Jun Yamamoto for his advice. Furthermore, I gratefully acknowledge the work of past and present members of our laboratory for their helpful discussions. Finally, I want to thank Rotary Yoneyama Memorial Foundation for their financial support.

I want to express my gratitude to my family for their moral support and warm encouragement. I also want to express my deepest gratitude to my friends for their support. But, most of all, I want to thank my cats, that helped me heal my heart during the critical doctoral period.

Nomenclature

a: Fixity coefficient for each echo sounder at LOG conversion. a depends on an echo sounder type.

a': Fixity coefficient that includes frequency characteristics and temperature characteristic for each echo sounder.

a_1 (m): Radius of calibration ball.

A (m^2): Scattering area for SS calculation.

A': The multiplication of atmospheric pressure values and nondimensional pressure correction factor in Boric acid acoustic absorption.

$AreaSA_{mean}$ (dB): Averaged value of SA_{mean}s for one month.

b: Directivity index. Function of direction describing the amplitude sensitivity.

B': The multiplication of atmospheric pressure values and nondimensional pressure correction factor in magnesium sulfate (MgSO4) acoustic absorption.

c (m/s): Sound speed in water.

c_1: The velocity of the compressional wave.

c_2: The velocity of the shear wave.

C': The multiplication of atmospheric pressure values and nondimensional pressure correction factor in fresh water acoustic absorption.

Cu: The calibration ball made of copper.

D (m): Central depth of the SV_{mean} cell.

Db (m): Distance of the SV_{mean} cell from the seabed.

E (V): Electrical voltage. Echo amplitude at preamplifier output.

E_{ts} (V): The electrical voltage at the point returned in the direction of the sound source from the target scatterer.

E_{ss} (V): The electrical voltage of echoes in the surface scattering for the propagation distance.

E_{sv} (V): The electrical voltage of multiple echoes synthesized in the scattering volume for the propagation distance.

EL (dBμV): Reception echo level.

f (kHz): Frequency of transducer.

f_1: The relaxation frequencies of Boric acid.

f_2: The relaxation frequencies of magnesium sulfate (MgSO4).

f_∞: The absolute value of form function, which is equal to the scattering amplitude at the infinite range.

F: The absolute value of scattering amplitude at infinity.

G: Gravel, a marine sediment.

G_R: Gain function of preamplifier.

G_{ts}: Time-varied-gain (TVG) correction factor.

GS: Gravel-sand, a marine sediment.

k: The velocity of the sound in the surrounding fluid.

k_1: The compressional waves in the scatterer.

k_2: The shear waves in the scatterer.

K_{TR}: Factor of transmit and receive.

KTR (dBV): The decibel value of K_{TR}.

KTRa: KTR as a result of this calibration.

KTRb: KTR as a result of previous calibration.

L (m): Total length of fish.

L (m): Distance from the shore (Chapter 5).

m: Integral Ping Number.

M: Receiving sensitivity.

ma (g): Total mass of wet sample and container.

mb (g): Total mass of sample and container after drying.

mc (g): Mass of container.

md (g): Mass of the beaker used to dissolve the wet sample.

me (g): Mass of the heat-resistant tray.

mf (g): Total mass of wet sample and beaker.

mg (g): Total mass of sample after drying.

mh (g): Total mass of gravel and tray after drying.

mi (g): Total mass of sand and tray after drying.

ME (dB): The decibel value of M.

n: Number of fish per unit volume.

n’: Number of echoes for integration.

n_k: Mean density per unit area of fish species k.

N: Estimated abundance index.

P (Pa): Acoustic pressure. Amplitude of the sound pressure variation.

P’ (Pa): The pressure of the atmosphere.

P_k: Percentage of total catch represented by species k.

P_o (Pa): Transmitted sound pressure. Sound pressure amplitude normalized to 1 m range.

P_i (Pa): Sound pressure reaching the scatterer.

P_{ts} (Pa): Reception sound pressure from one scatterer at the transducer terminals.

P_{sv} (Pa): Reception sound pressure from volume backscattering.

P_{ss} (Pa): Reception sound pressure from surface backscattering.

Ping: One dispatch pulse of the echo sounder systems.

r (m): Discrimination depth, which is the oblique distance from the transducer to the outer edge of the scattering surface.

ra (m): Radius of circular transducer.

R (m): Distance to scatterer / water depth.

R_p: Reflection coefficient of acoustic pressure amplitude.

R_w (m): Integral depth.

RG (dB): The decibel value of G_R.

S (psu): Salinity of seawater.

S': Sand, a marine sediment.

sa (m^2/m^2): Area scattering coefficient (linear measure).

SA (dB): Area backscattering strength. The decibel value of sa.

SA_{mean} (dB): Integrated mean SA.

SG: Sand-gravel, a marine sediment.

SL (dBμPa): Source level. dB measure usually re 1 μPa at 1 m from the source.

ss ($1/m^2$): Surface backscattering coefficient (linear measure).

SS (dB): Surface backscattering strength. The decibel value of ss.

ss_{mean} ($1/m^2$): Integrated mean ss.

SS_{mean}: Decibel value of ss_{mean}.

sv (m^2/m^3): Volume backscattering coefficient (linear measure).

SV (dB): Volume backscattering strength. The decibel value of sv.

sv_{mean} ($1/m^2$): Integrated mean sv, average volume backscattering coefficient (linear measure).

SV_{mean}(dB): Decibel value of sv_{mean}.

T (°C): Temperature of seawater.

ts: Target coefficient of one scatterer.

ts_k: Target coefficient per kg of fish species k.

TS (dB): Target strength of one scatterer. The decibel value of ts.

TS_k: Target strength per kg of fish species k.

TSm (dB): Mean value of measured TS.

TSt (dB): Theoretic TS.

V (m^3): Scattering volume for SV calculation.

w (%): Moisture ratio.

W (kg): Weight of fish.

WC: Tungsten carbide ball, a type of calibration ball.

z_1: Intrinsic acoustic impedance of the medium on the incident side.

z_2: Intrinsic acoustic impedance of transmitting medium.

α (dB/m): Acoustic absorption coefficients in dB per unit distance.

θ (rad): Beam angle. Angle from the acoustic axis.

θ_I (rad): Incident angle.

θ_t (rad): Transmission angle.

τ (s): Pulse width. Duration of a sonar transmission pulse, time from start to finish.

$d\Omega$: Element of solid angle.

Ψ: Equivalent beam angle of a transducer for volume scattering.

φ: Beam width. Azimuthal angle in the transducer plane.

Γ: Equivalent beam angle for surface scattering.

μ: Lambert coefficient.

γ (rad): Complementary angle of incidence.

ρ: The density of the fluid.

ρ_1: The density of the scatterer.

ω (rad/s): The angular frequency.

References

1. Abe, K. 2020. Mechanism of Acoustic Fisheries Resource Survey: Estimation of Existing Resources by Echo-Integral Method (<Feature> Survey Mechanisms). Kanrin: bulletin of the Japan Society of Naval Architects and Ocean Engineers, 33: 31-36.

2. Amaksu, K. 2019. Trends in Acoustic Survey Technology for Fishery Resources. Journal of the acoustical society of Japan, 75(1): 12-16.

3. Amakasu, K., Sadayasu, K. Abe, K. Takao, Y. Sawada, K. and Ishi, K. 2010. Swimbladder Shape and Relationship Between Target Strength and Body Length of Japanese Anchovy (*Engraulis japonicus*). The journal of the Marine Acoustics Society of Japan, 37(1): 46-59.

4. Anderson, J.T. 2007. Acoustic seabed classification of marine physical and biological landscapes. ICES cooperative research report, No. 286, 183 pp.

5. Aoki, I. and Sugimoto, T. 1988. Echo Surveying of Distribution and Abundance of Pelagic Fish Schools in Relation to Oceanographic Conditions in the Coastal Area of Kumano-nada Sea. Nippon Suisan Gakkaishi, 54(10): 1747-1755.

6. Aoyama, C., Hamada, E., Furusawa, M. and Saito, K. 1997. Calibration of Quantitative Echo Sounders by Using Echo from Water Tank Surface. Nippon Suisan Gakkaishi, 63(4): 570-577.

7. Aoyama, C., Hamada, E. and Furusawa, M. 1999. Total Performance Check of Quantitative

Echo Sounders by Using Echoes from Sea Bottom. Nippon Suisan Gakkaishi, 65(1): 78-85.

8. Aoyama, C. and Matsumoto, R. 2009. Acoustic Surveys of Methane Plumes by Quantitative Echo Sounder in Japan Sea and the Estimate of the Seeping Amount of the Methane Hydrate Bubbles. Journal of Geography, 118(1): 156-174.
9. Asami, T. and Koto, T. 1974. Fluctuations in sardine stocks in recent years 3-2. Bulletin of the Japanese Society of Fisheries Oceanography, 25: 156-160.
10. Burns, D.R., Queen, C.B., Sisk, H., Mullarkey, W. and Chivers, R.C. 1989. Rapid and convenient acoustic sea-bed discrimination for fisheries applications. Proceedings of the Institute of Acoustics, 11(3): 169-178.
11. Chen, C. and Millero, F. 1977. Speed of sound in seawater at high pressures. The Journal of the Acoustical Society of America, 62: 1129-1135.
12. Coetzee, J. 2000. Use of a shoal analysis and patch estimation system (SHAPES) to characterise sardine schools. Aquatic Living Resources, 13(1): 1-10.
13. Coppens, A.B. 1981. Simple equations for the speed of sound in Neptunian waters. The Journal of the Acoustical Society of America, 69: 862-863.
14. De Robertis, A. and Higginbottom, L. 2007. A post-processing technique to estimate the signal-to-noise ratio and remove echosounder background noise. ICES Journal of Marine Science, 64: 1282–1291.

15. Doiuchi, R., Takeda, Y. 2010. Stock managements of three-line grunt and round scad in Wakayama Prefecture, Japan. Fisheries biology and oceanography in the Kuroshio, 11: 9-12.

16. Ellingsen, K.E., Gray, J.S. and Bjornbim, E. 2002. Acoustic classification of seabed habitats using the QTC VIEW system. ICES Journal of Marine Science, 59(4): 825-835.

17. Fisheries of Japan - FY2018. 2019. Fisheries Agency

18. Fisher, F.H. and Simmons, V.P. 1977. Sound absorption in sea water. The Journal of the Acoustical Society of America 62: 558-564.

19. Foote, K.G., Knudsen, H.P., Vestnes, G., Brede, R. and Nielsen, L. 1981. Improved calibration of hydroacoustic equipment with copper spheres. ICES CM 1981, Document 8(20): 18.

20. Foote, K.G. 1982. Optimizing copper spheres for precision calibration of hydroacoustic equipment. The Journal of the Acoustical Society of America, 71: 742-747.

21. Foote, K.G. 1983. Linearity of fisheries acoustics, with addition theorems. The Journal of the Acoustical Society of America, 73: 1932-1940.

22. Foote, K.G. and MacLennan, D.N. 1984. Comparison of copper and tungsten carbide calibration spheres. The Journal of the Acoustical Society of America, (75): 612-616.

23. Fossati, A. and Wiegard, W. 2002. Policy evaluation with computable general equilibrium models. Routledge, London.

24. Francois, R.E. and Garrison, G.R. 1982. Sound absorption based on ocean measurements. Part II: Boric acid contribution and equation for total absorption. The Journal of the Acoustical Society of America 72: 1879-1890.

25. Fujii, M. and Nogi, Y. 2018. Acoustic mapping of the seafloor features: Implication for global environmental change. Low temperature science, 76: 269-284.

26. Fukuda, H. 2010. Fisheries ecology and prediction of the catch of Japanese jack mackerel *Trachurus japonicus* and spotted mackerel *Scomber australascicus* in the sea of Hyuda-nada. Fisheries biology and oceanography in the Kuroshio, 11: 55-66.

27. Fukuda, H. 2012. Fisheries ecology and prediction of the catch of round herring *Etrumeus teres* and Japanese sardine *Sardinops melanostictus* in the sea of Hyuga-nada. Fisheries biology and oceanography in the Kuroshio, 13: 75-85.

28. Fukuda, H. 2013. Characteristics of fishing season and fishing ground in purse seine fishing in the sea of Hyuga-nada. Fisheries biology and oceanography in the Kuroshio, 14: 61-67.

29. Furusawa, M. 1985. Consideration on TVG of Echo-sounder. Technical report of National Research Institute of Fisheries Engineering (Fishing boat and instrument), 6: 33-49.

30. Furusawa, M. and Takao, Y. 1990. A Versatile Quantitative Echo Sounding System. Bulletin of National Research Institute of Fisheries Engineering, 29(2): 139-147.

31. Furusawa, M. 1991. Designing quantitative echo sounders. The Journal of the Acoustical

Society of America, 90(26): 26-36.

32. Furusawa, M. and Sawada, K. 1991. Effects of Transducer Motion on Quantifying Single Fish Echoes. Nippon Suisan Gakkaishi, 57(5): 857-864.

33. Furusawa, M. Miyanohana, Y. Sawada, K. and Takao, Y. 1995. Calibration Manual for Quantitative Echo Sounders. Technical report of National Research Institute of Fisheries Engineering (Fishing boat engineering), 15: 9-37.

34. Furusawa, M. 2019. Quantitative Echo Sounder and Its Development. The Journal of the Acoustical Society of Japan, 75(12): 669-676.

35. Ginsburgh, V. and Keyzer, M. 1997. The structure of applied general equilibrium models. The MIT Press, Massachusetts Institute of Technology, Cambridge, Massachusetts 02142.

36. Goto, T. 2022. Relationship between fisheries and fish in Sanriku affected by the oceanographic dynamics. Journal for the integrated study of dietary habits, 32(4): 155-162.

37. Goto, N., Hashida, D., Nakao, H. and Tomiyama, T. 2020. Spatiotemporal distribution of two mackerel species, *Scomber japonicus* and *Scomber australasicus*, in the Bungo Channel, western Japan. Nippon Suisan Gakkaishi, 86(4): 295-301.

38. Hamano, A. 2019. Studies of Acoustic Method for Estimating Fishery Resources and Fishing Reef Grounds. Fisheries Engineering, 55(3): 175-185.

39. Hamilton, L.J. 2001. Acoustic Seabed Classification Systems. DSTO-TN-0401.

40. Harada, S. and Takeda, Y. 2014. Recent formation of fishing grounds in Jack mackerel, Round scad, Chub mackerel and Spotted mackerel of purse seine fisheries (two-boat operation) in outer waters adjacent to the Kii Channel. Fisheries biology and oceanography in the Kuroshio, 15: 37-43.

41. Harrison, G.W., Hougaard, S.E., Pedersen, L.H. and Rutherford, T.F. 2000. Using Dynamic General Equilibrium Models for Policy Analysis. North-Holland. Contributions to Economic Analysis Vol. 248.

42. Harada, S., Sumitomo, T., Miyazawa, Y., Saito, M. and Takeda, Y. 2015. Dispersal and recruitment processes of pelagic fish (Carangid). Nippon Suisan Gakkaishi, 81(3): 484.

43. Hinokio, R., Ishida, M. and Yamazaki, H. 2015. Effect of Substance Concentrations in Sediments using Various Types of Sediment Samplers: A study on surface sediments contamination by the Fukushima Daiichi Nuclear Power Station Accident. Environmental conservation engineering, 44(8): 452-459.

44. Hirai, K. 1999. Water temperature and fishing grounds for Spotted mackerels around the Izu Islands. Bulletin of the Japanese Society of Fisheries Oceanography, 63(4): 199-204.

45. Hokimoto, K. 2019. Study on "Meeting Held in the Branch of Fishery Cooperative" for Planning Fishing Village Revitalized Plan in Yamaguchi Prefecture. The journal of the Shimonoseki University of Fisheries, 67(4): 243-252.

46. Hokimoto, K. 2020. Operation Process and Difficulties Encountered in the Implementation of "Fishing Village Revitalizing Plans". The journal of the Shimonoseki University of Fisheries, 68(4): 97-106.

47. Hunsicker, M.E., Kappel, C.V., Selkoe, K.A., Halpern, B.S., Scarborough, C., Mease, L. and Amrhein, A. 2016. Characterizing driver–response relationships in marine pelagic ecosystems for improved ocean management. Ecological Applications, 26(3): 651-663.

48. Ichinokawa, M., Nishijima, S., Muko, S., Kurota, H. and Ohshimo, S. 2022. Alternative harvest control rules for achieving sustainable fisheries under the revised Fisheries Act in Japan: case studies in two Japanese sardine stocks. Nippon Suisan Gakkaishi, 88(4): 239-255.

49. Imazeki, A. Mine, Y. Takasu, Y. and Hamada, E. 1992. Calibration of Transmitting and Receiving System of Echo Sounder by used Ballbearing. Bulletin of the Japanese Society of Fisheries Oceanography, 56(2): 121-130.

50. Inoue, R. Shimizu, E. Yoshida, Y. and Li Y. 2009. Visualization of Spatial Distribution and Temporal Transition of Land Price in Tokyo 23 Wards Based on Spatio-Temporal Kriging Interpolation. Theory and Applications of GIS, 17(1): 13-24.

51. Ito, S., Kudo, M., Kuroki, K., Kurita, H. and Kuroki, T. 1985. Dispersal and migration of fry from horse mackerel spawning grounds. MRP progress report, 1-21.

52. Jackson, D.R. 1994. APL-UW high-frequency ocean environmental acoustic models handbook. Applied Physics Laboratory, University of Washington, Technical Report, 9407(102): IV21-IV36.

53. Kaneko, T. 2019. Effects and challenges of introducing ICT to wholesale markets. Nippon Suisan Gakkaishi, 85(2): 228.

54. Kang, M. 2006. Current technology of fisheries acoustics based on analyzed acoustic data using Sonar Data's Echoview. ACOUSTICS, 2006: 493-497.

55. Katayama, S. 2020. Future stock assessment and fisheries management of coastal resources. Fisheries biology and oceanography in the Kuroshio, 21: 3-7.

56. Katsukawa, T. 2020. Status of the ocean ecosystem and Japanese fisheries management. Environmental information science, 49(1): 6-10.

57. Kawano, M. 2020. Oceanographic Condition and Creatures in Waters off Yamaguchi Prefecture, Southwestern Sea of Japan (Review). Bulletin of Yamaguchi Prefectural Fisheries Research Center, 17: 33-48.

58. Kawano, M. and Kunimori, T. 2018. Spawning Ground and Movement of Distribution Area of Round Herring (*Etrumeus teres*) Eggs and Larvae in the Southwestern Sea of Japan. Bulletin of Yamaguchi Prefectural Fisheries Research Center, 15: 7-10.

59. Kondo, K. 1988. On the mode of distribution and migration of the Japanese Sardine,

Sardinops melanostictus at high level stock size. Bulletin of Tokai Regional Fisheries Research Laboratory, 124: 1-33.

60. Kobayashi, K., Zhu, Y., Oshiyama, D., Minami, K., Shirakawa, H. and Miyashita, K. 2021. Development of a biomass assessment method using fisheries echo sounder for monitoring whitebait fishery in Shizuoka Prefecture, Japan. Journal of Marine Science and Technology, 29(2): 168-174.
61. Mackenzie, K.V. 1981. Nine-term equation for sound speed in the oceans. The Journal of the Acoustical Society of America, 70: 807-812.
62. MacLennan, D.N. 1981. The theory of solid spheres as sonar calibration targets. Scottish Fisheries Research. Report Number 22.
63. MacLennan, D.N. and Dunn, J.R. 1984. Estimation of sound velocities from resonance measurements on tungsten carbide calibration spheres. Journal of Sound and Vibration. 97(2): 321-331.
64. MacLennen, D.N. 1989. Acoustical measurement of fish abundance. The Journal of the Acoustical Society of America, 87, 1-15.
65. MacLennan, D.N., Fernandes, G.P. and Dalen, J. 2002. A consistent approach to definitions and symbols in fisheries acoustics. ICES Journal of Marine Science, 59: 365-369.
66. Matsuda, S. 1969. The studies on fish eggs and larvae occurred in the Nansei regional waters

of Japan – species occurred and their seasonal variation. Bulletin of the Nansei Regional Fisheries Research Laboratory, 2: 49-83.

67. Matsuoka, M. 2001. Influence of Low Temperature on Hatching and Survival Rates at First−feeding Stage in the Japanese Sardine. Nippon Suisan Gakkaishi, 67(5): 894-895.

68. McCartney, B.S., and Stubbs, A.R. 1971. Measurements of the acoustic target strengths of fish in dorsal aspect, including swimbladder resonance. Journal of Sound and Vibration, 15(3): 405-420.

69. Miyanohana, Y., Ishii, K. and Furusawa, M. 1993. Spheres to Calibrate Echo Sounders at Any Frequency. Nippon Suisan Gakkaishi, 59(6): 933-942.

70. Miyanohana, Y. 1994. Ultrasonic Methods for Locating and Weighing Fish Stocks. Research journal of food and agriculture, 17(12): 22-26.

71. Miyamoto, Y., Uchida, K., Amakasu, K., Hasegawa, K., Theparoonart, Y., Anongponyoskun, M., Ishikawa, S., Minlee, Y. and Sasakura, T. 2016. Prototype pf a simple acoustic survey system for attachment to a GPS plotter echo sounder. The journal of the Marine Acoustics Society of Japan, 43(2): 71-78.

72. Murase, M., Hayashi, T. and Kitayama, T. 2014. Visualization of Higher Harmonic Generation at Contacting Surfaces. Journal of JSNDI, 63(6): 310-315.

73. Murase, H., Nagashima, H., Yonezaki, S., Matsukura, R. and Kitakado, T. 2009. Application

of a generalized additive model (GAM) to reveal relationships between environmental factors and distributions of pelagic fish and krill: a case study in Sendai Bay, Japan. ICES Journal of Marine Science, 66(6): 1417-1424.

74. Narita, H. 2016. Marine Observation Guidelines (Sediment Analysis). The Oceanographic Society Japan. Vol 5: 1-6.

75. Niida, N., Shimada, M., Hoshino, K., Hara, S. and Takei, M. 2005. On the Quantity Measurement of Remained Oil inside a Sunken Ship Using the Ultrasonic Pulse-echo. The Visualization Society of Japan, 25(1): 375-378.

76. Nishioka, T. 2019. Studies on the control measures of viral nervous necrosis (VNN) in seed production process of marine fish. Bulletin of Japan Fisheries Research and Education Agency, 48: 1-60.

77. Nozu, J. 1980. Fish ecology and fisheries formation of chub mackerel mainly in the Hyuga-nada. Bulletin of the Japanese Society of Fisheries Oceanography, 36: 50-53.

78. Okabe, K., Iwata, S. and Watanabe, S. 2009. Implication of effects of fluctuations in oceanographic condition and maturation process on migration of common mackerel (*Scomber japonicus*) in the fishing grounds around Izu Islands. Bulletin of the Japanese Society of Fisheries Oceanography, 73(1): 1-7.

79. Patterson, R.B. 1967. Using the Ocean Surface as a Reflector for a Self-Reciprocity

Calibration of a Transducer. The Journal of the Acoustical Society of America, 42: 653-655.

80. Pinilla. J. and Negrin. M. 2021. Non-Parametric Generalized Additive Models as a Tool for Evaluating Policy Interventions. Mathematics, 9(4): 299.

81. Saneyoshi. J. and Nakamura, K. 1952. Theory and Model Experiment on Reflection of Ultrasonic Waves from Numerous Reflectors. The Journal of the Acoustical Society of Japan, 8(3): 123-127.

82. Schulkin, M. and Marsh, H.W. 1962. ω: in Sea Water. The Journal of the Acoustical Society of America 34: 864-865.

83. Shida, O. 2019. Acoustic surveys of walleye pol lock by Hokkaido Research Organization using the quantitative echo sounder. Scientific reports of Hokkaido Fisheries Research Institutes, 95: 41-53.

84. Shimmonds, J. and Maclennan, D. 2006. Fisheries Acoustics-Theory and Practice Second Edition. Blackwell Publishing, Massachusetts, 63-65.

85. Shinada, A. 2021. Near-future predictions of sea surface temperature in the coastal areas around Hokkaido, Japan (Note). Scientific reports of Hokkaido Fisheries Research Institutes, 99: 19-23.

86. Siwabessy, P.J., Tseng, Y. and Gavrilov, A.N. 2004. Seabed habitat mapping in coastal waters using a normal incident acoustic technique. Proceedings of ACOUSTICS 2004, 3-5

November 2004, Gold Coast, Australia: 187-192.

87. Sugimoto, T. 2008. Recovery and collapse processes of sardine and anchovy stock. Kaiyo monthly, 40(3): 203-207.

88. Takasuka, A. 2007. Biological processes linking climate changes to sardine population dynamics. Nippon Suisan Gakkashi, 73(4): 758-762.

89. Takao, Y., Mizoguchi, H., Imaizumi, T., Fujita, K., Miyoshi, J., Oshima, T., Nishiyama, Y., Yamaguchi, S. and Ise, K. Construction and trial of a fishing vessel information aggregation system using the research vessel Takamaru. Fisheries engineering, 117-118.

90. Takeda, Y. 2002. Migration of Round Scad *Decapterus maruadi* in the waters around Kii channel. Bulletin of the Japanese Society of Fisheries Oceanography, 66(1): 26-33.

91. Tanaka, K. 2021. Assessment and Management of Fisheries Resources in Japanese Territorial Waters and EEZ - How do we weigh fish and catch them appropriately. Marine engineering: journal of the Japan Institution of Marine Engineering, 56(2): 206-209.

92. Tokeshi, T., Nakanishi, K. and Katayama, S. 2021. Long-term spatiotemporal variation in Miyazaki Prefecture coastal fishery catch in relationship to oceanographic conditions. Bulletin of the Japanese Society of Fisheries Oceanography, 85(2): 45-53.

93. Tang, Y. and Furusawa, M. 2003. Minimization of interference by sea surface and bottom reverberations in measuring surface fish abundance by scanning sonar. Nippon Suisan

Gakkaishi, 69(2): 153-161.

94. Kaneko, T. 2019. Effects and challenges of introducing ICT to wholesale markets. Nippon Suisan Gakkaishi, 85(2): 228.

95. Tanoue, H., Komatsu, T. and Hamano, A. 2013. Determination of upper boundary of an acoustic blind zone produced by the rugged bottom during a survey using a quantitative echosounder. Bulletin of the Japanese Society of Fisheries Oceanography, 77(2): 53-58.

96. Tao, L. and Motooka, S. 2005. Improvement of the Discrimination by Introducing the Reflection Properties of Different Seabed Materials. Steering committee of symposium on ultrasonic electronics, 26: 37-38.

97. Traynor, J.J. and Ehrenberg, J.E. 1990. Fish and standard-sphere target-strength measurements obtained with a dual-beam and split-beam echo-sounding system. Rapp. R-v. Réun. Cons. int. Explor. Mer, 189: 325-335.

98. Tokeshi, T., Horie, H. and Sajiki, T. 2020. The need of Miyazaki prefectural fishers for information on oceanic conditions. Nippon Suisan Gakkaishi, 86(5): 430-432.

99. Tsukamoto, Y. 2007. Ecological characteristics of Horse mackerel. Kaiyo monthly, 39(8): 495-499.

100. Uehara, S. and Mitani, T. 2007. Recruitment process of Horse mackerel in the southern pacific coast. Kaiyo monthly, 39(8): 539-544.

101. Voulgaris, G. and Collins, M. 1990. USP RoxAnn ground discrimination system: a preliminary evaluation. Admiralty Research Establishment, Portland, UK. University of Southampton, Department of Oceanography, Marine Consultancy Services, Technical Report No: SUDO/TEC/90/5C.

102. Wentworth, C.K. 1922. A Scale of Grade and Class Terms for Clastic Sediments. The journal of Geology, 30(5): 377-392.

103. Wong, H., and Chesterman, W.D. 1968. Bottom Backscattering near Grazing Incidence in Shallow Water. The Journal of the Acoustical Society of America, 44: 1713-1718.

104. Yagura, A. and Suzuki, M. 2019. Investigation of Ark Shell *Scapharca broughtonii* in South Sendai Bay. Miyagi Prefectural report of fisheries science, 19: 45-48.

105. Yamatani, K. 1990. About the Latest Echo Sounder Systems. The Society of Naval Architectsof Japan, 730: 208-214.

106. Yang, L., Chen, Y. and Zhang, J. 2019. Calibration of echosounder using standard target method. MATEC Web of Conferences, 283: 1-4.

107. Yokoyama, K., Umeda, M. and Yamazaki, H. 2005. Development of acoustic techniques for suspended sediment concentration measurement. Annual journal of hydraulic engineering, 49: 547-552.

108. Yokohama, H. and Ishihi, Y. 2009. Zoning of the inner part of Ariake Sound based on

principal component analysis of sediment factors. Nippon Suisan Gakkaishi, 75(4): 674-683.

109. Yosho, F., Shigeto, M., Sato, T. and Kuroki, T. 1984. Distribution of juvenile Horse mackerel. MRP progress report, 1-9.

110. Yukami, R., Ohshimo, S., Yoda, M. and Hiyama, Y. 2009. Estimation of the spawning grounds of chub mackerel *Scomber japonicus* and spotted mackerel *Scomber australasicus* in the East China Sea based on catch statistics and biometric data. Fisheries Science, 75: 167-174.

111. Zhu, Y., Minami, K., Iwahara, Y., Oda, K., Hidaka, K., Hoson, O., Morishita, K., Hirota, M., Tsuru, S., Shirakawa, H. and Miyashita, K. 2021. Seasonal variation in fish school spatial distribution and abundance under the Kuroshio regular pattern and the large meander in Suzu coastal waters. Plos one.